FINITE DIFFERENCE TIME DOMAIN (FDTD) ANALYSIS OF A LEAKY TRAVELING WAVE MICROSTRIP ANTENNA

THESIS

Gregory M. Zelinski, First Lieutenant, USAF

AFIT/GE/ENG/05-24

DEPARTMENT OF THE AIR FORCE
AIR UNIVERSITY

AIR FORCE INSTITUTE OF TECHNOLOGY

Wright-Patterson Air Force Base, Ohio

The views expressed in this thesis are those of the author and do not reflect the official policy or position of the United States Air Force, Department of Defense, or the United States Government.

AFIT/GE/ENG/05-24

FINITE DIFFERENCE TIME DOMAIN (FDTD) ANALYSIS OF A LEAKY TRAVELING WAVE MICROSTRIP ANTENNA

THESIS

Presented to the Faculty

Department of Electrical and Computer Engineering

Graduate School of Engineering and Management

Air Force Institute of Technology

Air University

Air Education and Training Command

In Partial Fulfillment of the Requirements for the

Degree of Master of Science in Electrical Engineering

Gregory M. Zelinski, B.S.E.E.

First Lieutenant, USAF

March 2005

AFIT/GE/ENG/05-24

FINITE DIFFERENCE TIME DOMAIN (FDTD) ANALYSIS OF A LEAKY TRAVELING WAVE MICROSTRIP ANTENNA

Gregory M. Zelinski, B.S.E.E.

First Lieutenant, USAF

Approved:

/signed/	21 Mar 2005
Maj Michael L. Hastriter (Chairman)	date
/signed/	21 Mar 2005
Dr. William P. Baker (Member)	date
/signed/	21 Mar 2005
Dr. Michael J. Havrilla (Member)	date
/signed/	21 Mar 2005
Dr. Andrew J. Terzuoli (Member)	date

Acknowledgements

First and foremost, I'd like to thank Dr. Gary Thiele for his patience, his advice, and his friendship. Dr. Thiele's curiosity in this project was a source of motivation. I couldn't have completed much of this work without Dr. Dan Janning, Josh Radcliffe, Ken Goss, "Cub" Corwin, John Reynolds, and all of the other "RASCAL's" that helped fabricate and measure antennas.

Many thanks to my advisor, Maj Larkin Hastriter. His "hands-off" style gave me the flexibility to learn a great deal more than I otherwise would have. Dr. Andrew Terzuoli deserves special recognition for finding a computer with increased memory to enable larger simulations. Thanks also to my committee for their support and direction when needed.

Finally, I'd like to thank my wife. I know it was as difficult for you as it was for me. It's your turn to go to school, now. To my daughters, the party is over.

Gregory M. Zelinski

Table of Contents

Page

List of Figures

List of Tables

Abstract

This thesis provides the groundwork that will enable development of a lightweight, inexpensive, aerodynamic, and broadband antenna. Whether for radar or communication, an antenna with these properties would be a force multiplier for the smaller, limited payload air vehicles the United States Air Force will pursue in the coming years.

Several microstrip antennas using the first higher order mode were simulated with the Finite Difference Time Domain (FDTD) method. The propagation constant of each antenna was extracted from the resulting field distribution for comparison with a transverse resonance approximation, measured far-field patterns, and other simulated antennas. Variations of the geometry were explored to investigate field propagation, improve the far-field pattern, and improve bandwidth. A simplified fabrication method was demonstrated that shorten production time and improved the far-field pattern.

FINITE DIFFERENCE TIME DOMAIN (FDTD) ANALYSIS OF A LEAKY TRAVELING WAVE MICROSTRIP ANTENNA

I. Introduction

The antenna, as defined in The Institute of Electrical and Electronic Engineers (IEEE) Standard 145-1983, is a means of radiating and receiving electromagnetic waves. In practice, an antenna is a component of a communication system that provides a connection between a remotely separated sender and receiver. Antennas allow the sharing of information without sharing a wire.

The need for more information sharing between individuals is making our world increasingly wireless. One need not look further than the incredible growth of cell phones, pagers, and wireless internet connections. Sometimes the sender or receiver is not even a person. Unmanned vehicles that operate in environments too expensive or too hostile for humans can be remotely controlled using an antenna, even as far away as Neptune! Many newer automobiles employ antennas to *see* behind them to alert the driver to an obstruction.

Aviation, particularly military aviation, uses many systems whose effectiveness hinges upon a properly functioning antenna. To avert mid-air collisions, aircraft must communicate in real-time with ground controllers as well as other aircraft. Landing, which is arguably the most difficult task in aviation, is made relatively simple by an instrument landing system (ILS) in which an antenna on the ground *talks* to an antenna on the aircraft. The safety and enjoyment of flights are enhanced by weather radar systems that allow flights to be diverted around storms. Navigation is greatly enhanced from systems that use antennas to communicate with satellites or scan the ground with radar. Mission effectiveness and aircraft survivability are increased by the radar warning receivers, which alert a pilot to the invisible dangers of enemy aircraft and surface to air missiles.

Historically, antennas have been the most expensive component in most communication systems. The price is due to the high development cost of designing a new antenna.

The electromagnetic interactions involved in the operation of an antenna can be extremely complicated. The ability to analytically characterize many new antennas is prohibitively time intensive. Attention is paid, instead, to numerically approximating the structure, although, an accurate model often requires much computing power. Adding to the price tag, an antenna must be manufactured under strict tolerances to operate as designed.

In recent years, antenna design has become less expensive. Exponential advances in computing resources together with more efficient algorithms have created a climate where elaborate simulations have become commonplace. Improved materials and new manufacturing techniques have made many types of antennas, such as microstrip, easy to fabricate.

1.1 Problem Statement

The U. S. Air Force has a need for a conformal, broadband antenna that is lightweight and inexpensive. A conformal antenna is more aerodynamic and tends to have a lower radar cross section. The less the aircraft weights, the more payload that can be carried. Likewise, the less the aircraft costs, the more aircraft that can be purchased, and in turn, the more payload that can be delivered. A broadband antenna reduces the need for multiple antennas, which further reduces the cost and weight of the aircraft. Microstrip inherently satisfies all of these requirements except bandwidth. A microstrip antenna operating in a leaky traveling wave configuration could provide the bandwidth needed.

A new antenna design proposed by Dr. Gary Thiele of Analytic Designs, Inc., is seen in Figure 1.1. The design is based on work by Menzel [23], whose antenna can be seen in Figure 1.2. Menzel's antenna uses seven slots cut from the conductor along the centerline to suppress the fundamental mode allowing leaky wave radiation via the first higher order mode. Menzel's antenna has been analyzed by a host of researchers over the past 25 years [2, 9, 10, 21, 24–26, 28–30, 34, 40, 42] and its performance is known and reproducible. Instead of transverse slots, Thiele's antenna uses a metal wall down the centerline of the antenna to block the fundamental mode. Symmetry along this metal wall invites the application of image theory. One entire side of the antenna is now an image of

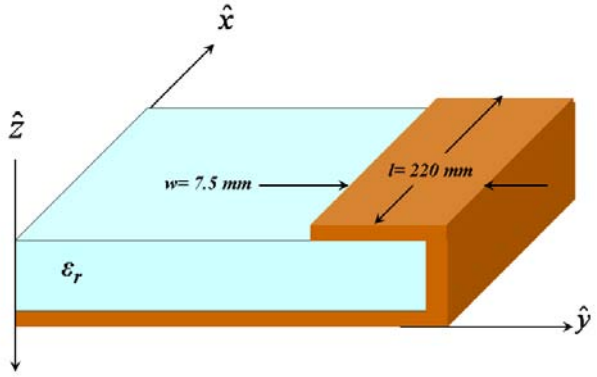

Figure 1.1: Thiele Half Width (THW) antenna.

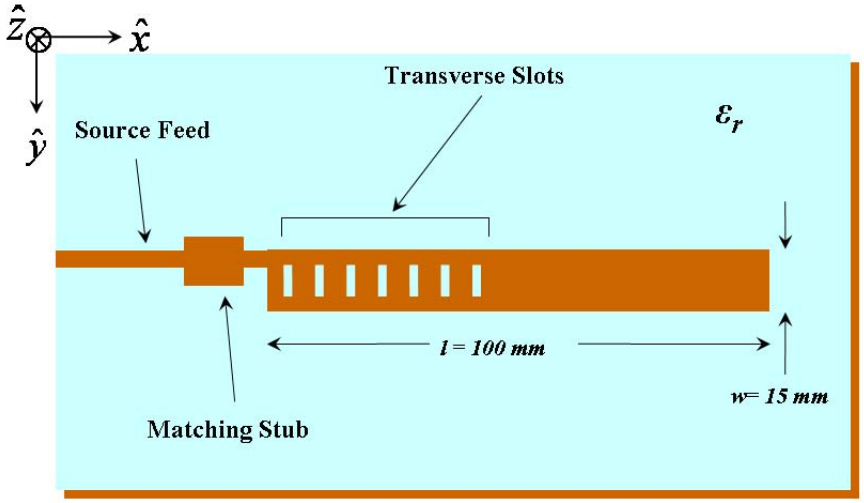

Figure 1.2: Menzel's original antenna [23].

the other side, making it redundant and unneeded. Thiele's resulting antenna is half the width of Menzel's antenna.

This thesis modelled Thiele's antenna with Finite Difference Time Domain (FDTD) techniques. Different geometries, including variations of curvature of the conductor strip, as well as thickness and composition of the substrate, were simulated. Different feeding methods were empirically evaluated.

A possible application of this new antenna could include an inexpensive replacement of the bulky cavity-backed spiral antennas used for the great majority of radar warning receivers.

1.2 Scope

The objective of this research was to characterize the propagation constant of a leaky mode traveling wave antenna. Understanding how the propagation constant is affected by modifying the geometry of the structure is vital to improving the far-field pattern and bandwidth of a traveling wave antenna. The Finite Difference Time Domain (FDTD) method, which is a computational electromagnetic (CEM) technique, was used to simulate different antenna geometries. The propagation constant was extracted from the field distribution resulting from the FDTD simulation. A design was fabricated and tested that incorporated improvements from simulations.

1.3 Resources

Code was written in Matlab starting from a program written by Keely Willis and Dr. Susan Hagness of the University of Wisconsin Computational Electromagnetics Laboratory. Fabrication required computer-aided design (CAD) software, microstrip material, coaxial feed materials, and milling equipment. Measurements required a network analyzer, an antenna test range, and associated supplies.

1.4 Overview

This thesis presents theories related to leaky wave microstrip antennas, methods of modelling such structures with Finite Difference Time Domain (FDTD), and both experimental and simulated results of several antennas based on Thiele's proposed design. Chapter II provides a literature review of work related to leaky wave microstrip antennas. Chapter III is a discussion of the FDTD method. Chapter IV describes development of the FDTD simulation. Chapter V presents results and analysis of tested antenna designs. Finally, Chapter VI states conclusions and suggests recommendations for future research.

II. Background on Microstrip Leaky Traveling Wave Antennas

2.1 Traveling Waves

Much like the waves produced by dropping a stone into a pond, a traveling wave is an electromagnetic disturbance that propagates with a constant phase. Since the wave maintains a constant phase, the wave travels with a constant phase velocity, v_p. Obeying Maxwell's equations dictates that this wave must also satisfy the Helmholtz wave equation. For instance, the source-free vector wave equation of a magnetic field in a lossless medium is:

$$(\nabla^2 + k^2)\mathbf{H} = 0 \tag{2.1}$$

The solution to Equation (2.1) for a complex magnetic field plane wave polarized in the $\hat{y}$ direction and traveling in the $+\hat{x}$ direction is:

$$\mathbf{H} = \hat{y} H_y e^{j(\omega t - kx)} \tag{2.2}$$

ω is the angular frequency of the excitation source. The propagation constant, k, is composed of a real portion, β, which is called the phase constant, and an imaginary component, α, called the attenuation constant:

$$k = \beta - j\alpha \tag{2.3}$$

The phase velocity is given by:

$$v_p = \frac{\omega}{\beta} = \frac{1}{\sqrt{\varepsilon\mu}} \tag{2.4}$$

where ε and μ are the constitutive parameters of the material in which the wave is propagating.

2.2 Traveling Wave Antennas

Most antennas operate in a resonance configuration by supporting standing waves of the currents, voltages, and fields along their length, which is analogous to the vibrations of a violin string. Standing waves can be described as a superposition of two traveling waves propagating in opposite directions. Dipoles and microstrip patches are common examples of antennas in which two waves of equal amplitude that are 180^o out of phase travel in opposite directions along their length. The current distribution is a standing wave with nulls at the ends, while the voltage distribution is a standing wave with maxima at the ends. The standing waves result when energy is excited at one end, travels the length of the antenna, reflects off of the opposite end, and returns toward the feed. A result of standing waves is limited bandwidth due to the destructive interference of the waves [41].

A solution to this problem is an antenna that uses a single traveling wave. The standing wave is prohibited by eliminating the wave in the return direction, which can be accomplished by placing an impedance at the far end to dissipate any remaining energy. Alternatively, the antenna can be made long enough so as to radiate nearly all of the energy before the forward wave from the feed reaches the opposite end, however, this requires the antenna to become unreasonably long. A general rule is to design the length, L, to radiate 90% of the applied power, P, and dissipate the remaining 10% with a load, as in Equation (2.5):

$$\frac{P(L)}{P(0)} = e^{-2\alpha L} = 0.1 \tag{2.5}$$

Equation (2.5) directly leads to Equation (2.6), which relates normalized α to normalized length.

$$\frac{L}{\lambda_0} \approx \frac{-0.183}{\frac{\alpha}{k_0}} \tag{2.6}$$

λ_0 is the excitation wavelength in free space and k_0 is the wavenumber in free space.

The simplest example of a traveling wave antenna is a long wire supported a distance, h, above the ground, also known as a Beverage antenna. Figure 2.1 shows a Beverage

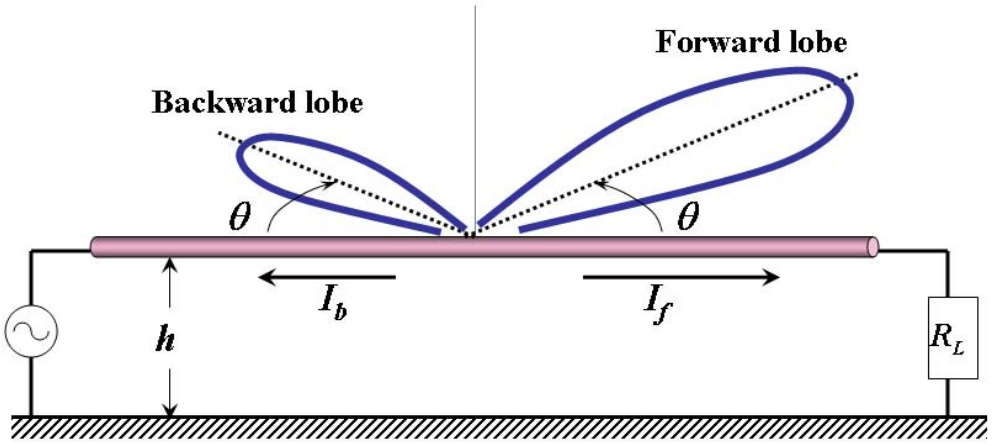

Figure 2.1: A long wire antenna, or Beverage antenna, illustrating the effects of a reflected traveling wave [4].

antenna excited by a forward current, I_f. Without a matched resistor, R_L, a backward current, I_b, is created by the reflection of I_f at the far end. A forward lobe is produced by I_f and a backward lobe is produced by I_b. In Figure 2.1, when the impedance of R_L is matched to the end of the wire antenna, I_b is eliminated, which removes the backward lobe associated with the returning traveling wave. Since an antenna that is designed to operate with a traveling wave will have uniform patterns of current and voltage, it behaves like a resistive circuit component. Matching the feed line to the antenna is simple since the antenna has a purely real input impedance.

2.3 Antenna Characteristics

The current can be approximated as a finite line source that radiates as an outward propagating spherical wave. The spherical wave can be approximated as a plane wave in the far-field. Equation (2.7) determines the far-field source (or observation) point distance, r, at which the phase varies by no more than $\frac{\lambda_0}{16}$ over half of the length, L, as depicted in Figure 2.2.

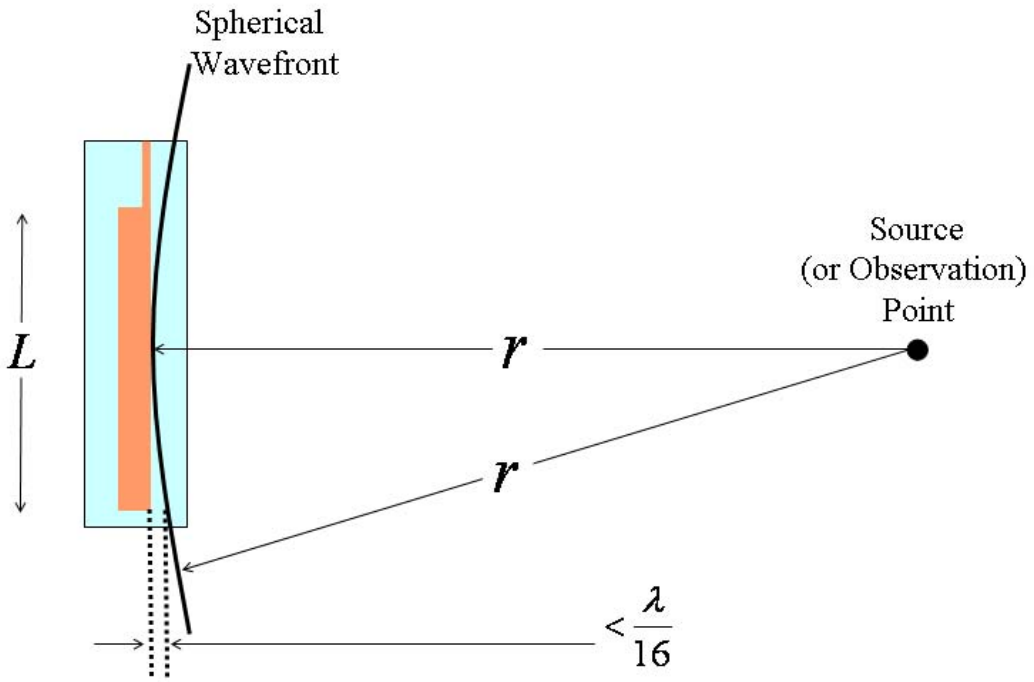

Figure 2.2: The far-field begins at distance r from the antenna at which the spherical wavefront varies by less than $\frac{\lambda_0}{16}$ over half of the antenna's longest dimension.

$$\begin{aligned} \left(r + \frac{\lambda_0}{16}\right)^2 &> r^2 + \left(\frac{L}{2}\right)^2 \\ \frac{r\lambda_0}{8} + \frac{\lambda_0^2}{256} &> \frac{L^2}{4} \\ r &> \frac{2L^2}{\lambda_0} \end{aligned} \tag{2.7}$$

The current distribution along the length of the traveling wave antenna is:

$$I = I_0 e^{-jkz} \tag{2.8}$$

The vector potential, $\mathbf{A}$(x,y,z), of an antenna with I is then:

$$\mathbf{A}(x,y,z) = \hat{z}A_z = \hat{z}\frac{\mu}{4\pi}\int_0^L \frac{I(z')e^{-jk_0 r'}}{r'}dz' \tag{2.9}$$

After making the far-field approximation, $A_r = 0$, the spherical coordinate equivalent vector potential is:

$$\mathbf{A}(r,\theta,\phi) = \hat{\theta}A_\theta = -\hat{\theta}A_z \sin\theta = -\hat{\theta}\frac{\mu I_0 e^{-jk_0 r}\sin\theta}{4\pi r}\int_0^L e^{j(k_0\cos\theta - k)z'}dz' \tag{2.10}$$

The electric field, $\mathbf{E}$, due to $\mathbf{A}$ follows:

$$\mathbf{E} = -j\omega\mathbf{A} = \hat{\theta}\frac{j\omega\mu I_0 e^{-jk_0 r}\sin\theta}{4\pi r}\int_0^L e^{j(k_0\cos\theta - k)z'}dz' \tag{2.11}$$

Solving the integral gives:

$$E_\theta = \frac{j\omega\mu I_0 e^{-jk_0 r}\sin\theta}{4\pi r}\left[\frac{e^{j(k_0\cos\theta - k)L} - 1}{j(k_0\cos\theta - k)}\right] \tag{2.12}$$

which can be separated into an element factor, E_0, and a pattern factor as in Equation (2.13):

$$E_\theta = E_0\frac{\sin\Omega}{\Omega} \tag{2.13}$$

where the element factor is:

$$E_0 = \frac{j\omega\mu I_0 L\sin\theta e^{-jk_0 r}}{4\pi r}e^{j\frac{L}{2}(k_0\cos\theta - k)} \tag{2.14}$$

and the pattern factor argument is:

$$\Omega = \frac{L}{2}(k_0\cos\theta - k) \tag{2.15}$$

The observation point is assumed in the $x - z$ plane, where $\phi = 0$. The pattern factor is a maximum when its argument, Ω, equals zero. This forms the main lobe at θ_m, given by Equation (2.16).

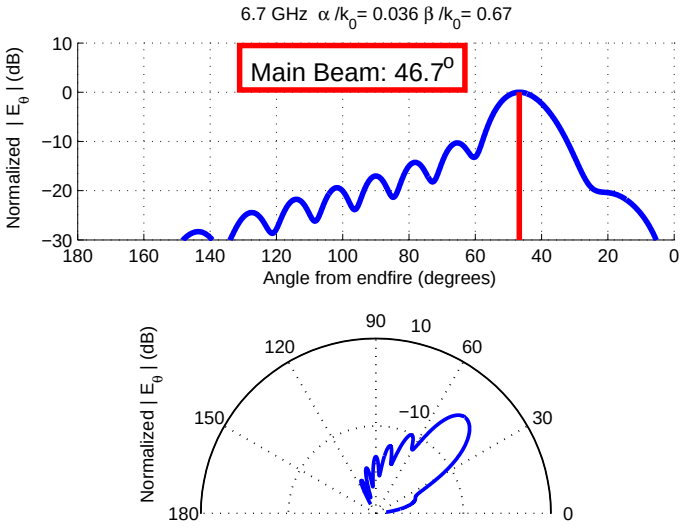

Figure 2.3: The far-field electric field pattern of a traveling wave antenna with aperture three wavelengths long.

$$\begin{aligned} \Omega = 0 &= k_0 \cos\theta_m - k \\ \theta_m &= \cos^{-1}\frac{\beta}{k_0} \end{aligned} \tag{2.16}$$

The magnetic field, $\mathbf{H}$, is found by:

$$\mathbf{H} = \frac{1}{\eta_0}\hat{r} \times \mathbf{E} \tag{2.17}$$

where η_0 is the impedance of free space.

Equations (2.13)-(2.15) produce the pattern seen in Figure 2.3 for the Thiele Half Width (THW) antenna of the dimensions in Figure 1.1, which is roughly three λ_β long. λ_β is the wavelength of the traveling wave. Notice the main beam is not directed at the angle predicted by Equation (2.16) of 44.9^o. The length must be greater than five wavelengths long and $\theta_m > 20^o$ for Equation (2.16) to provide an approximation within 1^o [41]. Figure 2.4 is a pattern of the same antenna lengthened to approximately 5 λ_β long.

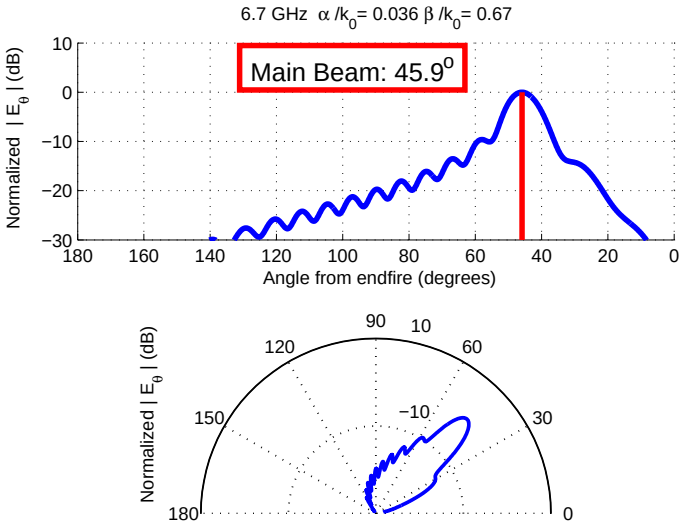

Figure 2.4: The far-field electric field pattern of the same antenna in Figure 2.3 with aperture increased to five wavelengths long.

The far-field pattern shown in Figures 2.3 and 2.4 only includes the forward traveling wave. Of course, a finite length antenna will have a finite amount of energy reflecting from the end, returning in the opposite direction, and producing a backward lobe. Figure 2.5 shows the effect of summing four traveling waves, using reflection coefficients of -1 at both ends.

When transmitting, the structure of the antenna is constructed to radiate as much energy as possible into free space for a given applied current. Gain is a typical measure of the efficiency of an antenna to radiate in a desired direction. In Equation (2.18), gain, G, is the dimensionless ratio of the radiation intensity at a given direction, $U(\theta, \phi)$, to the radiation intensity obtained if the input power, P_{in}, were radiated isotropically.

$$G = \frac{4\pi U(\theta, \phi)}{P_{in}} \tag{2.18}$$

There are two basic means of describing bandwidth, which is the range of frequencies of acceptable performance. The bandwidth of broadband antennas is often given by the ratio of the highest frequency, f_H, to the lowest frequency, f_L. For example, an antenna that operates on the band 2 - 20 GHz would have a 10:1 bandwidth. Narrowband antennas

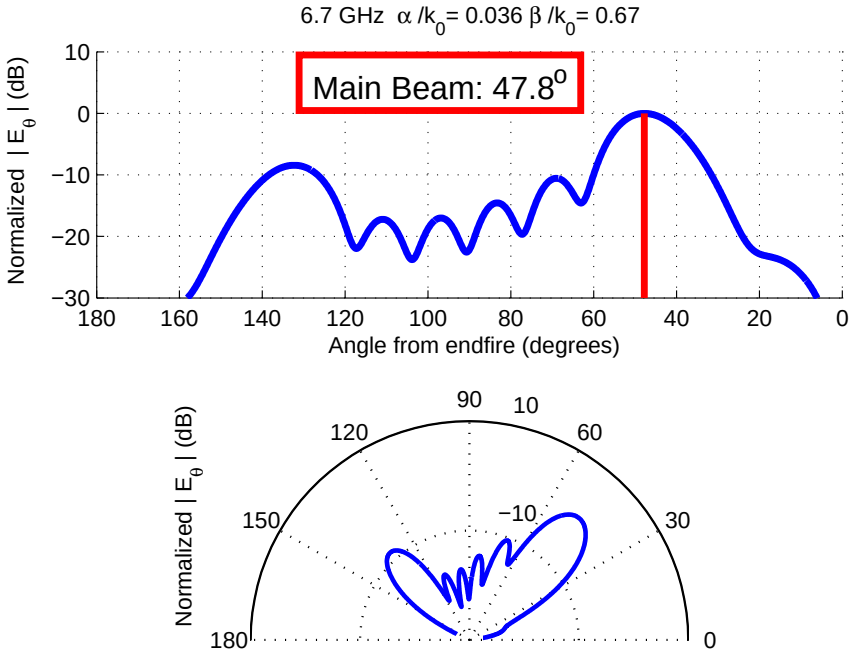

Figure 2.5: The far-field pattern generated by a traveling wave with three reflections at 6.7 GHz.

usually express their bandwidth as a percentage of the center frequency, f_c. An antenna that operates in the band 7 - 9 GHz would have the following bandwidth:

$$Bandwidth = \frac{f_H - f_L}{f_c} = \frac{9-7}{8} = 25\% \tag{2.19}$$

A result of the Lorentz reciprocity theorem, which is derived from Maxwell's equations, is that the gain pattern of an antenna is identical whether it is transmitting or receiving, as long as it is surrounded by a linear, isotropic medium. Simulation of transmission alone is all that is needed to fully characterize an antenna.

2.4 Propagation Modes

A mode is a particular configuration of the fields in a transmission line. A Transverse Electric and Magnetic (TEM) mode is a field distribution at which both the electric, **E**, and magnetic, **H**, field intensities are contained in an equiphase plane that is independent

of time [3]. This can also be described as both **E** and **H** being *transverse* to the direction of propagation. A higher order mode is a mode in which either **E** or **H** has a component in the direction of propagation. For example, a TE_n, or Transverse Electric mode, wave traveling in the $\hat{z}$ direction has a vector component of **H** in the $\hat{z}$ direction while all vector components of **E** are transverse to $\hat{z}$. The n signifies that there are an infinite number of these modes that can be found using Maxwell's equations. Likewise, TM_n signifies the nth higher order Transverse Magnetic mode. While many modes may be possible in a structure, the majority of the energy tends to dominate the lowest mode that can propagate.

In a given transmission line at a given excitation frequency, the modes that can exist are determined by each mode's cutoff frequency. A mode's cutoff frequency depends upon the dimensions of the structure and the medium inside the structure [3]. The modes which have a cutoff frequency equal to or smaller than the excitation frequency are supported and all others will quickly decay.

2.5 Microstrip

2.5.1 Physical Characteristics. Microstrip was first proposed by Deschamps in 1953 at the 3rd Air Force Symposium on Antennas [18], and it remained an academic novelty for nearly 20 years. Advances in materials and manufacturing processes in the 1970's made its production feasible. Microstrip antenna technology has been the most rapidly developing topic in antennas during the last twenty years [32]. Microstrip is an open structure that consists of a very thin metallic strip of a width, w, separated from a ground plate by a dielectric sheet called substrate (Figure 2.6). The thickness of the conductor, t, is much less than a wavelength. The height of the substrate, h, is usually very thin compared to the wavelength ($.0003\lambda \leq h \leq 0.05\lambda$) [31]. The substrate is designed to have a known relative permittivity, ε_r, that is homogeneous within specified temperature limits.

Figure 2.7 illustrates some of the many methods to feed a microstrip antenna. The antenna can be excited directly by a microstrip line, by a coaxial cable, or a combination of the two. The antenna can also be fed from a microstrip line without direct contact through electromagnetic coupling. Feeding by electromagnetic coupling through an aperture in the

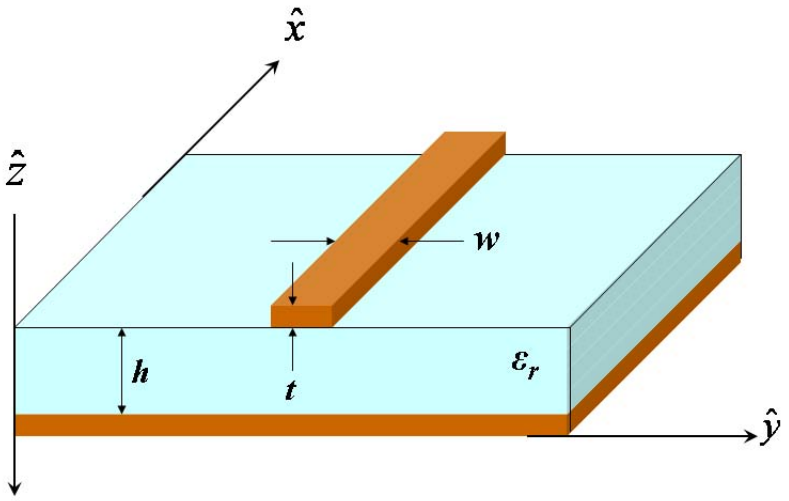

Figure 2.6: Geometry of a microstrip transmission line.

ground plane tends to improve bandwidth. To maximize efficiency, the impedance of the feed must be matched to the input impedance of the antenna. There are a variety of stubs, shunts, and other devices used for matching.

2.5.2 Advantages and Disadvantages. The advantages of microstrip lie in its physical characteristics. Circuits made with microstrip, especially antennas, can be essential to aircraft, spacecraft, satellite, and missile applications. Not only do these circuits have an inherently aerodynamic profile, but they can also be conformable to a surface. Microstrip is lighter and smaller than parabolic dishes and waveguide arrays, and generally cheaper and easier to manufacture and install [4, 18]. Mass production printed circuit and chemical etching technology have led to very low fabrication costs [18].

Compared to other microwave antennas, the major disadvantages of microstrip are lower gain and very narrow bandwidth [18]. Microstrip characteristically has low efficiency and low power handling ability [4,32]. In addition, antennas made with microstrip typically have poor polarization purity and poor scan performance [18].

2.5.3 Hybrid Modes. Operating above the cutoff frequency, the field lines of microstrip extend throughout the substrate as well as into the free space region above the substrate, as seen in Figure 2.8. The phase velocity of the field in the free space surrounding

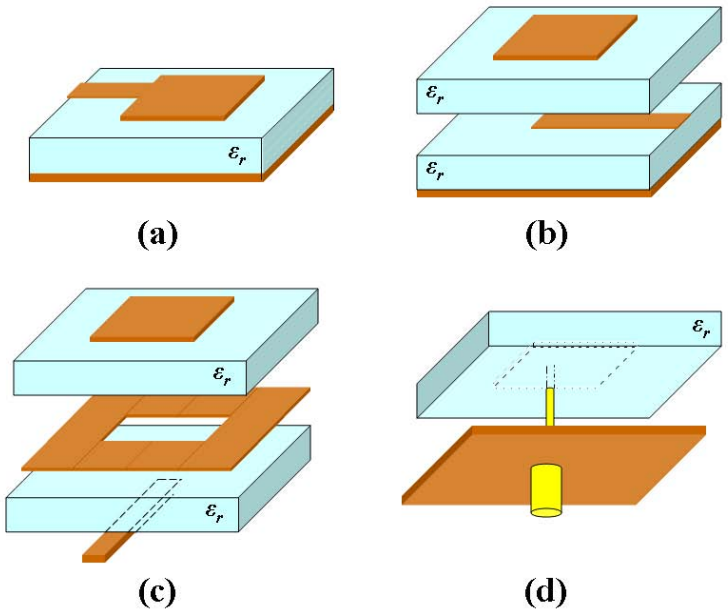

Figure 2.7: Exploded view of microstrip feed techniques for a square patch: (a) Direct. (b) Electromagnetic coupling. (c) Coupling through an aperture in the ground plane. (d) Direct coaxial connection [18].

the structure is the speed of light, c, and the phase velocity of the field in the substrate is given by Equation (2.20).

$$v_p = \frac{c}{\sqrt{\varepsilon_r}} \tag{2.20}$$

This difference in phase velocity at the interface between the substrate and free space makes the TEM mode impossible. Instead, the fundamental mode for microstrip is a quasi-TEM mode, usually annotated, EH_0, in which both the electric and magnetic fields have a component in the direction of propagation. Likewise, a higher order mode in microstrip is not purely TE or TM, but a *hybrid* combination of the two. The nth higher order mode is termed the EH_n mode.

The fundamental mode of microstrip, as seen in Figure 2.8, does not radiate since the fields produced do not decouple from the structure. If the fundamental mode is not allowed to propagate, the next higher order mode will dominate. Figure 2.9 shows the

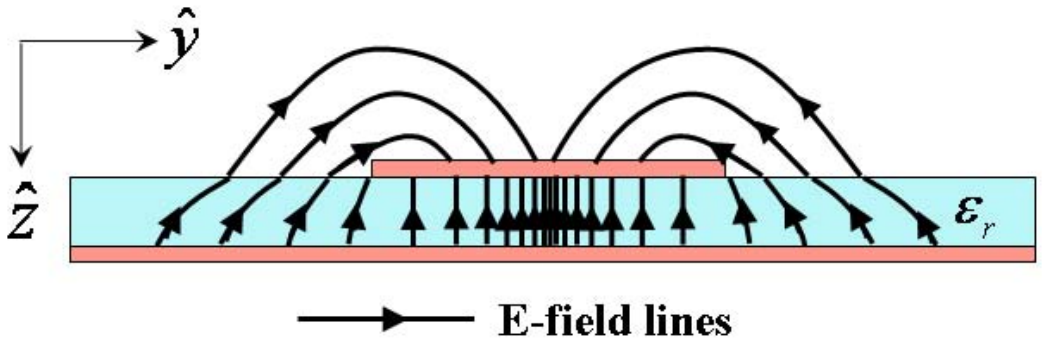

Figure 2.8: Field pattern associated with the fundamental mode of microstrip, EH_0.

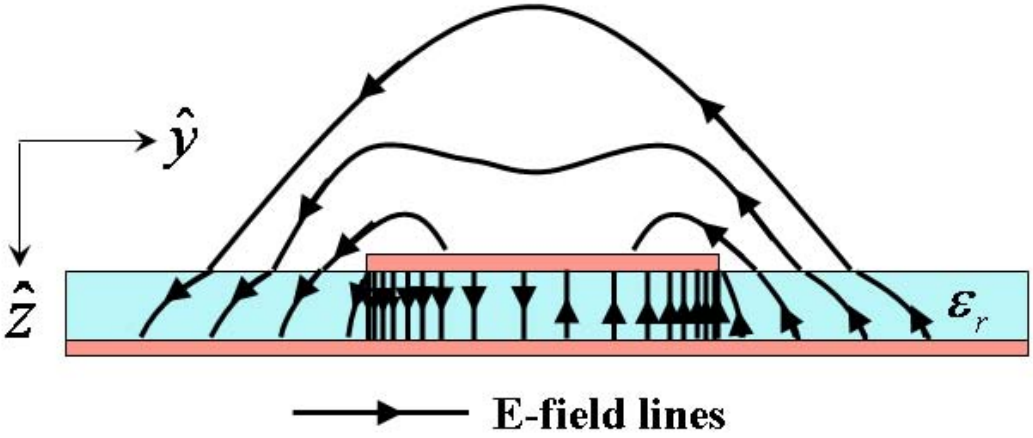

Figure 2.9: Field pattern associated with the first higher order mode of microstrip, EH_1.

fields due to the first higher order mode, EH_1. A phase reversal, or null, appears along the centerline, allowing the fields to decouple and radiate.

2.6 Propagation Mechanisms

Higher order modes on microstrip transmission lines can be described as exhibiting three distinct propagation mechanisms above the cutoff frequency, f_c: bound wave, surface wave, and leaky wave. These mechanisms can be described by analyzing the general dispersion relation of Equation (2.21):

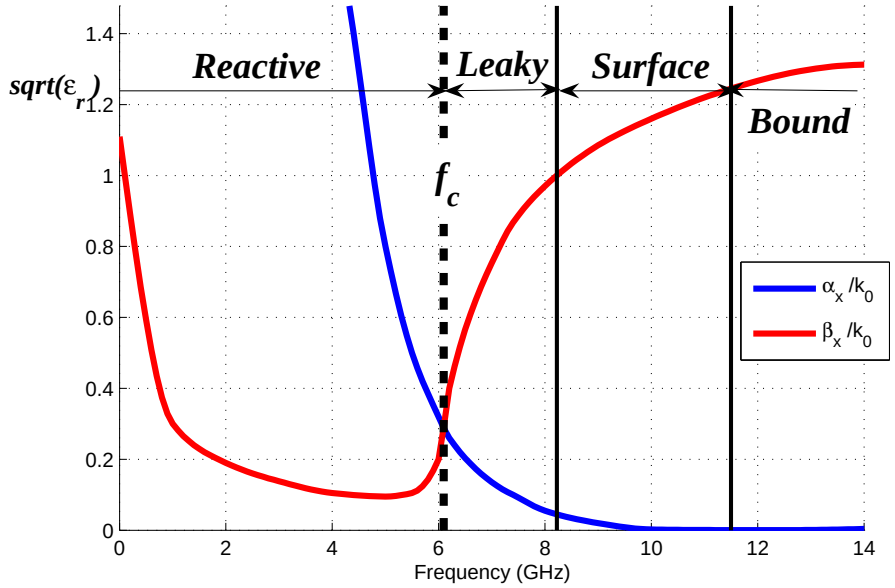

Figure 2.10: The typical normalized attenuation constant, $\frac{\alpha_x}{k_0}$, and phase constant, $\frac{\beta_x}{k_0}$, in the direction of propagation of the first higher order mode, EH_1. There are four frequency regions associated with propagation regimes: Reactive, Leaky, Surface, and Bound.

$$k^2 = k_x^2 + k_y^2 + k_z^2 \tag{2.21}$$

where the complex wavenumbers are composed of a phase constant, β, and an attenuation constant, α:

$$\begin{aligned} k_x &= \beta_x - j\alpha_x \\ k_y &= \beta_y - j\alpha_y \\ k_z &= \beta_z - j\alpha_z \end{aligned} \tag{2.22}$$

Following the orientation of Figure 2.6, k_x is the wavenumber in the direction of propagation. Figure 2.10 is a typical plot of k_x over each of the propagation mechanism regions. Below the cutoff frequency, α_x is quite large causing the transmission line to

function as a reactive load. Unsurprisingly, this region is frequently called the *reactive* region.

As the frequency is raised to f_c, $\beta_x = \alpha_x$ resulting in the commonly used cutoff frequency expression: $k_x^2 = 0$. The dispersion relation at this point is:

$$\begin{aligned} k^2 &= \beta_y^2 + \beta_z^2 \\ &= \omega^2 \varepsilon \mu \end{aligned} \tag{2.23}$$

which can be manipulated to find the cutoff frequency, f_c:

$$f_c = \sqrt{\frac{\beta_y^2 + \beta_z^2}{4\pi^2 \varepsilon \mu}} \tag{2.24}$$

Directly above cutoff is the leaky region where energy begins to propagate down the transmission line as β_x grows larger than α_x. Field losses due to α_x are not ohmic. Although surface waves are present, losses in the leaky wave region are mostly due to the radiation of energy *leaking* from the microstrip [2]. A purely real k_z allows power to radiate, or couple per unit length from the structure into free space [13].

The leaking wave travels away from the antenna at an angle, θ, measured from the endfire direction as seen in Figure 2.11. At the lower limit of the leaky transition region, the beam is nearly broadside. θ decreases as the frequency increases. Simple geometry shows the relation between frequency and θ in Equation (2.25), which is equivalent to Equation (2.16). The main beam approaches endfire as the frequency approaches the leaky region upper limit, at which point $\beta_x = k_0$.

$$\theta = \cos^{-1}\left[\frac{\beta_x}{k_0}\right] = \cos^{-1}\left[\frac{\beta_x c}{\omega}\right] \tag{2.25}$$

For any frequency in the leaky region, there is a curious property whereby the fields due to the leaky wave actually *increase* moving *away* from the structure. The reason for this is simply that less energy leaks per unit length as the wave travels down the

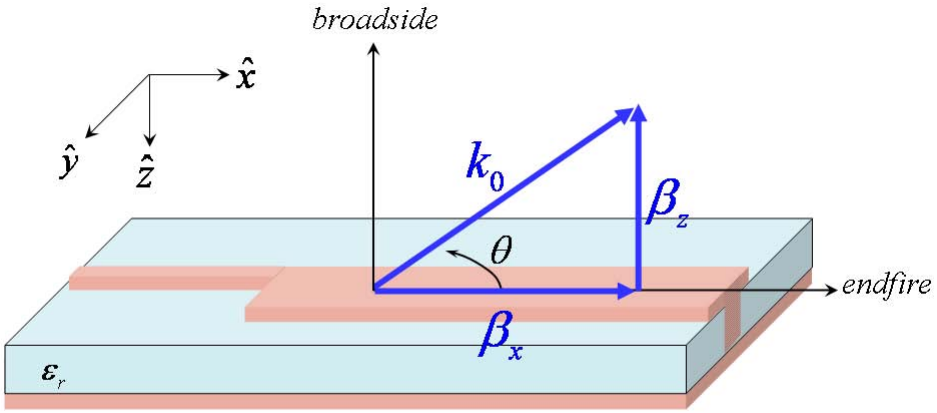

Figure 2.11: The direction of the main beam radiation occurs at an angle created by β_x and k_0.

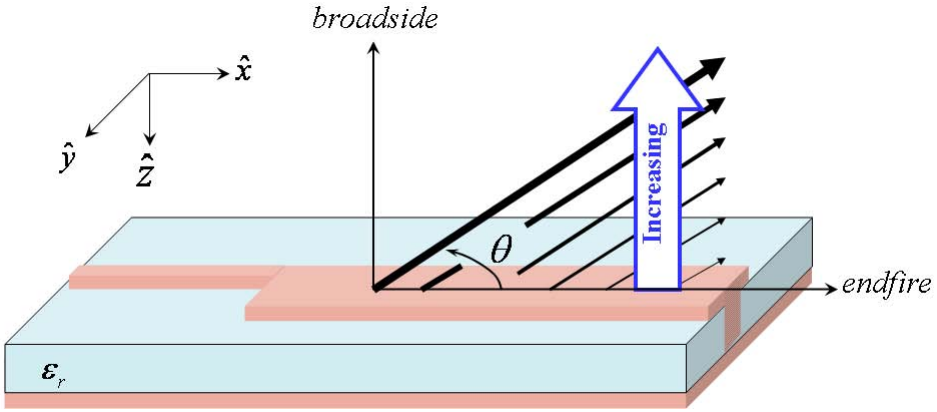

Figure 2.12: The intensity of fields radiating from a leaky wave antenna increase moving away from the structure.

structure. In Figure 2.12, the strength of the leaking field is depicted by the thickness of the line. The fields increase exponentially to a distance above the antenna, z_{max}, given by Equation (2.26), and then quickly decay [29].

$$z_{max}(x) = x \tan\theta \tag{2.26}$$

where x is the distance from the source feed in the $\hat{x}$ direction. Rotating angle θ about the $\hat{x}$ axis of the antenna forms a bowl-shaped main lobe.

Leaky waves are considered *fast waves* since the phase front travels faster than the speed of light. A leaky wave is generally an efficient means to radiate energy, but it is typically narrow-banded since it occurs only for frequencies in a transition region, as seen in Figure 2.10.

Above the frequency at which $\beta_x = k_0$, α_z increases causing the leaky wave to attenuate. The surface wave, however, remains. Surface waves are unbounded losses that are supported by a dielectric layer on a ground plate. The magnitude of a surface wave decays exponentially as it travels away from the transmission line in the $-\hat{z}$ direction since k_z has a large imaginary component, therefore, these waves are associated only with the *surface* of a structure. Surface waves can emanate from discontinuities in the physical structure that disrupt and decouple the bound waves from the surface. Discontinuities can include ends, corners, feeding structures, and also curvature. Generally these surface waves are classified as slow waves since their phase velocity is less than the speed of light. Surface waves are the means by which desired coupling takes place in certain microwave circuits such as coupled line filters, however, more often, they tend to complicate both antenna and circuit design by introducing additional loss and unwanted coupling [6].

Just like leaky waves, surface waves travel outward from the microstrip at an angle, θ. Referring to Figure 2.13, the wavenumber of the surface wave, k_s, has a component in the $\hat{x}$ direction, β_x, and a component in the $\hat{y}$ direction, β_y. The resulting dispersion relation, Equation (2.27), shows that $\beta_x < k_0\sqrt{\varepsilon_r}$ for surface waves to exist:

$$\begin{aligned} \beta_y^2 &= k_s^2 - \beta_x^2 \\ \beta_y &= \sqrt{k_0^2\varepsilon_r - \beta_x^2} \end{aligned} \tag{2.27}$$

Above the frequency at which $\beta_x = k_s$, α_y increases causing the surface wave to attenuate. The field waves are then *bound* to the immediate vicinity of the structure. This regime is typically the state at which most microwave circuits are designed to operate. The operating frequency is generally chosen to be 20% above f_c to ensure leaky and surface wave losses are not present.

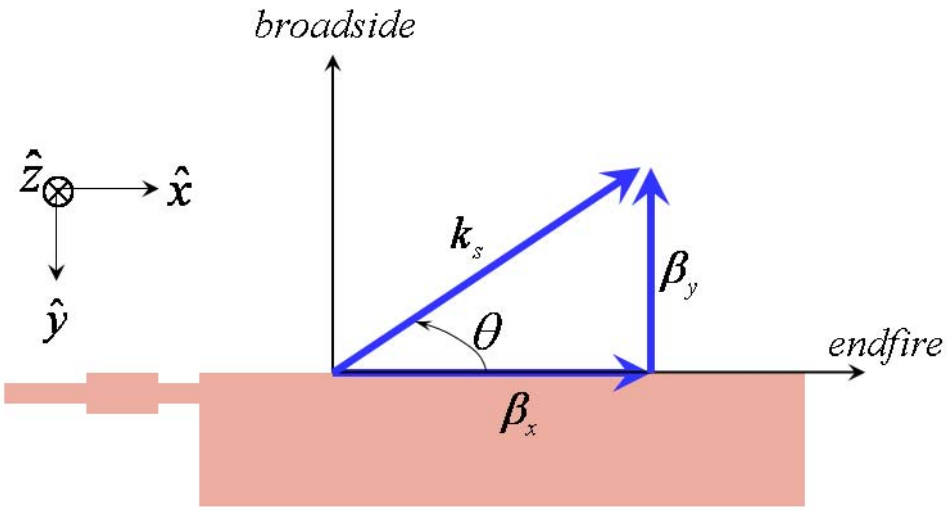

Figure 2.13: The surface wavenumber, k_s, has an $\hat{x}$ component, β_x, and a $\hat{y}$ component, β_y.

2.7 Menzel's Original Antenna

Microstrip structures do not radiate for the fundamental mode, therefore, a higher order mode must be excited. In 1979, Menzel, published the first account of a traveling wave microstrip antenna that used a higher order mode to produce leaky waves [23]. This method of producing radiation by exciting higher order modes in a transmission line has been documented since the 1950's [11]. By the 1970's, rectangular waveguides, circular waveguides, and coaxial cables were in use as leaky traveling wave antennas. However, until Menzel, the jump to microstrip had not been made.

By looking at a cross section of microstrip excited in the fundamental mode, the **E** field is strongest in the center and tapers off to zero at the sides, as depicted in Figure 2.8. If the electric field down the centerline is suppressed, the fundamental mode will be prohibited, forcing the energy to propagate at the next higher mode, EH_1. As seen in Figure 2.9, EH_1 mode causes **E** to be strongest at the edges. Menzel attempted to force the EH_1 mode using several means. Feeding two equal magnitude waves 180^o out of phase with a "T" or "Y" feed produced EH_1 as desired, but did not fully eliminate the EH_0 mode. Metal posts, known as vias, inserted down the centerline eliminated the fundamen-

tal mode and produced the anticipated radiation. A drawback of using vias was difficulty constructing an antenna that was no longer planer. Easier to produce and providing an even better response was given using transverse slots down the centerline (Figure 1.2). The multiple feeds were not necessary to produce the EH_1 mode when the fundamental mode was suppressed.

Menzel demonstrated that the beam angle can be predictively steered by input frequency if the electrical length of the antenna is at least 3λ. If the length is less than 3λ, too little of the incident wave is being radiated and a resonance standing wave pattern is forcing the beam toward broadside.

Qualitative analysis shows that the beamwidth of Menzel's antenna is not frequency dependent, however, it is inversely related to length. The 3 dB beamwidth approaches 10^o for electrical length of over 6λ and approaches nearly 90^o for fractions of a wavelength.

Menzel's gain varied from 7 dB for $l = 0.2\lambda$ to 14 dB for $l = 4\lambda$. 7 dB is comparable to a similar sized resonant antenna. An antenna longer than $l = 4\lambda$ would have an even higher gain as the radiation aperture increases.

2.8 Analysis of Menzel's Work

Lee notes that Menzel assumed that his antenna should radiate simply because the phase constant due to his operating frequency was less than k_0 [20]. If Menzel had considered the complex propagation constant, he would have realized that his antenna was operating in a leaky regime. The length would need to be roughly 220 mm, or more than twice as long as his design, to radiate at 90% efficiency. Radiation patterns in Menzel's paper clearly show the presence of a large backlobe due to the reflected traveling wave.

Ermert, who conducted a mode matching analysis of a similar microstrip structure, did not investigate normalized phase constants below $\beta = k_0$. Ermert specifically refused to include leaky modes citing Marcuvitz, who declared these waves not part of the complete set of eigenmodes [10, 22]. Marcuvitz rejected these modes since their magnitude appears to increase indefinitely away from the antenna and, hence, do not satisfy the radiation conditions at infinity. As mentioned earlier, Figure 2.12 shows that the field strength

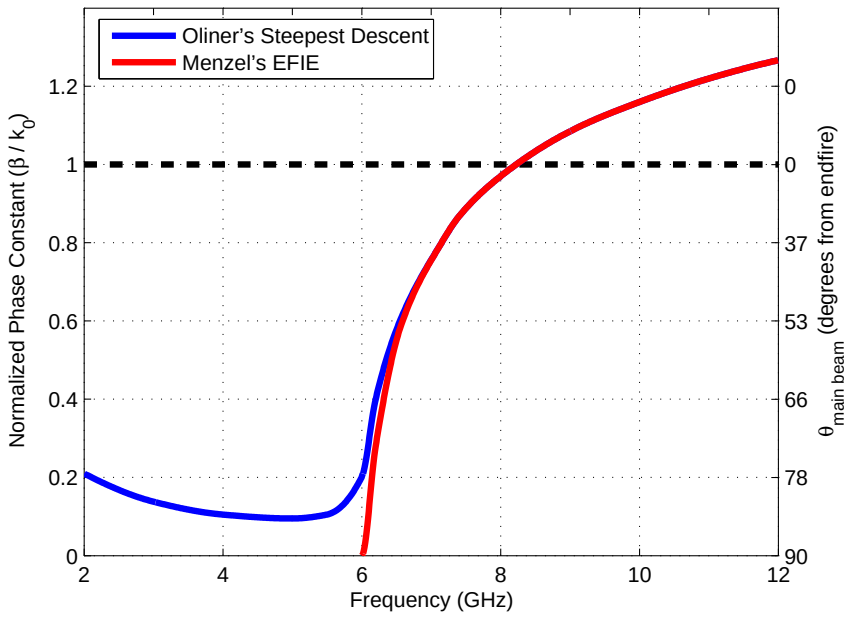

Figure 2.14: Predictions of normalized phase constant for Menzel's antenna [29].

increases exponentially, but it's maximum is at a finite distance given by Equation (2.26). Bagby, Grimm, Nyquist et al showed that while leaky modes *are indeed* nonspectral, a Steepest Descent Contour (SDC) integration can be used to demonstrate that these modes approximate the continuous radiation spectrum [2, 12].

Oliner used a transverse resonance formulation to also show that the leaky region should not be neglected. The normalized phase constant in Figure 2.14 predicted by Menzel's calculations, which ignores the leaky region, is shown atop that predicted by Oliner, which accounts for the leaky regime [23, 29]. Oliner demonstrated the reason for the less than expected bandwidth experienced by Menzel was due to his neglecting of the leaky region. Oliner's Steepest Descent Plane analysis predicts that the useful bandwidth of the higher order modes can be quite substantial.

Michalski and Zheng devised a rigorous Mixed Potential Electric Field Integral Equation (MPEFIE) solution that was applicable to an arbitrary cross section. For Menzel's antenna, Michalski and Zheng's MPEFIE dispersion curves are in agreement with Oliner's [26, 29].

The four analytical methods mentioned, Steepest Descent, Transverse Resonance, Mode Matching, and MPEFIE, all provide much needed insight into the physical nature of the leaky wave phenomenon, however, they all have the very serious drawback that the solution must be reformulated for each geometry. The formulation of these methods is quite complicated and time-intensive.

Sheen et al introduced an S-parameter extraction technique to determine the complex propagation constant through network analyzer measurements. The method has been validated with the spectral domain approach of [2, 12]. Near-field probing measurements conducted by Thiele show promise to directly measure k_x. The problem with any measurement is that the fields must necessarily be disturbed by the testing equipment.

In lieu of analytical methods and measurement methods, this work attempted to develop a numerical simulation of a leaky microstrip antenna that would be easy to modify for new geometries. The Finite Difference Time Domain approach was chosen since the technique directly solves for the fields in the time domain using Maxwell's equations.

III. Finite Difference Time Domain

Finite Difference Time Domain (FDTD) is a computational electromagnetic (CEM) technique that directly solves the differential form of Maxwell's equations,the curl equations, in the time domain using a discretized space-time grid. Compared to an integral equation solution of Maxwell's equations, such as Method of Moments (MoM), FDTD offers the benefits of no linear algebra, well-understood error sources, impulse behavior that is treated naturally, nonlinear behavior that is treated naturally, enhanced visualization of the wave interactions, and a systematic approach that does not require reformulations of integral equations for each new structure.

Yee first proposed using finite differencing for electromagnetic problems in 1966 [43]. Taflove conducted much of the initial research into Yee's method in the 1970's and coined the term FDTD in 1981 [39]. Although there are other methods of gridding the computational space, the grid in this project follows the Yee Cell, as seen in Figure 3.1. The Yee cell uses rectangular coordinates and places each of the components of the magnetic field a half grid space apart from the orthogonally directed electric field components. The same must necessarily be true for the electric field with respect to the magnetic field. Not only are the **E** and **H** fields a half of a cell width apart, but they are also updated a half of a time step apart. The Yee method involves a leap frog approach in which the **E** field is updated, then the **H** field, then **E**, then **H**, and so on. One time step is counted after both **E** and **H** have been updated once.

3.1 Formulation

Yee's Finite Difference scheme uses central differencing that is second order accurate in both space and time. Starting with Maxwell's curl equations:

$$\frac{\partial \mathbf{B}}{\partial t} = -\nabla \times \mathbf{E} - \mathbf{M} \tag{3.1}$$

$$\frac{\partial \mathbf{D}}{\partial t} = \nabla \times \mathbf{H} - \mathbf{J} \tag{3.2}$$

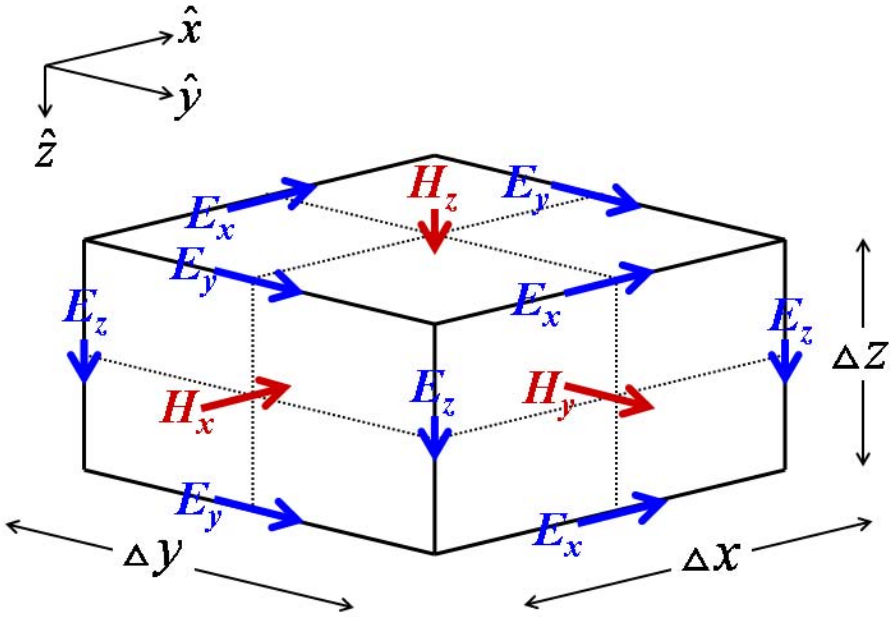

Figure 3.1: The Yee Cell [39, 43].

Noting that:

$$\mathbf{J} = \mathbf{J}_{source} + \sigma \mathbf{E} \tag{3.3}$$

$$\mathbf{M} = \mathbf{M}_{source} + \sigma^* \mathbf{H} \tag{3.4}$$

Equations (3.1) and (3.2) can be manipulated into a more usable form that is applicable for all linear, isotropic, nondispersive, lossy materials:

$$\frac{\partial \mathbf{H}}{\partial t} = -\frac{1}{\mu} \nabla \times \mathbf{E} - \frac{1}{\mu} (\mathbf{M}_{source} + \sigma^* \mathbf{H}) \tag{3.5}$$

$$\frac{\partial \mathbf{E}}{\partial t} = \frac{1}{\varepsilon} \nabla \times \mathbf{H} - \frac{1}{\varepsilon} (\mathbf{J}_{source} + \sigma \mathbf{E}) \tag{3.6}$$

Considering only the source-free case and separating Equations (3.5) and (3.6) into the vector components yields:

$$\frac{\partial H_x}{\partial t} = \frac{1}{\mu}\left[\frac{\partial E_y}{\partial z} - \frac{\partial E_z}{\partial y} - \sigma^* H_x\right] \tag{3.7}$$

$$\frac{\partial H_y}{\partial t} = \frac{1}{\mu}\left[\frac{\partial E_z}{\partial x} - \frac{\partial E_x}{\partial z} - \sigma^* H_y\right] \tag{3.8}$$

$$\frac{\partial H_z}{\partial t} = \frac{1}{\mu}\left[\frac{\partial E_x}{\partial y} - \frac{\partial E_y}{\partial x} - \sigma^* H_z\right] \tag{3.9}$$

$$\frac{\partial E_x}{\partial t} = \frac{1}{\varepsilon}\left[\frac{\partial H_z}{\partial y} - \frac{\partial H_y}{\partial z} - \sigma E_x\right] \tag{3.10}$$

$$\frac{\partial E_y}{\partial t} = \frac{1}{\varepsilon}\left[\frac{\partial H_x}{\partial z} - \frac{\partial H_z}{\partial x} - \sigma E_y\right] \tag{3.11}$$

$$\frac{\partial E_z}{\partial t} = \frac{1}{\varepsilon}\left[\frac{\partial H_y}{\partial x} - \frac{\partial H_x}{\partial y} - \sigma E_z\right] \tag{3.12}$$

The finite difference implementation of Equation (3.7) is as follows:

$$\begin{aligned}\frac{H_x|^{n+1/2}_{i,j+1/2,k+1/2} - H_x|^{n-1/2}_{i,j+1/2,k+1/2}}{\triangle t} &= \frac{1}{\mu_{i,j+1/2,k+1/2}} \\ \cdot\left[\frac{E_y|^n_{i,j+1,k+1/2} - E_y|^n_{i,j,k+1/2}}{\triangle z}\right. &- \frac{E_z|^n_{i,j+1/2,k+1} - E_z|^n_{i,j+1/2,k}}{\triangle y} \\ &\left. - \sigma^*_{i,j+1/2,k+1/2} H_x|^n_{i,j+1/2,k+1/2}\right]\end{aligned} \tag{3.13}$$

The convention used here is to update the **E** fields on integer time steps, $n+1$, and update the **H** fields during half time steps, $n + \frac{1}{2}$. Noting that the **H** field cannot be updated twice in one time step, the last term of Equation (3.13) is approximated as:

$$H_x|^n_{i,j+1/2,k+1/2} = \frac{H_x|^{n+1/2}_{i,j+1/2,k+1/2} + H_x|^{n-1/2}_{i,j+1/2,k+1/2}}{2} \tag{3.14}$$

After incorporating Equation (3.14) into Equation (3.13) and combining terms:

$$H_x|_{i,j+1/2,k+1/2}^{n+1/2} = D_a \cdot H_x|_{i,j+1/2,k+1/2}^{n-1/2} + D_b \cdot \left[\frac{E_y|_{i,j+1,k+1/2}^{n} - E_y|_{i,j,k+1/2}^{n}}{\triangle z} - \frac{E_z|_{i,j+1/2,k+1}^{n} - E_z|_{i,j+1/2,k}^{n}}{\triangle y} \right] \tag{3.15}$$

where the coefficients, D_a and D_b, are composed of the material parameters of the cell being updated:

$$D_a = \frac{2\mu_{i,j,k} - \sigma^*_{i,j,k}\Delta t}{2\mu_{i,j,k} + \sigma^*_{i,j,k}\Delta t} \tag{3.16}$$

$$D_b = \frac{2\Delta t}{2\mu_{i,j,k} + \sigma^*_{i,j,k}\Delta t} \tag{3.17}$$

Analyzing Equation (3.15) in conjunction with Figure 3.1, it is clear that the value of the H_x field component at a particular cell is based on the previous value of that cell's H_x field as well as the adjacent orthogonal **E** fields that were updated one half of a time step ago. A similar corresponding analysis is true of the other five field components. Equations for the other components follow in much the same manner:

$$H_y|_{i-1/2,j+1,k+1/2}^{n+1/2} = D_a \cdot H_y|_{i-1/2,j+1,k+1/2}^{n-1/2} + D_b \cdot \left[\frac{E_x|_{i-1/2,j+1,k+1}^{n} - E_x|_{i-1/2,j+1,k}^{n}}{\triangle z} - \frac{E_z|_{i,j+1,k+1/2}^{n} - E_z|_{i-1,j+1,k+1/2}^{n}}{\triangle x} \right] \tag{3.18}$$

$$H_z|^{n+1/2}_{i-1/2,j+1/2,k+1} = D_a \cdot H_z|^{n-1/2}_{i-1/2,j+1/2,k+1}$$

$$+D_b \cdot \left[\frac{E_y|^n_{i,j+1/2,k+1} - E_y|^n_{i-1,j+1/2,k+1}}{\triangle x} - \frac{E_x|^n_{i-1/2,j+1,k+1} - E_x|^n_{i-1/2,j,k+1}}{\triangle y} \right] \tag{3.19}$$

$$E_x|^{n+1}_{i-1/2,j+1,k+1} = C_a \cdot E_x|^n_{i-1/2,j+1,k+1}$$

$$+C_b \cdot \left[\frac{H_y|^{n+1/2}_{i-1/2,j+1,k+3/2} - H_y|^{n+1/2}_{i-1/2,j+1,k+1/2}}{\triangle z} \right.$$

$$\left. - \frac{H_z|^{n+1/2}_{i-1/2,j+3/2,k+1} - H_z|^{n+1/2}_{i-1/2,j+1/2,k+1}}{\triangle y} \right] \tag{3.20}$$

$$E_y|^{n+1}_{i,j+1/2,k+1} = C_a \cdot E_y|^n_{i,j+1/2,k+1}$$

$$+C_b \cdot \left[\frac{H_z|^{n+1/2}_{i+1/2,j+1/2,k+1} - H_z|^{n+1/2}_{i-1/2,j+1/2,k+1}}{\triangle x} \right.$$

$$\left. - \frac{H_x|^{n+1/2}_{i,j+1/2,k+3/2} - H_x|^{n+1/2}_{i,j+1/2,k+1/2}}{\triangle z} \right] \tag{3.21}$$

$$E_z|^{n+1}_{i,j+1,k+1/2} = C_a \cdot E_z|^{n}_{i,j+1,k+1/2}$$

$$+C_b \cdot \left[\frac{H_x|^{n+1/2}_{i,j+3/2,k+1/2} - H_x|^{n+1/2}_{i,j+1/2,k+1/2}}{\triangle y} \right.$$

$$\left. - \frac{H_y|^{n+1/2}_{i+1/2,j+1,k+1/2} - H_y|^{n+1/2}_{i-1/2,j+1,k+1/2}}{\triangle x} \right] \tag{3.22}$$

where:

$$C_a = \frac{2\varepsilon_{i,j,k} - \sigma_{i,j,k}\Delta t}{2\varepsilon_{i,j,k} + \sigma_{i,j,k}\Delta t} \tag{3.23}$$

$$C_b = \frac{2\Delta t}{2\varepsilon_{i,j,k} + \sigma_{i,j,k}\Delta t} \tag{3.24}$$

3.2 Absorbing Boundary Condition (ABC)

Simulations seek to explore a model in known conditions. For this simulation, as is commonly the case, the antenna was to be simulated in unbounded free space. Since it is clearly not possible to simulate a model in an environment whose extent is infinite in all directions, the antenna was enclosed in an Absorbing Boundary Condition (ABC). An ABC seeks to *absorb* outward propagating waves before they can be reflected inward toward the model.

In the early days of FDTD, ABC's consisted of an expansion of the wave equation, called a radiation operator [5]. Many radiation operators were developed in the 1970's and 1980's. Commonly used, was the Bayliss-Turkel operator, in which a weighted sum of the spatial derivative in the outgoing direction, the spatial derivative in the transverse direction, and the time derivative were taken of neighboring fields [39]. This method

worked based on a diminishing remainder term. In 1981, Mur proposed a finite-difference ABC based on the one-way approximation of the wave equation [5, 27]. This method was used extensively for the next 15 years despite the drawback that Mur's absorbtion was very sensitive to frequency. Schemes for surrounding the computational domain with a lossy medium whose impedance matches that of free space were attempted by several, however, all had the result of no reflection only for plane waves at normal incidence [5]. Plane waves at normal incidence can necessitate a rather large computational domain.

In 1994, Berenger made Mur's ABC all but obsolete when he introduced an alternative called Perfectly Matched Layer (PML) [33]. PML is composed of a layer cells modelling a dissipative material surrounding the FDTD computational domain whose wave impedance is perfectly matched to the space it surrounds. Berenger's hypothetical material was based on a mathematical model of an anisotropic medium in which each component of magnetic field is split into two new components. For example, in the 2-D TE case, Equation (3.25):

$$\mu_0 \frac{\partial H_z}{\partial t} + \sigma_m H_z = \frac{\partial E_x}{\partial y} - \frac{\partial E_y}{\partial x} \tag{3.25}$$

is replaced by Equations (3.26) and (3.27).

$$\mu_0 \frac{\partial H_{zx}}{\partial t} + \sigma_m x H_{zx} = -\frac{\partial E_y}{\partial x} \tag{3.26}$$

$$\mu_0 \frac{\partial H_{zy}}{\partial t} + \sigma_m y H_{zy} = \frac{\partial E_x}{\partial y} \tag{3.27}$$

Berenger demonstrated that the effectiveness of this *split-field* PML was independent of frequency and independent of incidence angles, providing the incidence angle is within 75^o from normal [5]. These results for a 2-D implementation were verified by [1]. Katz also verified Berenger and was the first to extend PML to 3-D [16]. Kantartzis compiled a comprehensive comparison of PML, Mur, higher order Mur, and higher-order radiation operators, and concluded that PML was *absolutely superior* to all other ABC's [14]. Also

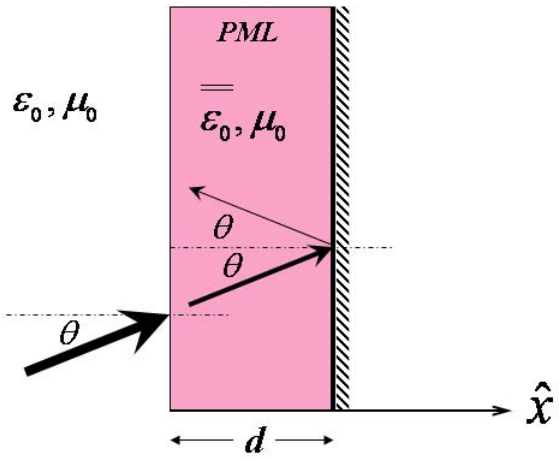

Figure 3.2: UPML covering a PEC wall normal to $\hat{x}$.

in 1994, Chew and Weedon introduced a PML based on complex coordinate stretching variables whose effect is much like Berenger's [8, 33].

Sacks et al developed a diagonally anisotropic layer, later termed Uniaxial PML (UPML) by Taflove, which results in equivalent performance to split-field and stretched coordinate PML's. UPML is easier to implement since it does not involve modifying Maxwell's equations and is able to match anisotropic media. UPML seeks to attenuate the fields by creating an imaginary component of the permittivity in the direction normal to a PEC boundary wall. Figure 3.2 illustrates UPML on a wall that is normal to the $\hat{x}$ direction. Adding an imaginary component to ε_x will attenuate E_x, and in turn, the other five field components. Permittivity in the PML in Figure 3.2 is chosen to be:

$$\varepsilon_{x,\ pml} = \varepsilon_x \cdot \left(1 - j\frac{\sigma_x}{\omega\varepsilon_0}\right) \tag{3.28}$$

The reflection coefficient for a wave entering this UPML of a thickness, d, at an arbitrary incident angle, θ, is given by:

$$\begin{aligned}\Gamma(\theta) &= Re\Big\{e^{-j\ 2k_x d}\Big\} \\ &= Re\Big\{e^{-j\ 2k_0\cos\theta\left(1-j\frac{\sigma_x}{\omega\varepsilon_0}\right)d}\Big\} \\ &= e^{-2\sigma_x\eta_0 d\cos\theta}\end{aligned} \tag{3.29}$$

Reflection is least when the wave impacts at normal incidence and approaches total reflection as incidence approaches grazing angle. Of course, UPML is intended to have zero reflection. This appears to be possible by simply making σ_x very large, however, as σ_x becomes large, the UPML ceases to be matched to the material it is surrounding and creates reflection at the surface. Most PML's, therefore, use a grading scheme to make σ_x small at the material boundary gradually increasing to a larger value at the PEC. The UPML used in this study is polynomial graded, using:

$$\sigma_x(x) = \left(\frac{x}{d}\right)^m \sigma_{x,max} \tag{3.30}$$

where σ_x is zero at the material boundary and rises as an mth degree polynomial to a maximum value of $\sigma_{x,max}$ at the PEC wall. $\sigma_{x,max}$ is not without bound. If the rise of loss is too rapid, discretization error instabilities will dominate any effects of loss. Equation 3.29 can be updated with Equation 3.30 to become:

$$\begin{aligned}\Gamma(\theta) &= e^{-2\ \eta_0\cos\theta\int_0^d \sigma_x(x)\ dx} \\ &= e^{\frac{-2}{m+1}\ \sigma_{x,max}\ \eta_0 d\cos\theta}\end{aligned} \tag{3.31}$$

Taflove [39] states that much empirical evidence indicates that the optimum balance between absorbtion rate and stability occurs when $\sigma_{x,max}$ is given by:

$$\sigma_{x,max} = \frac{0.8(m+1)}{\eta_0\ dx} \tag{3.32}$$

Using Equation (3.32) with Equation (3.31) results in nearly 140 dB reduction at normal incidence for a ten-cell-thick PML:

$$\begin{aligned} \Gamma(0) &= e^{\frac{-2}{m+1}\left(\frac{0.8(m+1)}{\eta_0\ dx}\right)\ \eta_0 d\cos(0)} \\ &= e^{-1.6\frac{d}{dx}} = e^{-16} = -139\ dB \end{aligned} \tag{3.33}$$

The UPML derivations for the faces normal to the other five directions are analogous.

3.3 Materials specification

Each cell is a homogeneous material specified by it's constitutive parameters: permittivity, ε, permeability, μ, electrical conductance, σ, and magnetic conductance, $\sigma*$. These parameters can be complex.

The conductor can be specified using cells with the actual constitutive parameters of the material, however, the conductor can instead be modelled as an infinitesimally thin layer of PEC by simply setting the tangential electric fields to zero at the desired cell boundaries. The boundary condition on the normal magnetic field, $\hat{n} \cdot \mathbf{H} = 0$, is automatically satisfied by the finite difference equations if the tangential electric fields have been zeroed, $\hat{n} \times \mathbf{E} = 0$.

Figure 3.3 illustrates a simulated PEC strip 2 cells in the $\hat{y}$ direction by 3 cells in the $\hat{x}$ direction. Sheen reported that this method can be used to quite accurately represent a number of simple microstrip circuits and antennas [35].

In his dissertation, Sheen later discussed a slightly more accurate method of modelling PEC, shown in Figure 3.4 [36]. The difference equations developed in this chapter relied on a central difference approximation, in which case, PEC is equivalent to forcing the *average* value of $\hat{n} \times \mathbf{E}$ to zero.

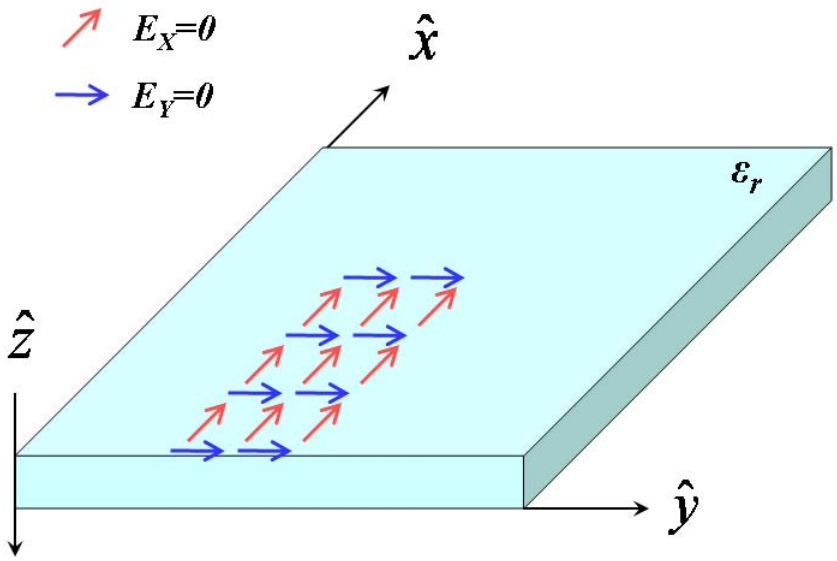

Figure 3.3: PEC can be modelled by setting the appropriate boundary Electric field components to zero [35].

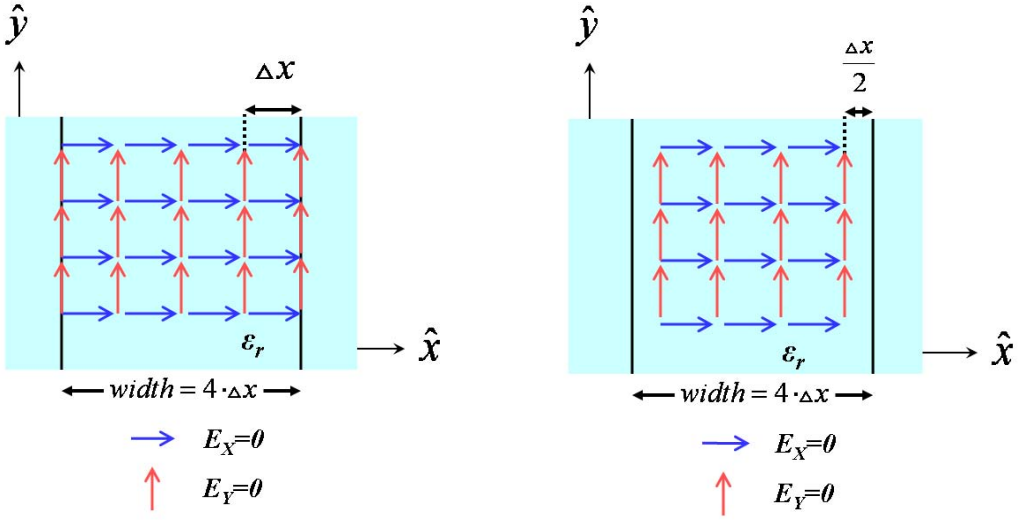

Figure 3.4: (a) PEC borders can be defined as the last tangential **E** components that are zeroed. (b) A more accurate method defines the PEC borders $\frac{1}{2}$ cell beyond the zeroed components.

The difference equations of (3.15), (3.18), (3.19), (3.20),(3.21), and (3.22) show that, in this formulation, the fields are dependent on only the fields in the directly neighboring cells. For a stable solution, a propagating wave, therefore, must not travel more than one cell in any direction during one time step. The maximum time step that will prevent this instability is given by the dispersion relation for a plane wave propagating in a FDTD grid. To derive the finite difference dispersion relation, first reduce the source-free Maxwell's Equations to the wave equations for free space:

$$\nabla^2 \mathbf{E} = \frac{1}{c^2} \frac{\partial^2 \mathbf{E}}{\partial t^2} \tag{3.34}$$

$$\nabla^2 \mathbf{H} = \frac{1}{c^2} \frac{\partial^2 \mathbf{H}}{\partial t^2} \tag{3.35}$$

which can be represented as:

$$\Big(\frac{\partial^2}{\partial x^2} + \frac{\partial^2}{\partial y^2} + \frac{\partial^2}{\partial z^2}\Big)\psi = \frac{1}{c^2} \frac{\partial^2 \psi}{\partial t^2} \tag{3.36}$$

where ψ is any vector component of $\mathbf{E}$ or $\mathbf{H}$. In general, the plane wave solution to Equation (3.36) is of the form:

$$\psi(x, y, z, t) = Re\Big\{e^{j(\omega t - k_x x - k_y y - k_z z)}\Big\} \tag{3.37}$$

where k_x, k_y, and k_z are the wavenumber components in rectangular coordinates. Equation (3.37) can be discretized in space and time as:

$$\psi(n_x, n_y, n_z, n_t) = Re\Big\{e^{j(\omega n_t \triangle_t - k_x n_x \triangle_x - k_y n_y \triangle_y - k_z n_z \triangle_z)}\Big\} \tag{3.38}$$

where n_x, n_y, and n_z are the number of cells in each of the rectangular directions and n_t is the number of time steps, $\triangle_t$. Each cell is uniform and has the dimensions $\Delta_x \times \Delta_y \times \Delta_z$. Defining the central difference operator in the $\hat{x}$ direction, δ_x, as:

$$\delta_x \psi = \frac{\psi(n_x + \frac{1}{2}, n_y, n_z, n_t) - \psi(n_x - \frac{1}{2}, n_y, n_z, n_t)}{\triangle_x} \tag{3.39}$$

and using Equation (3.38) with Equation (3.39) results in:

$$\begin{aligned} \delta_x \psi &= \frac{e^{-j\ k_x \frac{\triangle_x}{2}} - e^{j\ k_x \frac{\triangle_x}{2}}}{\triangle_x} \psi \\ &= \frac{-2j}{\triangle_x} \sin\Big(\frac{k_x \triangle_x}{2}\Big) \psi \end{aligned} \tag{3.40}$$

The second derivative operator is simply the square of the first derivative operator:

$$\delta_x^2 \psi = (\delta_x \psi) \cdot (\delta_x \psi) = \frac{-4}{\triangle_x^2} \sin^2\Big(\frac{k_x \triangle_x}{2}\Big) \psi \tag{3.41}$$

Defining δ_y^2, δ_z^2, and δ_t^2 analogously, the scalar wave equation of Equation (3.36) becomes:

$$\begin{aligned} \Big(\delta_x^2 + \delta_y^2 + \delta_z^2\Big)\psi &= \frac{1}{c^2} \delta_t^2 \psi \\ \frac{\sin^2 \frac{k_x \triangle_x}{2}}{\triangle_x^2} + \frac{\sin^2 \frac{k_y \triangle_y}{2}}{\triangle_y^2} + \frac{\sin^2 \frac{k_z \triangle_z}{2}}{\triangle_z^2} &= \frac{1}{c^2} \frac{\sin^2 \frac{\omega \triangle_t}{2}}{\triangle_t^2} \end{aligned} \tag{3.42}$$

which is the dispersion relation for a plane wave propagating on the FDTD computational grid. Solving for ω, which must be purely real for a stable solution, Equation (3.42) becomes:

$$\omega = \frac{2}{\triangle_t} \sin^{-1}(\xi) \tag{3.43}$$

where

$$\xi = c\triangle_t \sqrt{\frac{\sin^2 \frac{k_x \triangle_x}{2}}{\triangle_x^2} + \frac{\sin^2 \frac{k_y \triangle_y}{2}}{\triangle_y^2} + \frac{\sin^2 \frac{k_z \triangle_z}{2}}{\triangle_z^2}} \tag{3.44}$$

The upper bound of ξ gives rise to the Courant condition for the 3D case of uniform cell size free space [39]:

$$\triangle_t \leq \frac{1}{c\sqrt{\frac{1}{\Delta_x^2} + \frac{1}{\Delta_y^2} + \frac{1}{\Delta_z^2}}} \tag{3.45}$$

If no free space is used in the grid, c should be replaced in Equation (3.45) with v_{max}, which is the maximum propagation velocity through any medium in the grid space.

The Courant condition of Equation 3.45, which is also known as the Courant-Fredericks-Levy (CFL) criteria, only holds for the case of this central-difference formulation. Higher order difference equations may depend on fields of more than one cell's distance, which allows a wave to travel more than one cell per time step in a stable solution. Fewer time steps is a great benefit of higher order FDTD formulations [19].

Instability can present itself in several ways depending on the output product of the simulation. Figure 3.5 shows the effects of an instability that develops while a traveling wave distribution is developing. Due to an unstable condition, the waveform develops small spikes, which are barely visible near cell number 600 of Figure 3.5(a). The instability may or may not originate in the vicinity of cell 600 since the spikes could have travelled many cells before they were visible. The magnitude of the spikes increases as the spikes travel to the right in Figure 3.5(b). Figure 3.5(c) shows the spikes impact the PML near cell 1200 and are partially attenuated. The reduced magnitude spikes reflect and begin traveling to the left, as seen in Figure 3.5(d). The spikes again increase in magnitude (Figure 3.5(e)) until they overtake the waveform (Figure 3.5(f)). A video of the fields shows checkerboard pattern of neighboring highs and lows spreading outward in all directions from the point of instability, as seen in the stills of Figure 3.6. Notice that the checkerboard pattern alternates each timestep.

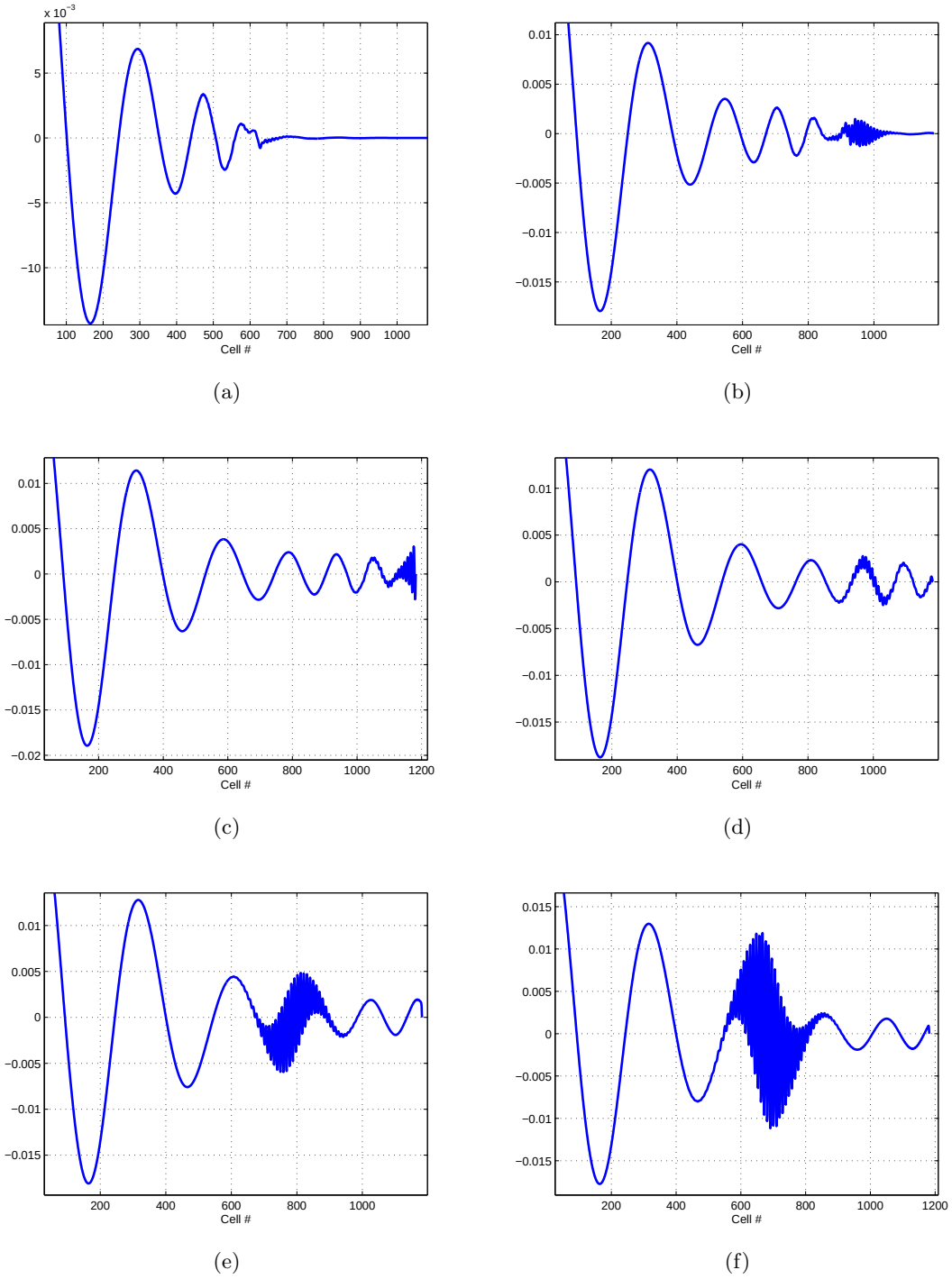

Figure 3.5: (a) An instability causes barely visible spikes near cell number 600. The magnitude of the spikes increases as the spikes travel to the right in (b). (c) shows the spikes impact the PML near cell 1200 and are partially attenuated. The reduced magnitude spikes reflect and begin traveling to the left, as seen in (d). The spikes again increase in magnitude (e) until they overtake the waveform (f).

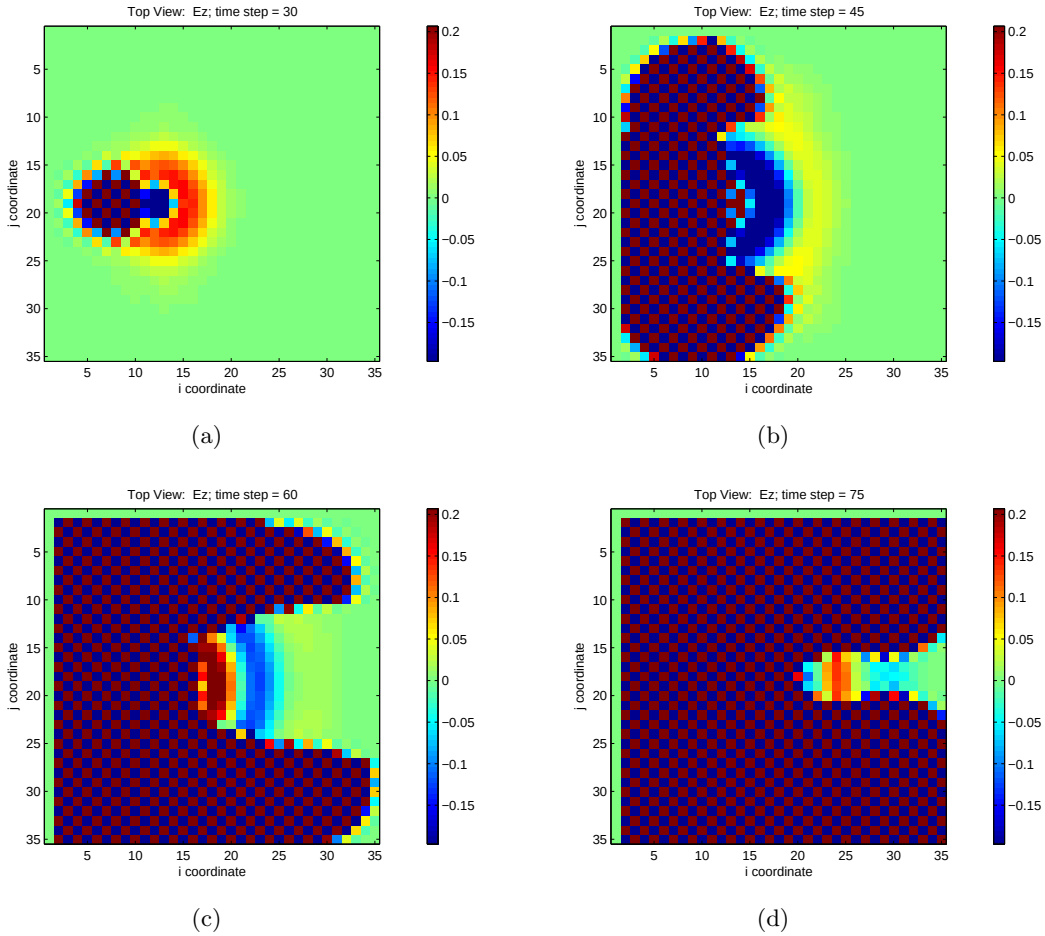

(a) (b)

(c) (d)

Figure 3.6: An instability quickly overtakes the entire computational space.

The first step of applying an FDTD formulation to a structure is gridding the computational space. The cell size chosen has implications for accuracy of the resulting data, time required, and computing resources needed. As with nearly all areas of CEM, larger discretizations bring less computations, but more error.

The most significant error in the case of FDTD is grid dispersion, which is a cumulative phase error. Dispersion is a product of the discretization of space as well as time. Since a wave travels a certain distance specified by Equation (3.45) each time step, a phase front traveling along the direction diagonal to the grid will propagate faster than the same wave traveling along a grid axis. Simplifying Equation (3.42) for a 2-D square grid with a monochromatic traveling wave:

$$\left[\frac{1}{c\triangle_t}\sin\left(\frac{\omega\triangle_t}{2}\right)\right]^2 = \left[\frac{1}{\triangle}\sin\left(\frac{k_x\triangle}{2}\right)\right]^2 + \left[\frac{1}{\triangle}\sin\left(\frac{k_y\triangle}{2}\right)\right]^2 \tag{3.46}$$

where $\triangle$ is the length of a grid cell edge and $\triangle_t$ is the period of a time step. To satisfy the Courant condition of Equation (3.45), let:

$$\frac{\triangle}{c\triangle_t} = 2 \tag{3.47}$$

Using the resolution, N, to equal the number of cells per wavelength, Equation (3.46) can be rewritten as:

$$4\sin^2\left(\frac{\pi}{2N}\right) = \sin^2\left(\frac{\triangle k\cos\theta}{2}\right) + \sin^2\left(\frac{\triangle k\sin\theta}{2}\right) \tag{3.48}$$

Equation (3.48) is a transcendental equation that can be solved for k using Newton's method with the help of trigonometric identities [39]:

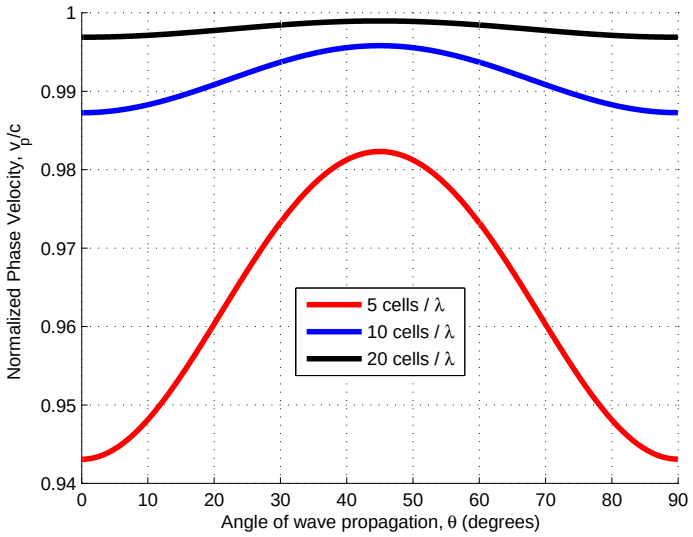

Figure 3.7: The magnitude of phase velocity error, or *dispersion* [39].

$$k_m = k_{m-1} - \frac{\sin^2\left(\frac{k_{m-1}\triangle\cos\theta}{2}\right) + \sin^2\left(\frac{k_{m-1}\triangle\sin\theta}{2}\right) - 4\sin^2\left(\frac{\pi}{2N}\right)}{\frac{\triangle\cos\theta}{2}\sin(k_{m-1}\triangle\cos\theta) + \frac{\triangle\sin\theta}{2}\sin(k_{m-1}\triangle\sin\theta)} \tag{3.49}$$

where m is simply the iteration number. The normalized phase velocity can be found using k_m from the final iteration of Equation (3.49) as:

$$\frac{v_p}{c} = \frac{2\pi}{k_m} \tag{3.50}$$

Figure 3.7 is a plot of $\frac{v_p}{c}$ showing that the amount phase velocity error is proportional to the resolution and the direction of travel. As expected, the phase velocity is fastest in the diagonal direction, 45^o, and is slowest along a grid axis. This anisotropy of phase velocity is reduced as the number of cells per wavelength is increased. Similar to MoM, $\lambda/10$ is a benchmark cell size that works acceptably in many situations. $\lambda/20$ or finer resolution may be needed if the scattering from a complicated structure is desired. Some researchers have found cells as large as $\lambda/4$ acceptable, particularly if the waves modelled have few interactions [39].

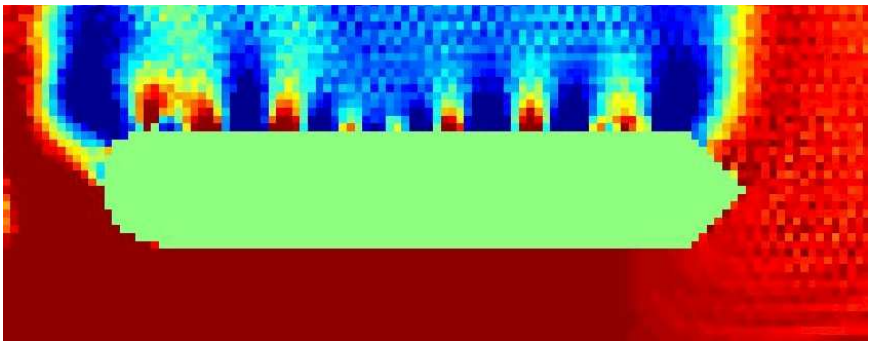

Figure 3.8: Rectangular gridding results in stair-step approximations of curves and diagonal lines.

3.6 Geometric Distortion

It doesn't take long to notice the staircase effect from the use of rectangular cells to simulate a curve, as seen in Figure 3.8. The obvious solution is the use of finer gridding, but this leads to longer run times and more computational resources. Curves are better represented with cylindrical or spherical coordinates, however the difference equations, particularly involving the PML, become cumbersome. Conformal grids have been used to reduce distortion of complex shapes, particularly microstrip with curvature [15, 38]. Subgridding, or finer gridding in only certain regions, has been used by many researchers beginning with Yee [38]. Attention must be paid to the boundaries between unlike cell sizes to properly model the field coupling between fine and course grids. Updating the fields on the boundary can be accomplished using interpolation of both space and time. Kunz developed a method that requires two runs, the first to update the fields in the course grid, the second to update the fields in the fine grid using the coarse-grid fields as a boundary [19]. A common solution to geometric distortion is a hybrid technique employing FDTD and MoM or FDTD and Geometrical Theory of Diffraction (GTD).

3.7 Source

There are two types of sources that can be used: a hard source or a soft source. For a hard source, the field at one or more cells is forced to have a certain value regardless of the neighboring fields. Waves cannot travel through these hard source cells and appear to reflect off in the same manner as if the cell was a perfect electric conductor (PEC). For a

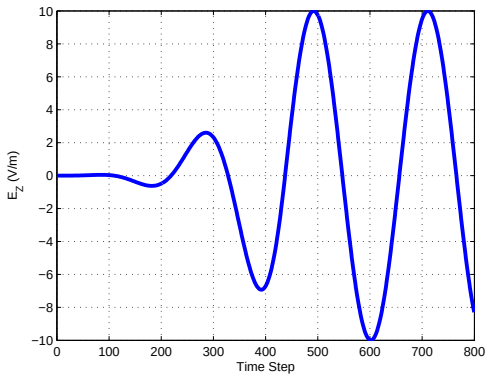

Figure 3.9: Cubic growth over the first few periods eliminates problematic high frequency components of rapid transitions.

soft source, the introduced value is only added to the existing field of the cell or cells. Soft sources are beneficial when you do not have prior knowledge of the fields in the vicinity of the source as these cells allow waves to travel through. Hard sources have the ability of being turned off more easily than soft sources.

The waveform of the source also must be considered. A sharp start or stop transition in the source wave will create *messy* propagating waves. These discontinuities contain many higher frequency components that can disturb the surrounding fields to such an extent that a source may even enter *runaway mode* and fail to turn off. Taflove notes that FDTD has an intrinsic low pass filter effect since computations are only based on neighboring cells [39]. Theoretically, the high frequency components, if left long enough, would eventually disappear. Typically, these discontinuities are eliminated by a gaussian pulse, which is a sinusoidal function attenuated by an exponential, as seen in Equation (3.51).

$$source_{n_t} = \sin(\omega n_t \triangle_t) \cdot e^{(-\zeta^2 n_t^2)} \tag{3.51}$$

where ζ is an attenuation constant that is typically related to the resolution, or number of cells per wavelength. For this study, I chose a constant source, so I was not concerned with a *stop* transition. I decided to use a sinusoidal source with a cubic growth over the first three periods, which is illustrated in Figure 3.9.

IV. Simulation Development

This chapter presents the methodology by which an FDTD simulation was developed to analyze antennas of different geometries.

4.1 Hagness-Willis Code

To save time, I obtained a working 3-D FDTD program with a UPML absorbing layer. The UPML was a 10-cell-thick, 4th order polynomial graded, and PEC-backed on all six faces. This "beta" version Matlab code was provided by Dr. Susan Hagness and one of her Ph.D. students, Keely Willis, both of the University of Wisconsin Computational Electromagnetic Laboratory. The Hagness-Willis code will be featured in the upcoming edition of Taflove and Hagness's book *Computational Electromagnetics: The Finite-Difference Time Domain Method, 3rd Ed.* The program was extensively modified for my purposes and, as a result, I used little more than their UPML implementation.

The first design simulated was the 220 mm long full width Thiele antenna using a solid wall down the centerline, as seen in Figures 4.1 and 4.2. Since the UPML of the Hagness-Willis code was matched to free space, I surrounded the entire antenna with a 20-cell-thick layer of free space. Above the antenna, I included an additional 20 cells, for a total of 40 cells of free space between the top UPML boundary and the top of the antenna. The open substrate was extended outward one antenna-width in both $\hat{y}$ directions. The following paragraphs detail the procedure I used to pare away unnecessary cells revealing only the minimum number of cells required to accurately model the structure.

4.2 Copper

I began modelling the copper as 1-cell-thick layer of $\varepsilon_0,\ \mu_0,\ \sigma = 5.8 \times 10^7$ S/m. Designs were fabricated with Rogers Corporation 5870 RT/Duroid with 1 ounce copper cladding, which is 35μm thick. If the FDTD cells were nearly cubic, the substrate would need to be 22 cells thick and the entire computational space would require nearly 900 million cells. From smaller trials that I have run, I estimate that this would call for upwards of 1 TB of memory for even the lossless case. I abandoned this method and instead approxi-

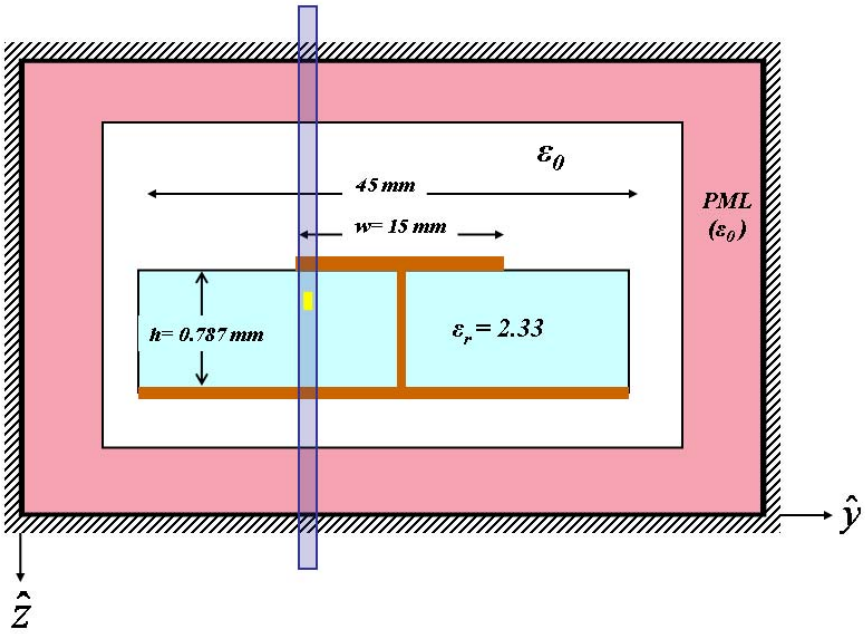

Figure 4.1: The $\hat{y} - \hat{z}$ cross-section slice of the Thiele Full Width (TFW) antenna surrounded by free space (not to scale). The source cell is shown in gold. The $\hat{x} - \hat{z}$ slice of Figure 4.2 is shaded in blue.

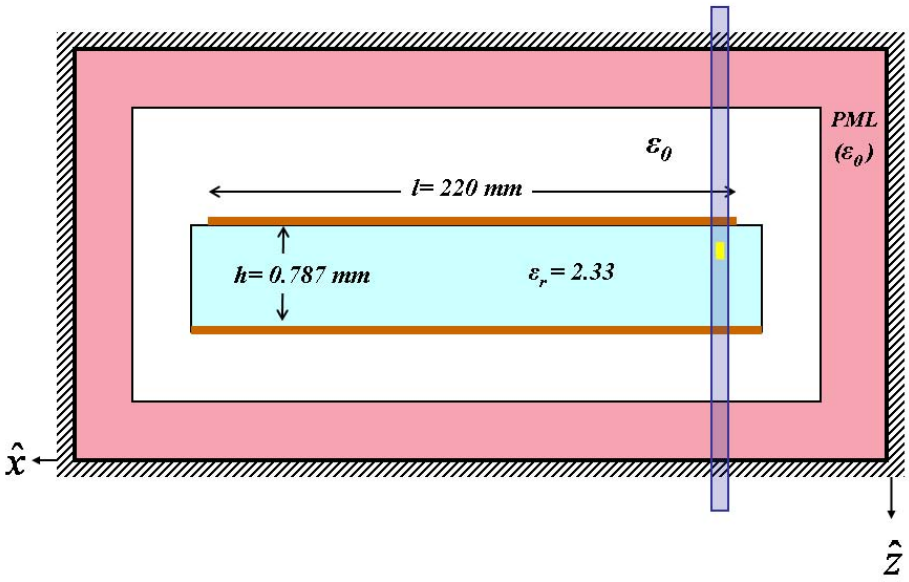

Figure 4.2: The $\hat{x} - \hat{z}$ longitudinal-section slice of the TFW antenna surrounded by free space (not to scale). The source cell is shown in gold. The $\hat{y} - \hat{z}$ slice of Figure 4.1 is shaded in blue.

mated the copper conductor as a perfect electric conductor (PEC) of zero thickness. This approximation allowed for much larger cells, decreasing the total number. For example, by making the substrate only 5 cells thick, the simulation is cut from 900 million cells down to roughly 50 million cells, a 94 % decrease.

4.3 PML

The UPML of the Hagness-Willis code is matched to free space, therefore, my antenna was first surrounded by a layer of free space, which was then surrounded by the UPML cells. To extract the propagation constant of the forward traveling wave, I needed to eliminate reflections from the free space boundaries at the ends of the substrate. This was accomplished by extending the substrate directly into the UPML, and modifying the affected UPML cells to match the substrate. The resulting grid space is seen in Figures 4.3 and 4.4. Notice that the UPML layer under the ground plate has also been removed since it is redundant. The UPML now absorbs all outward propagating waves in the substrate allowing the forward traveling wave to develop exclusively. At this point, the UPML is inhomogeneous in the $\hat{z}$ direction. If the electric flux density, D_z, is discontinuous between the two materials, Gauss's Law states that a surface charge will develop at the boundary. A charge building between two bordering cells is a source of instability for the FDTD method. This problem was averted in the UPML development, since the imaginary component of the UPML permittivity in Equation (3.28) was chosen to be normalized to free space permittivity instead of the material's permittivity. The number of cells to simulate the antenna after the removal of the surrounding free space was reduced over 71% to 14.2 million cells, which was still much too large.

4.4 Material Surrounding the Antenna

Since the PML absorbs nearly all of the outward propagating energy, the amount of free space above and the amount of open substrate extending outward from the structure has no effect on k_x as long as the PML 1s at least two cells away from the structure. The resulting grid space with only the required number of cells, a further reduction of almost 80 %, is seen in Figures 4.5 and 4.6.

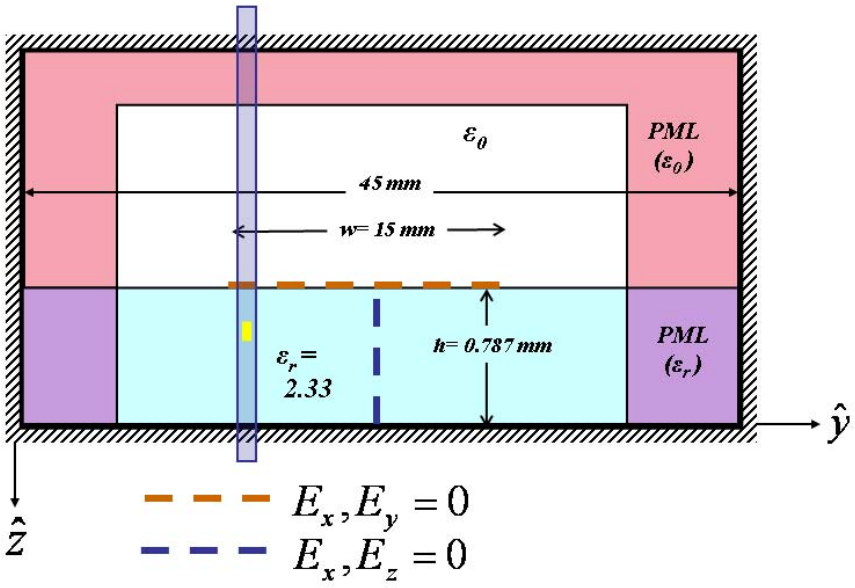

Figure 4.3: The cross-section of the TFW antenna extending into the UPML (not to scale). The source cell is shown in gold. The $\hat{x} - \hat{z}$ slice of Figure 4.4 is shaded in blue.

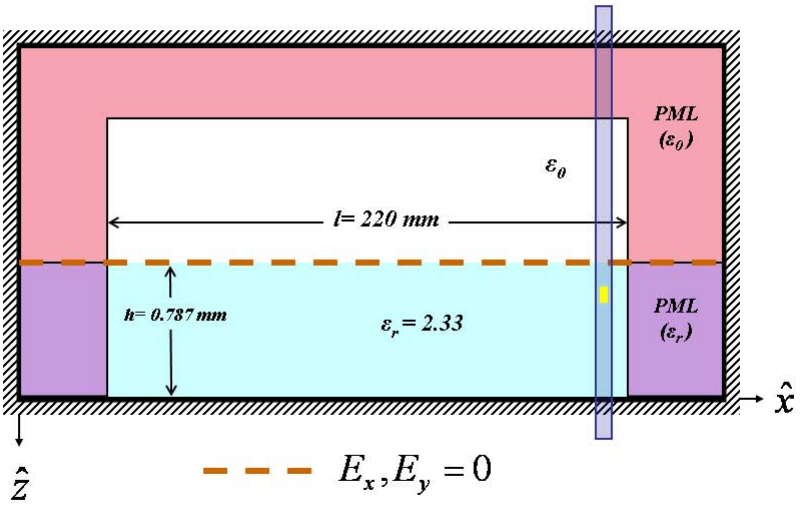

Figure 4.4: The longitudinal-section of the TFW antenna extending into the UPML (not to scale). The source cells are shown in gold. The $\hat{y} - \hat{z}$ slice of Figure 4.3 is shaded in blue.

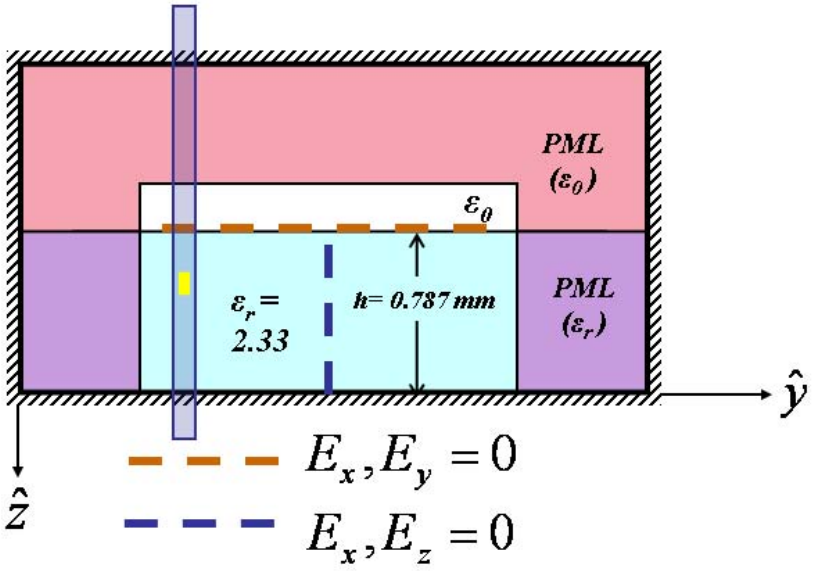

Figure 4.5: The $\hat{y} - \hat{z}$ slice of the TFW antenna extending into the UPML with unneeded material removed (not to scale). The source cells are shown in gold. The $\hat{x} - \hat{z}$ slice of Figure 4.6 is shaded in blue.

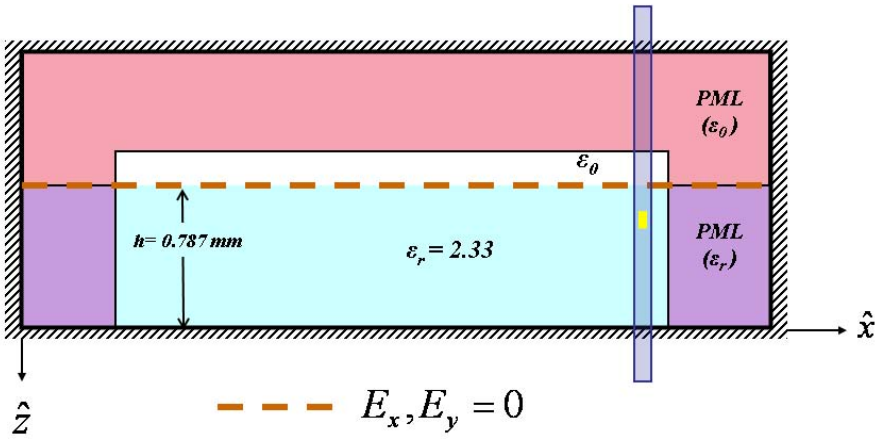

Figure 4.6: The $\hat{x} - \hat{z}$ slice of the TFW antenna extending into the UPML with unneeded material removed (not to scale). The source cells are shown in gold. The $\hat{y} - \hat{z}$ slice of Figure 4.5 is shaded in blue.

4.5 Resolution and Cell Size

I ran several trials to determine if the cell size could be changed. By keeping the cross section square and elongating the cells in the $\hat{x}$ direction, Figure 4.7(a) shows that at the leaky band's center frequency, 7 GHz, there is less than 1% error of β_x if the cell size is 6:1:1 or less. The error is with respect to the transverse resonance solution. Figure 4.7(b) is a plot of the error due to varying cell sizes while keeping the cells square in the $\hat{x}$ and $\hat{y}$ directions. Cell size must be 1.5:1.5:1 or less to stay within 0.5% of transverse resonance. Figure 4.7(c) shows that keeping the height of the substrate to at least 5 cells ensures agreement with transverse resonance to within 0.5%. Using a cell size of 5:1:1 with a five-cell-thick substrate, the grid of Figures 4.5 and 4.6 is only 572,000 cells.

The worst resolution will occur at areas with the shortest wavelength and largest cells. All subsequent trials used five-cell-thick substrate and sizes of either 3:1:1 or 5:1:1. Since the only substrate thickness used was 787 μm, the cells were 472.2 $\times$ 157.4 $\times$ 157.4 μm or 787 $\times$ 157.4 $\times$ 157.4 μm, respectively. The shortest wavelength encountered in the simulation was in the substrate outside of the antenna, given by:

$$\lambda_{substrate} = \frac{\lambda_0}{\sqrt{\varepsilon_r}} \tag{4.1}$$

Therefore, the worst resolution is given by Figure 4.8 for the largest dimension of each of the two cell sizes. The resolution of the traveling wave inside the structure was in the *hundreds* of cells per wavelength.

4.6 Source

Many source geometries and locations were tried to find the optimum. At least one source cell must be more than two cells from the PML or too much energy will be absorbed for the traveling wave to adequately develop. A source cell centered vertically in the substrate allows a traveling wave of the largest magnitude to develop. A source cell directly on the antenna's open edge prevents establishment of the traveling wave by allowing the source energy to propagate away from the antenna and not in the structure. Following these findings, all contiguous geometries consisting of single cells, rows of cells

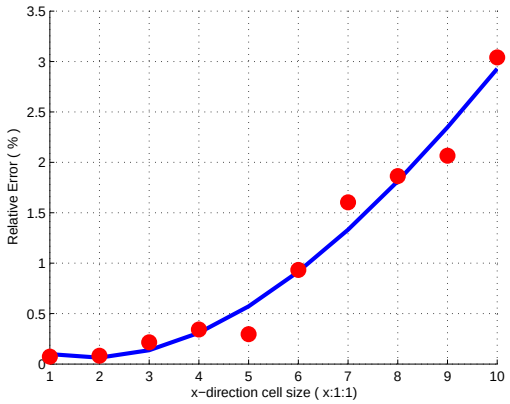

(a)

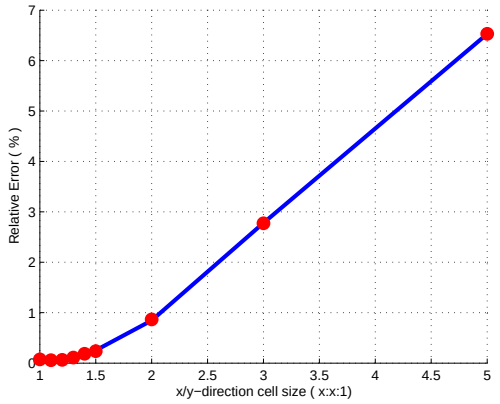

(b)

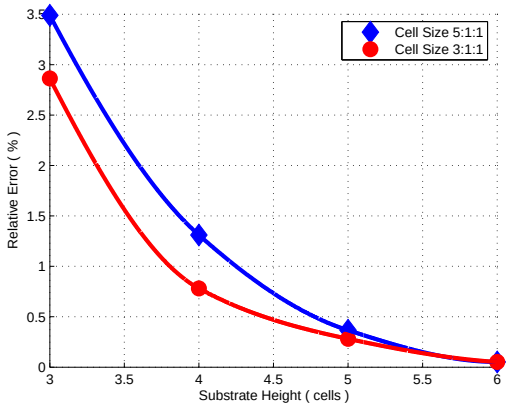

(c)

Figure 4.7: (a) Plot of the error of β_x as a function of elongating the $\hat{x}$ direction of the cells while keeping the other dimensions square. (b) Plot of the error of β_x as a function of cell size for cells square in the $\hat{x}$ and $\hat{y}$ directions. (c) Plot of the error of β_x as a function of the height of the substrate in cells. For all figures, the error is with respect to the transverse resonance solution and the curve is a cubic least-squares fit of the data points.

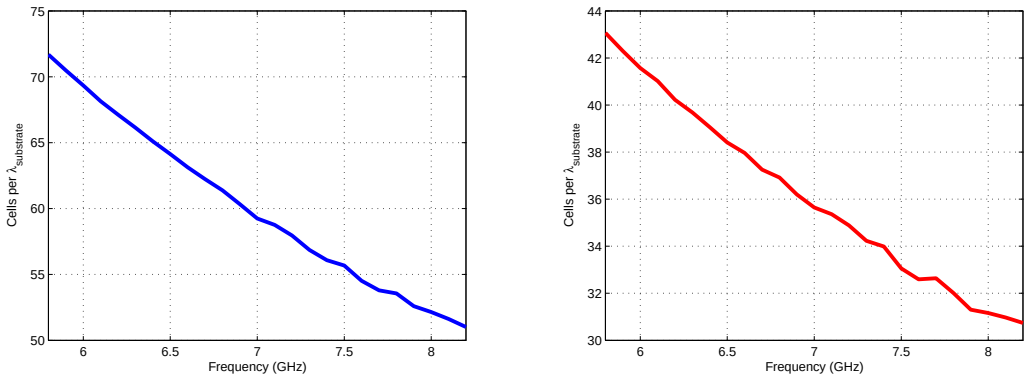

(a) (b)

Figure 4.8: The worst resolution encountered in Thiele antenna simulations with 5-cell-thick substrate for cell sizes of (a) 3:1:1 and (b) 5:1:1.

in each of the three rectangular directions, and walls of cells normal to each of the three directions, performed identically. All subsequent trials used a single source cell midway between the ground plate and the conductor strip, two cells inside from the open edge of the antenna and five cells from the PML.

4.7 Loss

Simulating substrate with loss requires nearly twice the computer RAM compared to the lossless case since each field component of each cell must have a real and imaginary portion. Rogers Duroid 5870 high frequency laminate has a loss tangent of only 0.0012. Neglecting this loss showed no noticeable effect on the extracted propagation constant, as can be seen in Figure 4.9. All subsequent trials were treated as lossless freeing 50% of the memory allowing a larger simulation.

4.8 Precision

Matlab defaults to double precision unless specified otherwise. Trials run in single precision used roughly 40% less memory and the results were consistent with double precision, as seen in Figure 4.10. All subsequent trials remained double precision unless the size of the simulation required more memory than was available.

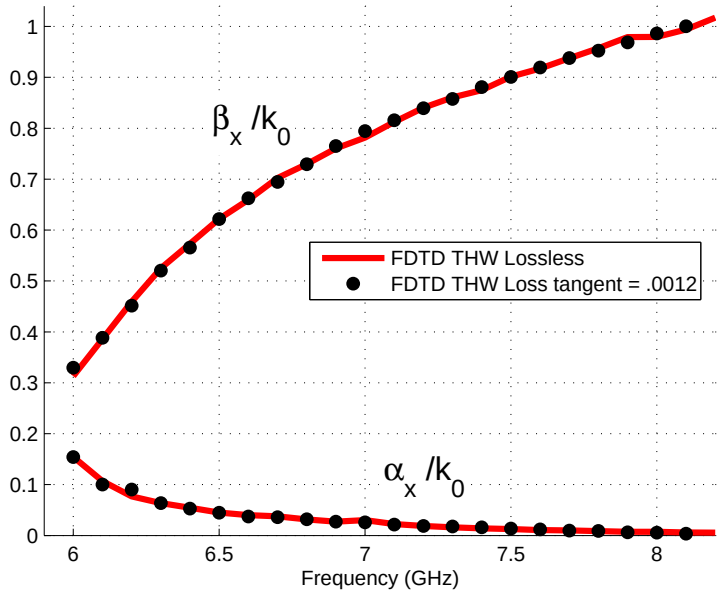

Figure 4.9: No noticeable error of the extracted propagation constant due to neglecting loss for the Thiele Half Width (THW) antenna.

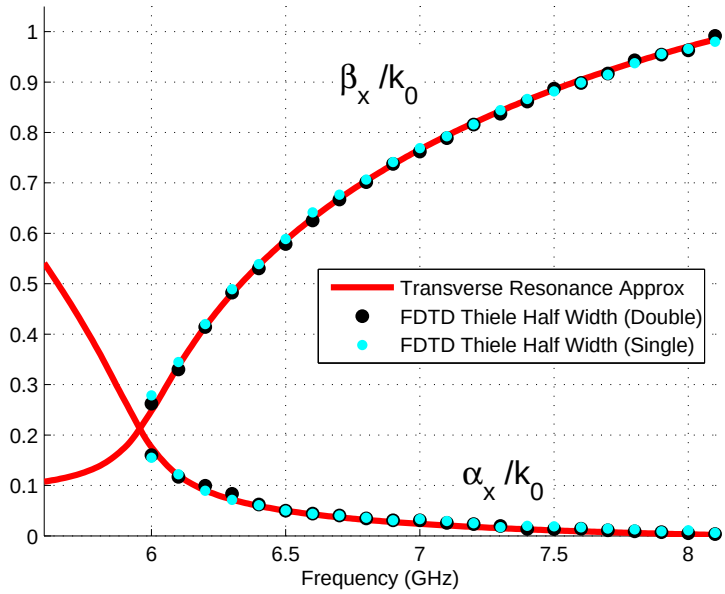

Figure 4.10: Propagation constant extracted from the fields following a single precision simulation does not differ significantly from the double precision results.

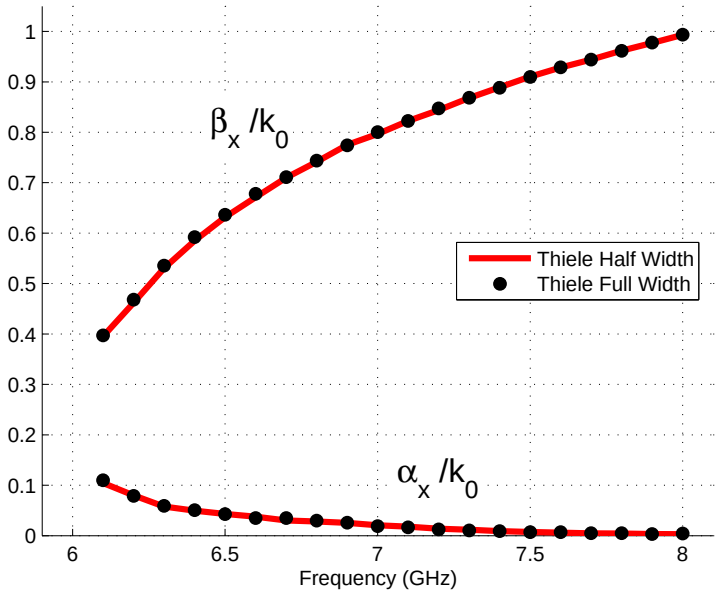

Figure 4.11: The propagation constant data extracted from the THW antenna is indistinguishable from the TFW antenna.

4.9 Full Width vs. Half Width

Figure 4.11 illustrates the agreement between the propagation constants of the Thiele Half Width (THW) and Thiele Full Width antennas (TFW) to within 1% over the entire leaky band. Simulation of the THW antenna uses approximately 45% less memory than the TFW simulation.

4.10 Determination of Leakage Constant and Phase Constant

The objective of the antenna simulations was limited to providing the propagation constant of the vertical component of the electric field, E_z, inside the substrate between the top conductor and the bottom ground plate. The E_z data was retrieved from a single row of cells stretching the length of the antenna, as depicted in green in Figure 4.12. As discussed in Chapter 2, the attenuation constant, α_x, and the phase constant, β_x, components of the propagation constant give an accurate means of comparing the bandwidth, leakage rate, main beam direction, and approximate far-field pattern of different traveling wave antennas.

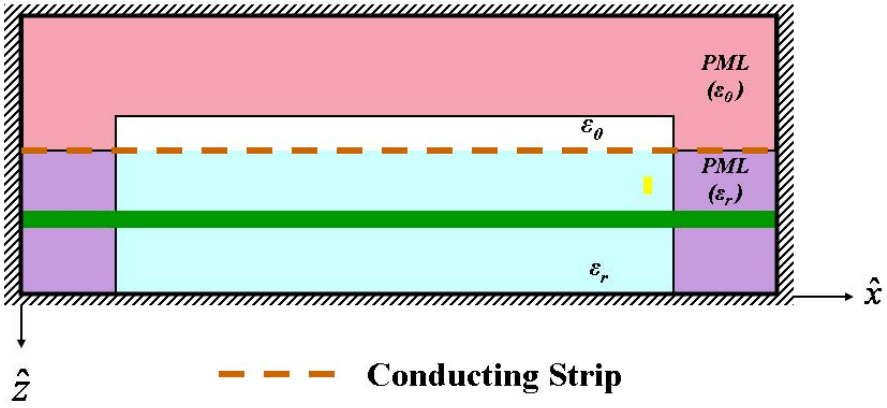

(a)

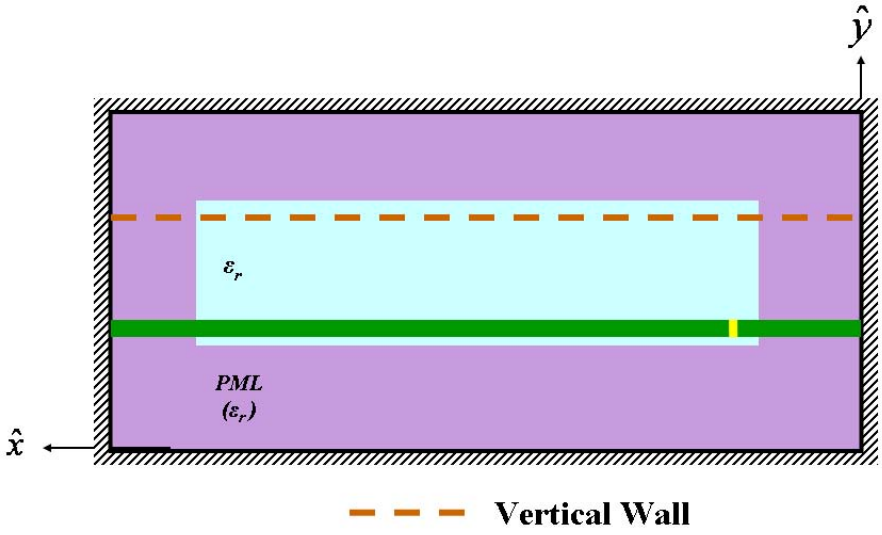

(b)

Figure 4.12: 4.12(a) is a vertical slice and 4.12(b) is a horizontal slice of the computational domain (not to scale). E_z was retrieved from the cells in green to be used to determine the propagation constant. The source cell is shown in gold.

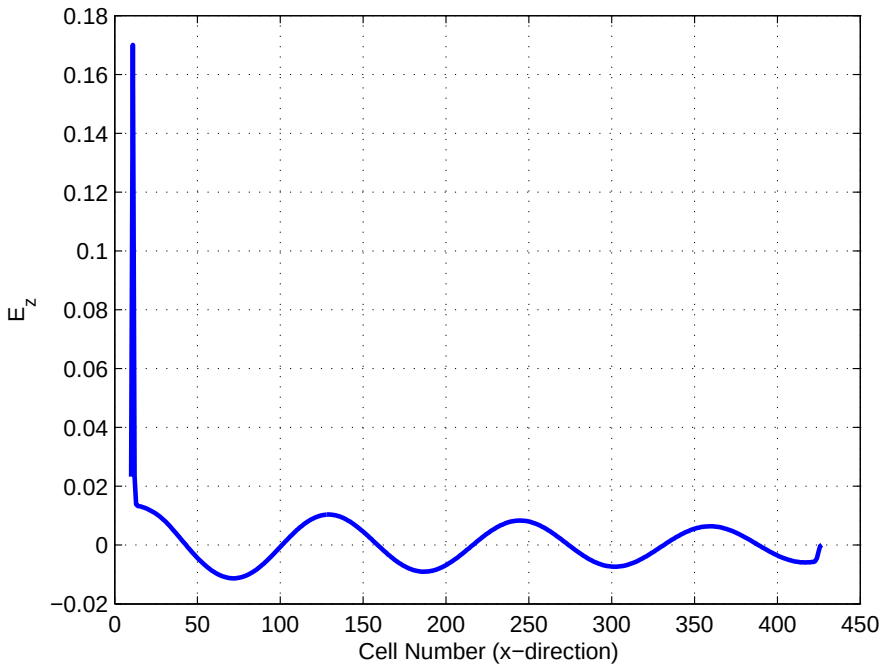

Figure 4.13: The raw E_z data retrieved following simulation.

Typical raw data following a simulation is plotted in Figure 4.13. The source is seen as the large spike at cell number 13. At cell 420, the PML begins to dampen the waveform. At least two periods of the waveform of Figure 4.13, starting from the first absolute maximum (cell 72), were normalized for analysis. A recursive, least-square procedure was used to best fit a known exponential curve. The peak values were compared to find α_x and the zero crossing locations were compared to find β_x. Figure 4.14 shows the best fit curve on top of the FDTD data. The procedure was automated to process an entire set of simulation trials and output the propagation constants to an excel spreadsheet. This procedure works well for most frequencies, however, its use for the lowest 15% of a leaky band is problematic for two reasons.

First, good agreement with a best fit method is not adequate with less than two periods of data. The wavelength of the traveling wave at the lower end of the leaky band is more than five times the wavelength at the highest frequency in the band, as seen in Figure 4.15. Therefore, the computational domain must be five times longer, which requires five times the memory. Even worse, the processing time will be increased by more than

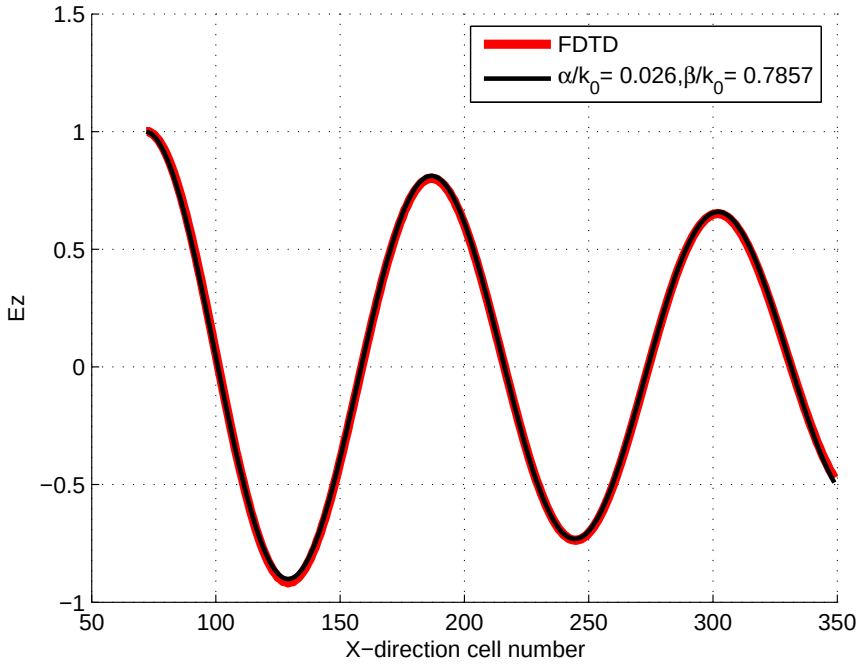

Figure 4.14: The data from Figure 4.13 has been normalized and matched with its best-fit exponential curve.

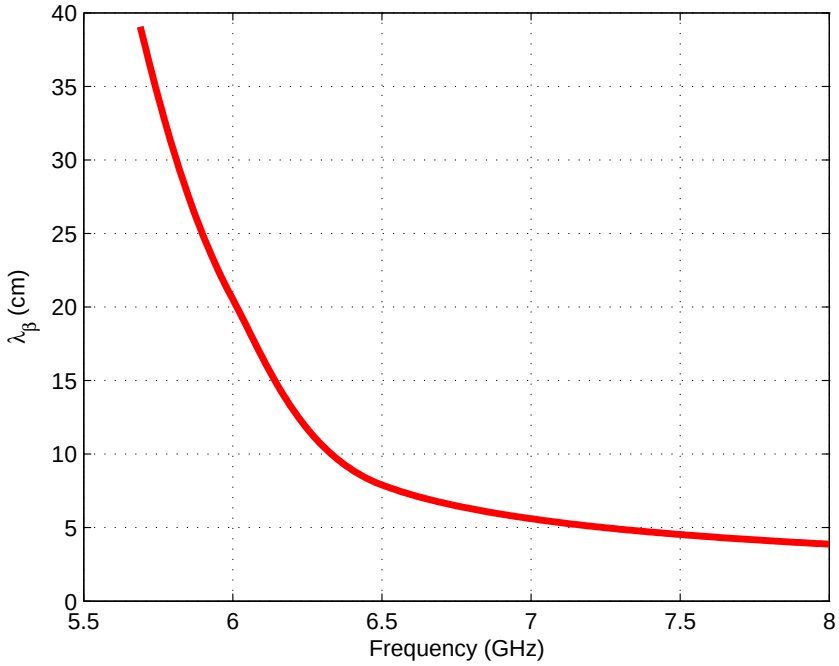

Figure 4.15: The phase constant wavelength, λ_β, is much longer for lower frequencies.

25 times, since each time step will take five times longer and the waveform will need five times the steps to propagate the length of the antenna. A large simulation is difficult and time-consuming, but possible.

The second problem was a bigger roadblock. For frequencies at which $\frac{\alpha_x}{k_0}$ is greater than 0.1, the waveform attenuates too rapidly to find sufficient peaks or zero crossings. Instead, a much simpler method was developed from the logarithm of the normalized "FDTD" waveform of Figure 4.14 using Equation (4.2):

$$\begin{aligned} E_z &\propto e^{(\alpha_x - j\beta_x)x} \\ \ln E_z &\propto \ln e^{(\alpha_x - j\beta_x)x} = \alpha_x x - j\beta_x x \end{aligned} \tag{4.2}$$

As shown in Figure 4.16, α_x is simply the slope of the peaks of the $\ln E_z$ waveform, shown as a dotted line, and β_x is found from the separation of nulls using:

$$\beta_x = \frac{2\pi}{\lambda_\beta} \tag{4.3}$$

If the simulation has run long enough to ensure that the traveling wave distribution has a constant wavelength, only $\frac{\lambda_\beta}{2}$ is needed for determination of the propagation constant. A computational space that is just one-half wavelength long is a $\frac{5}{6}$ reduction from the best-fit method that required three wavelengths.

4.11 Validating FDTD Code

4.11.1 Transverse Resonance. The FDTD simulation was validated by comparison of the extracted α_x and β_x with the propagation constant given by a transverse resonance solution, which was verified by a comparison with the Steepest Descent Contour (SDC) method by Lee and Oliner [20, 30]. Figure 4.17 shows a transmission line model that is applicable to the cross section of the Menzel, TFW, and THW antennas. Each structure can be modelled as a dielectric-filled parallel plate waveguide of admittance, $Y_{0\varepsilon}$, terminated at one end by a short circuit and the other end by admittance Y_t. The **E** null

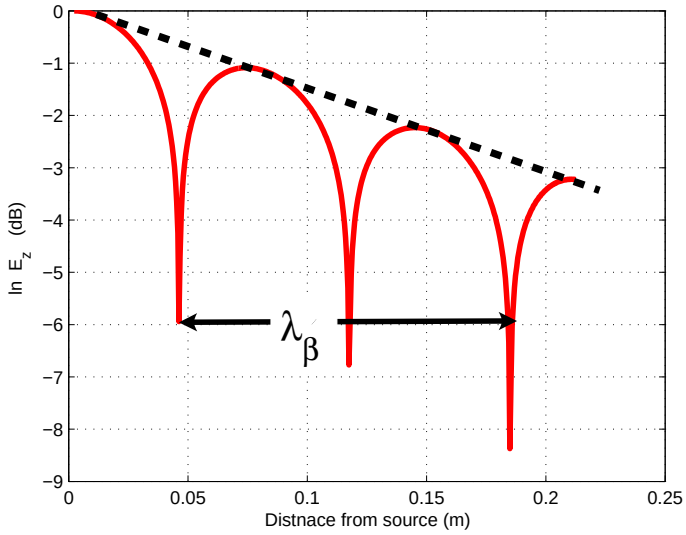

Figure 4.16: The natural logarithm of the simulation data can be used to determine the propagation constant.

generated in the EH_1 mode by a vertical wall or transverse slots is represented by a short circuit. Y_t is an approximation of the admittance of an open edge of microstrip developed by Chang and Kuester [7, 17] using the Weiner-Hopf technique to analyze a TEM wave that is completely reflected.

Chang and Kuester state applicability to only *thin* substrates in which:

$$h \ll \frac{1}{\omega \sqrt{\varepsilon\mu}} \tag{4.4}$$

For a substrate thickness, h, of $787\mu m$, Equation (4.4) requires frequencies $\ll$ 40 GHz, which is five times higher than the highest frequency of this leaky band. At 6.7 GHz, Figure 4.18 shows that FDTD and transverse resonance begin to disagree as the height of the substrate increases past the *thin* criteria, near h= 1.1 mm. By Equation 4.4, the frequency should be much less than approximately 28.4 GHz at this point. This suggests that, for the THW antenna ($\varepsilon_r = 2.33$ and w= 7.5 mm), Equation (4.4) is more precisely:

$$h < \frac{28.4}{2\pi 6.7 \sqrt{\varepsilon\mu_0}} < \frac{4.2}{\omega \sqrt{\varepsilon\mu_0}} \tag{4.5}$$

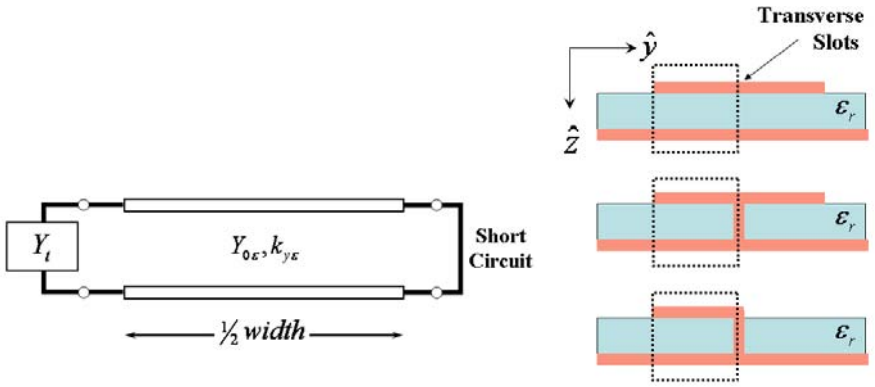

(a) (b)

Figure 4.17: (a) is a transmission line circuit that approximates the cross section of each of the three structures in (b) operating in mode EH_1. The cross sections in (b) represent Menzel (top), TFW (center), and THW (bottom).

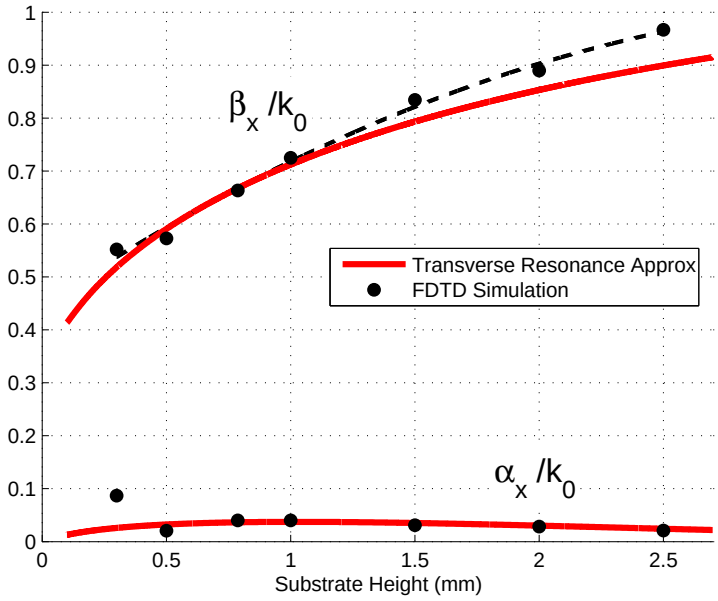

Figure 4.18: The effect of the height of the substrate on the propagation constant at 6.7 GHz for the THW antenna ($\varepsilon_r = 2.33$; w = 7.5 mm.) The dashed line is a quadratic least square of the FDTD data points.

The transverse resonance relation, Equation (4.6), must hold for all points in the transverse direction, $\hat{y}$.

$$\Gamma_{right}(y) \cdot \Gamma_{left}(y) = 1 \tag{4.6}$$

The reflection coefficient from the admittance of the end of the microstrip, Y_t, is unity with a phase shift, χ [7, 17]. At a point $y = y_a$ just to the right of Y_t,

$$\Gamma_{right}(y_a) = -e^{-j2k\frac{w}{2}} \tag{4.7}$$

$$\Gamma_{left}(y_a) = e^{j\chi} \tag{4.8}$$

where k is the wavenumber in the substrate and w is the width of the structure. Equation (4.6) becomes:

$$\begin{aligned} -e^{-j2k\frac{w}{2}} \cdot e^{j\chi} &= 1 \\ \chi - kw &= \pm n\pi \quad n = 1, 3, 5, ... \end{aligned} \tag{4.9}$$

For the EH_1 mode, n=1.

The approximation can be modified to meet changes in h, w, and ε_r, providing that Equation (4.4) is still valid. It cannot, however, be applied to curves or tapers since the Y_t approximation is no longer valid. Figure 4.19 shows that the transverse resonance approximation is in agreement within 1% of the FDTD-derived β_x data over the entire leaky band.

4.11.2 Measurements. Validation was also shown by comparison with existing measurements. The Thiele Half Width antenna was fabricated at the Radiation and Scattering Compact Antenna Laboratory (RASCAL) by Dr. Thiele using vias spaced $\lambda/10$ to

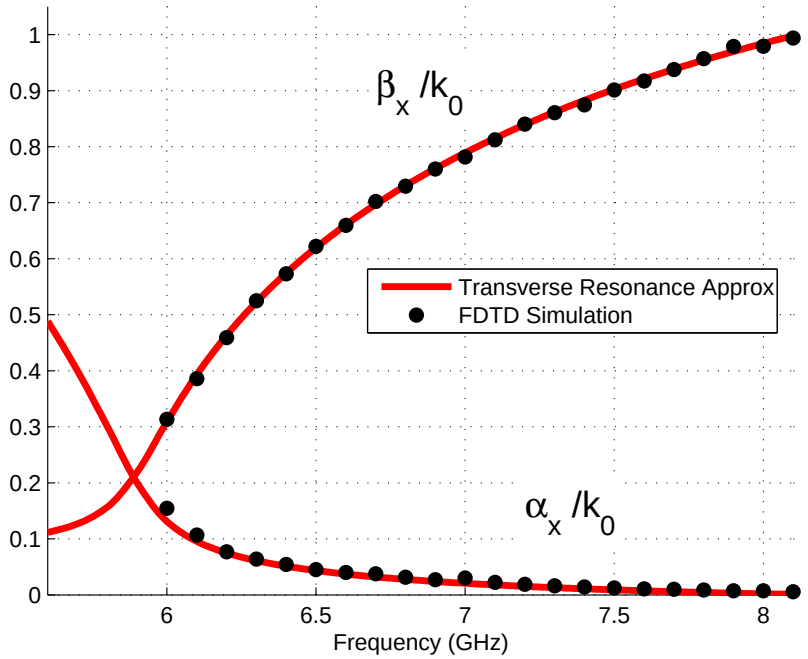

Figure 4.19: The FDTD simulation of the THW is in agreement with the transverse resonance approximation.

form the wall. Both far-field pattern measurements as well as near-field probing measurements were conducted.

The near field measurements produced the data seen in Figure 4.20, from which the propagation constant was extracted in much the same manner as with the FDTD data. Figure 4.21 shows that the data is not very smooth, but β_x corresponding to the peaks does agree to within 3% of both FDTD and transverse resonance.

Far-field H-plane measurements were taken at RASCAL's compact range. The set-up is depicted in Figure 4.22. Figure 4.23 shows the normalized far-field H-plane **E** field pattern of the THW antenna made with vias by Dr. Thiele. For comparison, the data is plotted along with the line source pattern of the corresponding data from both the FDTD simulation and the transverse resonance approximation. The magnitude of the backward lobe is higher for the measured THW antenna demonstrating a lower attenuation constant, α_x. The location of the measured main lobe is closer to endfire, which indicates a higher β_x than the numerical solutions.

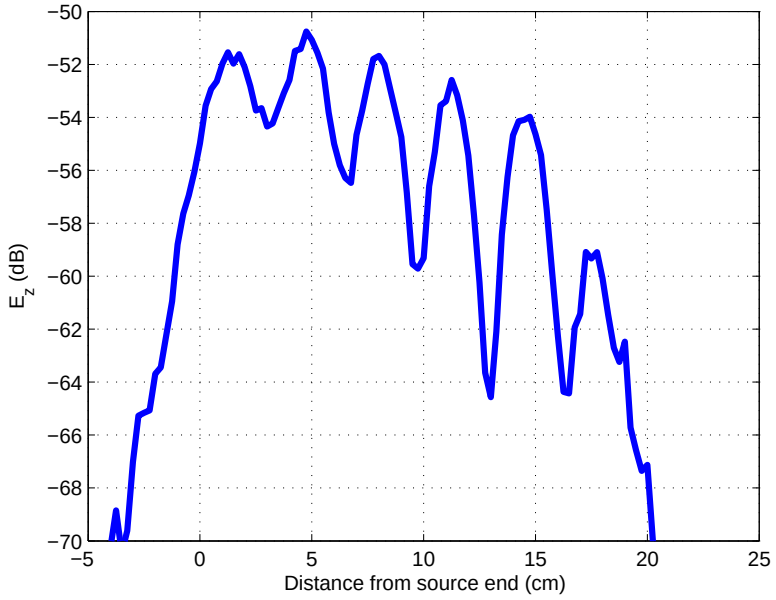

Figure 4.20: The raw data resulting from probing the near field of the Thiele half width antenna at 6.7 GHz.

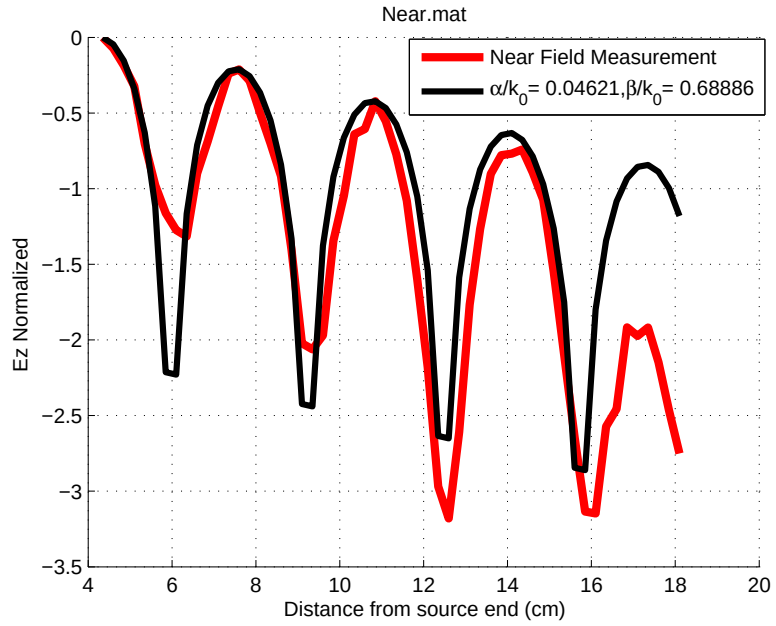

Figure 4.21: Extraction of the propagation constant from the near field measurements (6.7 GHz).

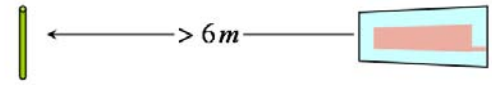

(a)

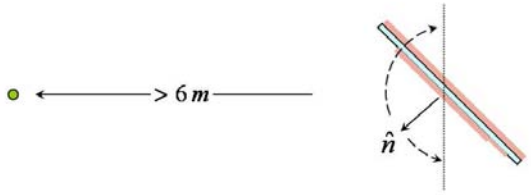

(b)

Figure 4.22: Far-field H-plane measurements of the **E** field taken in RASCAL's compact range. (a)Horizontal view and (b) View from above showing placement of antenna under test and the probe of the receive horn (left).

The estimated propagation constant of the Thiele antenna can be determined by a best fit with the line source. Figure 4.24 shows the line source pattern matched to that of the THW antenna. As discussed in Chapter 2, the main beam position is only within 1^o if the antenna is over 5 λ_β long. The length of all antennas fabricated was limited to 19 cm due to material availability. This length is less than 3 λ_β at 6.7 GHz and less than 4 λ_β at 7.2 GHz. To extract the propagation constant, 5% was added to the line source α_x and β_x to accurately match the main beam location within 1%. The propagation constants of the THW antenna determined from Figure 4.24 are summarized in Table 4.1.

Table 4.1: Line source best fit of the Thiele antenna made with vias.

	6.7 GHz	7.2 GHz
Measured k_x/k_0	0.715 - j0.019	0.85 - j0.0135
FDTD k_x/k_0	0.677 - j0.040	0.816 - j0.0252
β_x Relative error	5.7 %	4.2 %

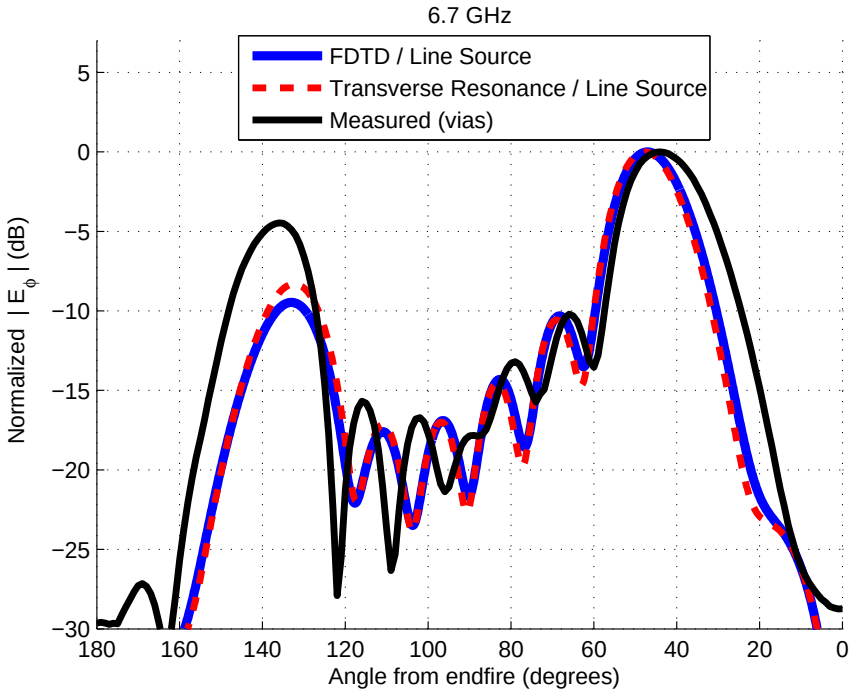

(a)

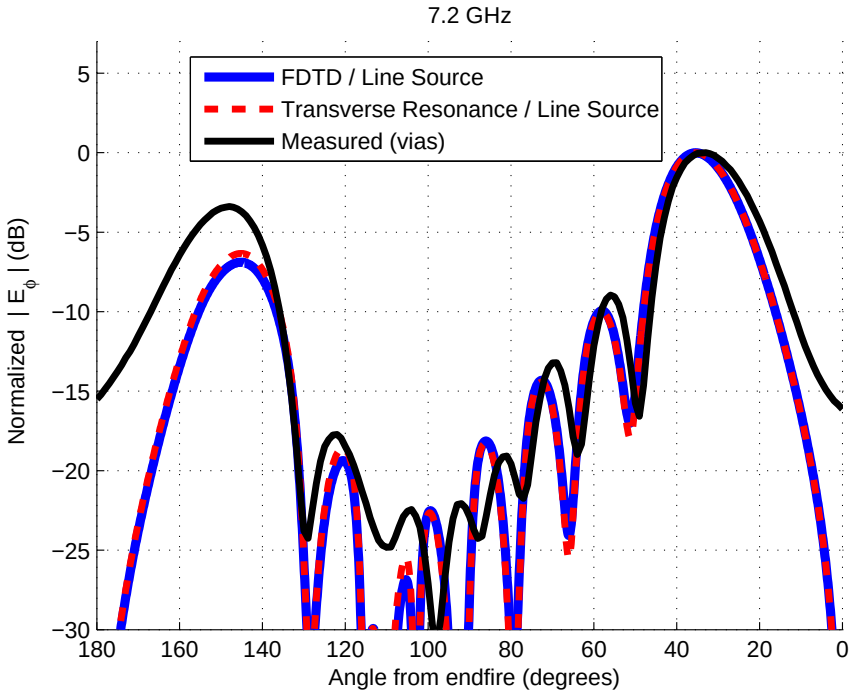

(b)

Figure 4.23: Far-field radiation pattern of the THW fabricated with vias compared to the line source pattern generated with FDTD and Transverse Resonance data (a) at 6.7 GHz and (b) at 7.2 GHz.

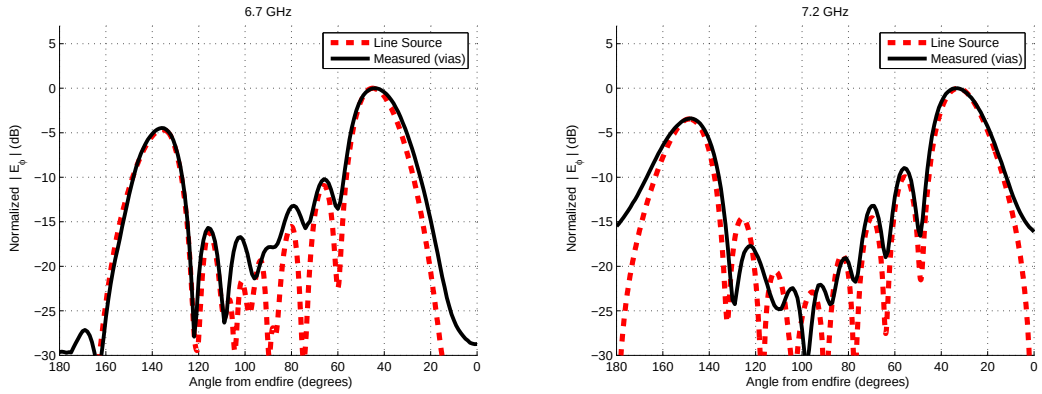

(a) (b)

Figure 4.24: Measured data with a best fit line source to estimate the propagation constant (a) at 6.7 GHz and (b) at 7.2 GHz.

4.12 Curvature

The effect of curvature on the propagation constant was tested by constructing a 180^o bend of the THW design. Figure 4.25 illustrates the view from above the curved computational domain, looking in the $+\hat{z}$ direction. The substrate is shown as cyan, the PML is maroon, and the top conducting strip is colored green. For viewing, the wall has been colored blue and the cells from which E_z were recorded are colored orange. The source is the single dark cell near (20,140). The antenna was bent with the wall on the inside (Figure 4.25(a)) as well as with the wall on the outside (Figure 4.25(b)).

Geometrical distortion was expected to pose a problem. Figure 4.26 is a blown-up view of the cells at a curve. A cell size of 1.5:1.5:1 was used to keep the cells square in the plane of curvature to minimize distortion.

The most difficult task involved in simulating curvature in a rectangular coordinate system is accurately processing the data. As seen in Figure 4.26, the cells from which the field data is taken are not on a precise curve. Worse, the cell data is not stored in the order the traveling wave propagates. These matters were solved by storing the angle to each field cell with respect to the lower PML boundary as seen by the cell at the center of the semi-circle, cell (138,141). The output data from this simulation was, therefore, a

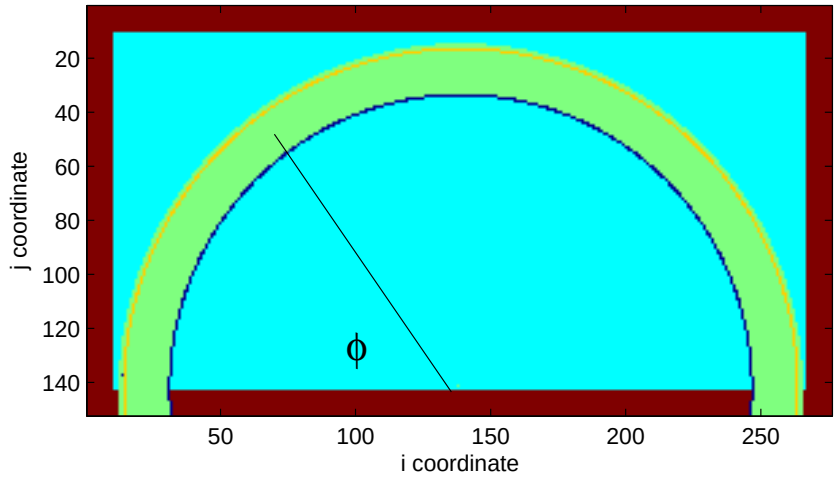

(a)

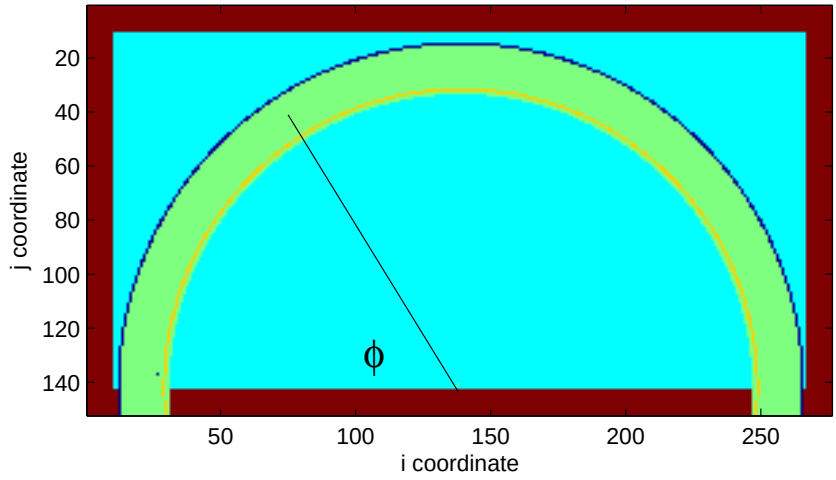

(b)

Figure 4.25: The computational space of the THW antenna curved 180^o in Matlab. (a) shows the wall (in blue) on the inside while (b) shows the wall on the outside

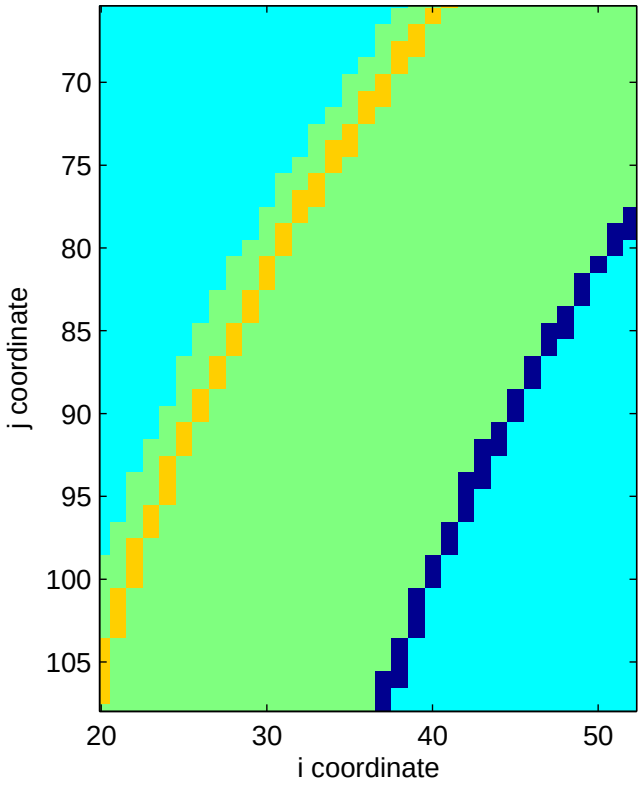

Figure 4.26: The curved THW antenna is approximated by rectangular cells.

vector called *EZDATA*, which contained the E_z component field data from the orange cells in Figure 4.4.25, and a vector of *EZDATA*'s corresponding angles, named *ANGLES*.

Figure 4.27 depicts the processing using the angle information. Figure 4.27(a) shows the *ANGLES* data following simulation. The phase is unwrapped in Figure 4.27(b). Next, both *EZDATA* and *ANGLES* are re-ordered based on the *ANGLES* data to put the data in the order encountered by the traveling wave propagating in the antenna, as seen in Figure 4.27(c). Finally, the vertical axis of Figure 4.27(d) shows the *ANGLES* have been translated into arc distances from the source cell to allow computation of the propagation constant from the *EZDATA*. The propagation constant can then be extracted in the same manner as the straight antennas.

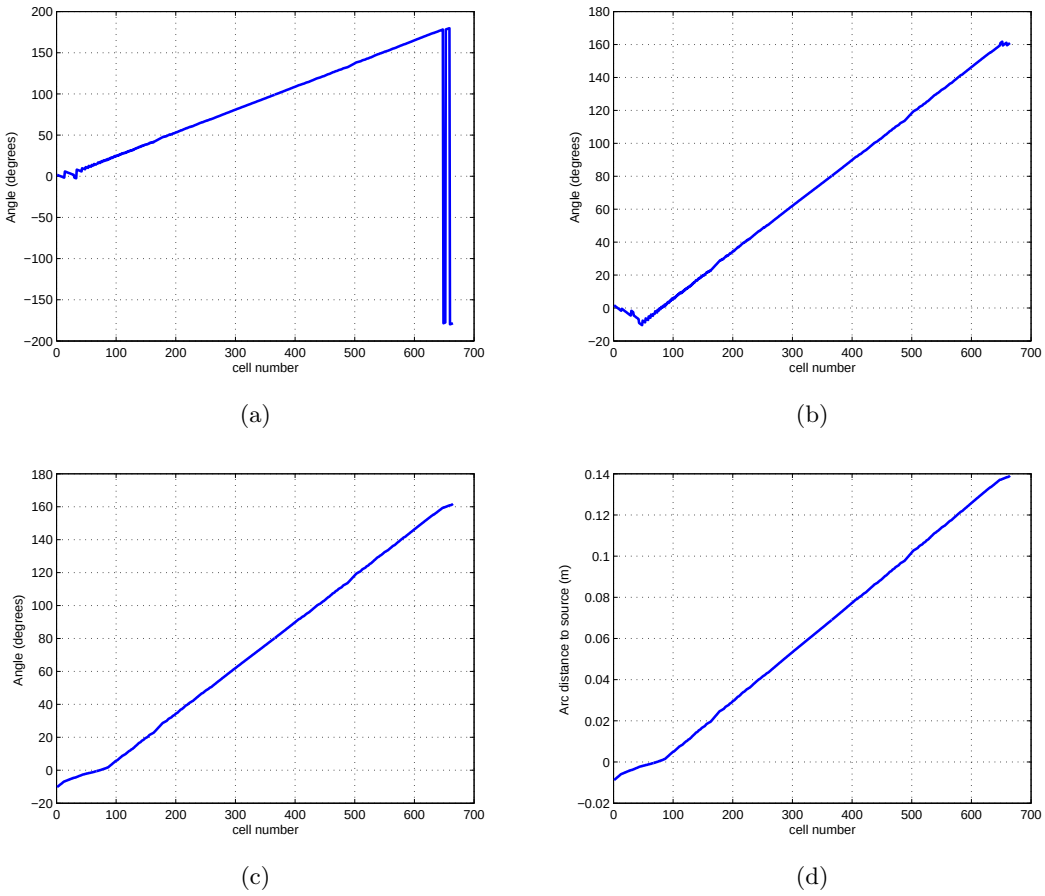

Figure 4.27: Following the curved THW simulation, processing of the (a) raw angle data involved (b) unwrapping the phase, (c) ordering, and (d) converting the angle to an arc distance from the source.

V. Results

Analysis of the Thiele Half Width (THW) antenna began by a examining the field distribution of its predecessors, the Menzel antenna and the Thiele Full Width (TFW) antenna. One of the primary uses of determining the propagation constant of a traveling wave antenna is bandwidth prediction. Antennas were simulated with varying geometrical parameters and the resulting effects on the propagation constants were analyzed to find means of increasing the bandwidth. A preliminary look into the effects of an array of THW elements determined the required spacing to prevent mutual interaction of multiple elements. The current method of fabricating the THW antenna is an imprecise, tedious process of drilling holes and soldering vias. An improved fabrication technique replacing the vias with conducting copper tape is documented.

5.1 Reduction of Memory for Simulation

The simulation development steps taken in the previous section allowed the trials to be accurately run on personal computers with only 1 GB of RAM. Table 5.1 summarizes means that can be used to eliminate unnecessary cells and the corresponding decrease in memory use observed. These steps reduced the initial simulation of 900 million cells over 99.9% to only 572,000. Unless otherwise annotated, all trials modelled the THW antenna as a five-cell-thick lossless substrate with uniform cells of size 3:1:1 using double precision. These approximations enable simulations of up to 1 million cells.

Table 5.1: Ways the size of the simulation was reduced.

Assumption	Memory Reduction
Modelling copper as zero thickness	over 94 %
Extraction of k_x using log	over 80 %
Cell size 5:1:1 (3:1:1)	80 % (60 %)
Elimination of unneeded substrate	nearly 80 %
5-cell-thick substrate	nearly 80 %
No free space surrounding structure	over 70 %
Lossless substrate	50 %
Remove non-excited side of TFW	approx 45 %
Single precision	approx 40 %
Total	**over 99.9** %

5.2 Menzel antenna

The wall of the Thiele design is clearly superior to transverse slots at suppression of the fundamental mode. The transverse slots of the Menzel design created field distributions that made FDTD extraction of the propagation constant difficult for higher frequencies and virtually impossible for the lower half of the leaky band, as shown in Figure 5.1. The patterns of Figures 5.1(b) and 5.1(c) suggest destructive interference from the presence of the EH_0 mode in addition to EH_1. The right half of the pattern enclosed in a dotted box of Figures 5.1(d) and 5.1(e) is a waveform useable for propagation constant extraction and yields data within 5% of both the transverse resonance approximation and the THW simulation. An attempt to improve the waveform by enlarging the transverse slots is seen in Figure 5.2. The lower frequencies are still unusable, but the usable portion of the higher frequencies has been increased slightly.

5.3 Thiele Full Width (TFW) antenna

Figure 5.3 illustrates an investigation into the fields inside the TFW antenna. The source cell seen in the upper left corner of Figure 5.3(a) has an E_z component with a negative (red) value that induces positive (blue) fields in the immediately surrounding cells on the excited (top) side. As the positive (blue) fields fill the excited side, negative (red) fields are induced into the non-excited side (bottom) past the vertical PEC wall. Figures 5.3(b)-5.3(e) show that these induced fields form a traveling wave in the non-excited side that travels in the same $+\hat{x}$ direction and has roughly the same wavelength, λ_β, as the excited side. Since the energy propagated along a longer path, the non-excited side is not 180^o out of phase but less than 90^o. Like those of the excited side, the fields of the non-excited side attenuate as they travel. This attenuation indicates that radiation is also occurring on the non-excited side. Due to the less than 90^o phase difference with respect to the excited side, the radiation from the non-excited side is likely decreasing the ability of the structure to radiate. Extracting k_x from simulations does not support any difference between the THW and the TFW. However, Dr. Thiele reports that previous measurements comparing the far-field pattern of both antennas indicate that the THW does in fact radiate with higher gain than the TFW.

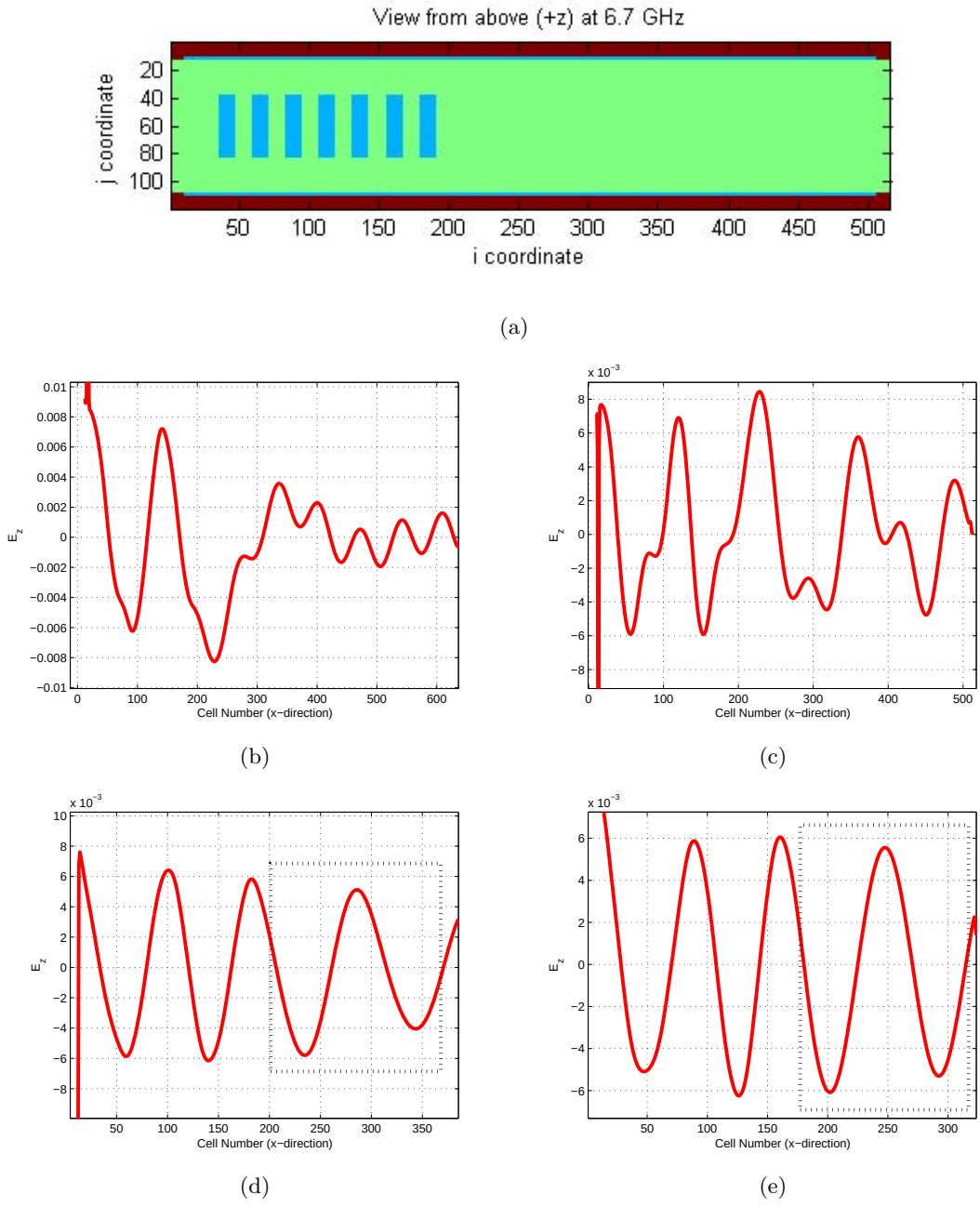

Figure 5.1: (a) The original Menzel antenna as simulated in Matlab at 6.7 GHz. The PML appears maroon, PEC green, and substrate blue. The antenna yielded the following traveling wave distributions: (b) at 6.2 GHz, (c) at 6.7 GHz, (d) at 7.2 GHz, and (e) at 7.7 GHz. The only useable data is surrounded by a dotted line.

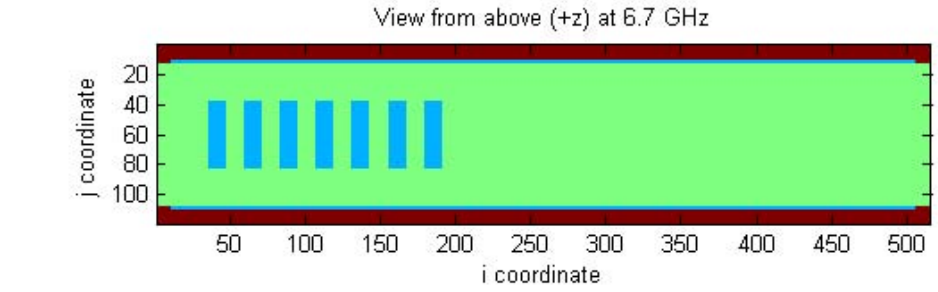

(a)

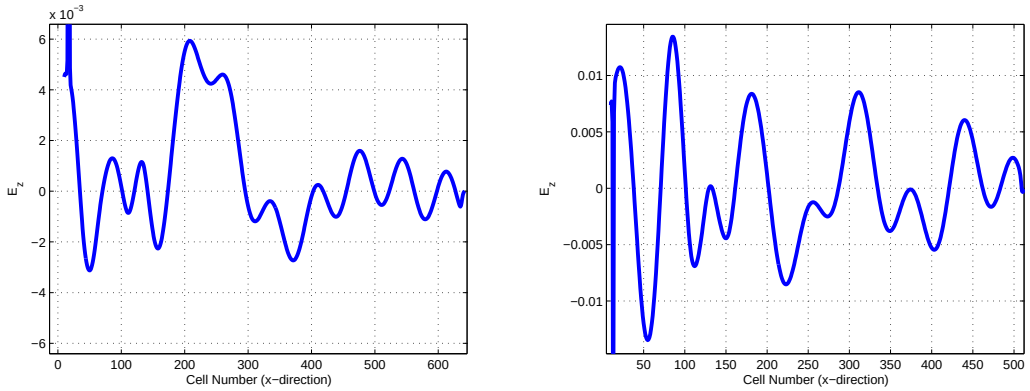

(b)

(c)

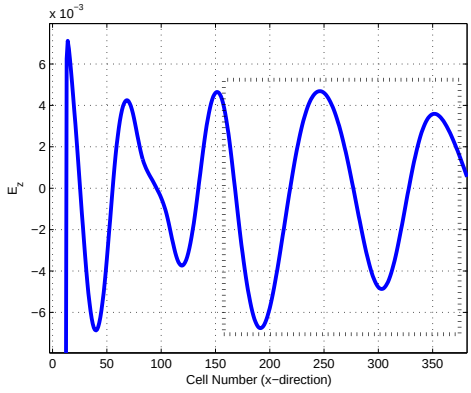

(d)

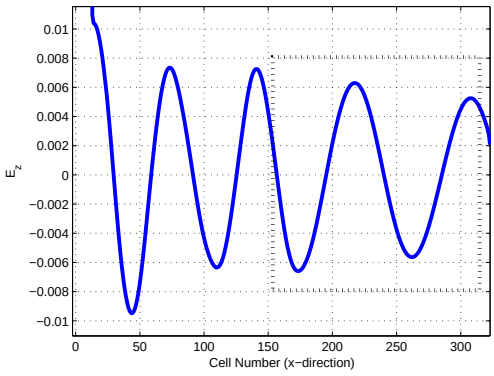

(e)

Figure 5.2: (a) The Menzel antenna with larger transverse slots as simulated in Matlab at 6.7 GHz. The PML appears maroon, PEC green, and substrate blue. This antenna yielded the following traveling wave distributions: (b) at 6.2 GHz, (c) at 6.7 GHz, (d) at 7.2 GHz, and (e) at 7.7 GHz. The only useable data is surrounded by a dotted line.

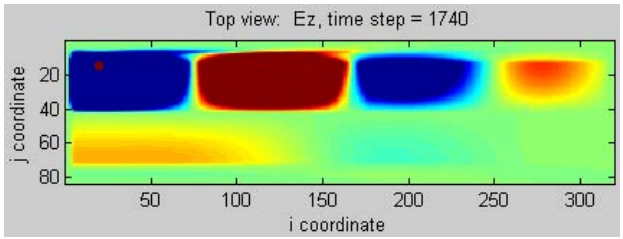

(a)

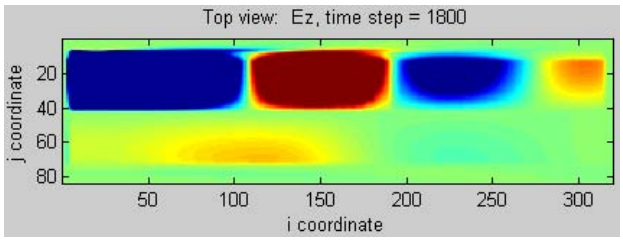

(b)

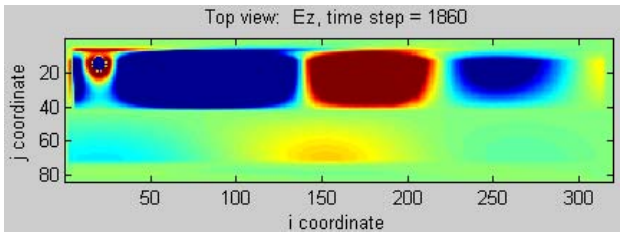

(c)

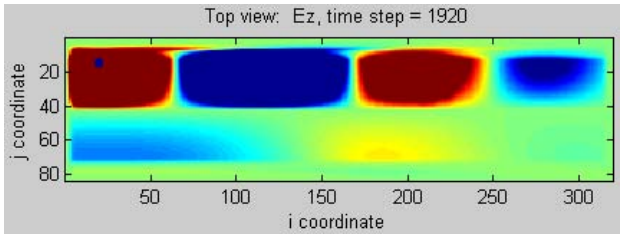

(d)

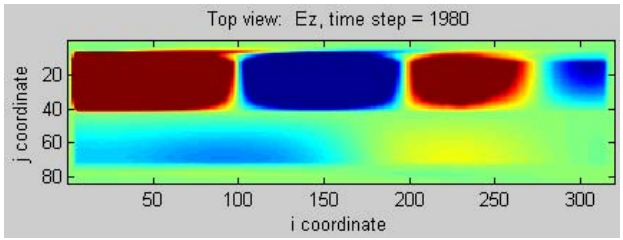

(e)

Figure 5.3: The excited side (top of each figure) of the TFW antenna induces a traveling wave on the non-excited side (bottom) that also travels to the right ($+\hat{x}$) and attenuates as it radiates. The source cell can be seen in the upper left corner of (a), (c), and (d).

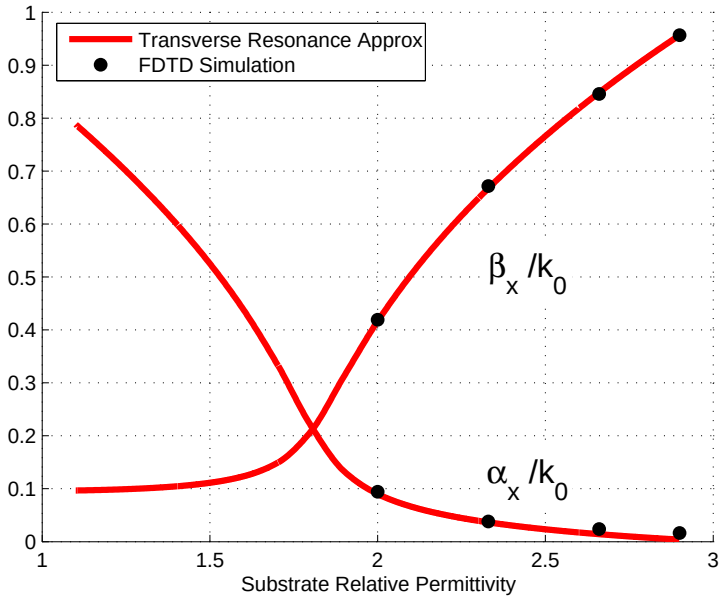

Figure 5.4: The propagation constant's dependence on dielectric constant at 6.7 GHz for the THW antenna (h = 0.787 mm; w = 7.5 mm.)

5.4 Modifying dimensions to meet bandwidth specifications

A bandwidth centered around a desired center frequency, f_c, can be achieved by scaling the width of the conducting strip, the height (or thickness) of the substrate, and/or the permittivity of the substrate. The bandwidth can be increased, to a limited extent, by the selection of the substrate material. As a fraction of the center frequency, the bandwidth will be unaffected by altering the height and width, although f_c can be shifted readily. The choice of substrate material and thickness is usually dictated by cost or availability of material, therefore, the width is the easiest of the three to manipulate.

5.4.1 Varying Dielectric Constant. Figure 5.4 illustrates the relationship between the relative permittivity of the substrate and the propagation constant. Figure 5.5 shows the bandwidth as a function of substrate permittivity overlayed with common substrates. Bandwidth increases rapidly as the substrate dielectric constant nears that of free space. The drawback of lower dielectric constant is a very low α_x across most of the leaky band, as seen in Figure 5.6. Low α_x results in little energy radiating per unit length.

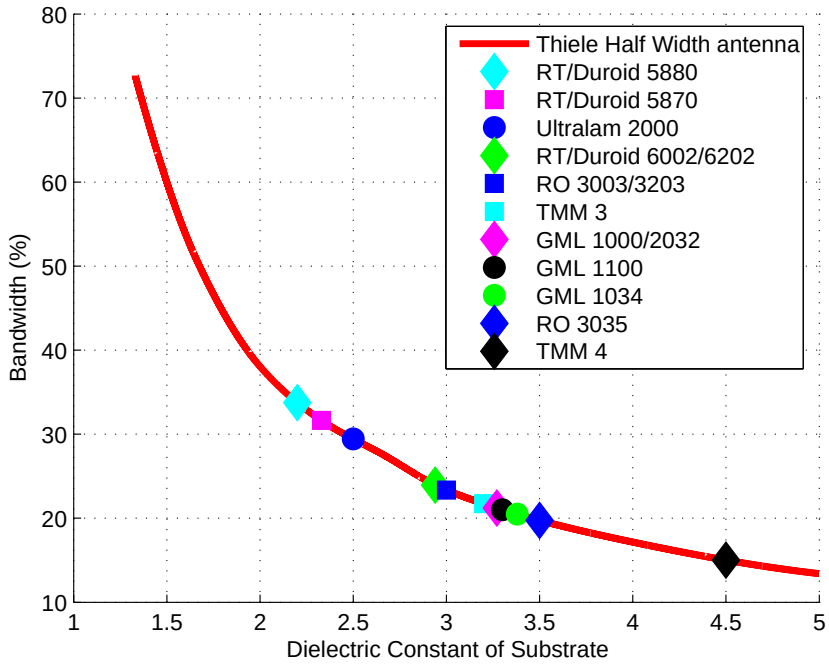

Figure 5.5: The bandwidth as a function of substrate permittivity for the THW Antenna (h = 0.787 mm; w = 7.5 mm.) Common, commercially available substrates are overlayed

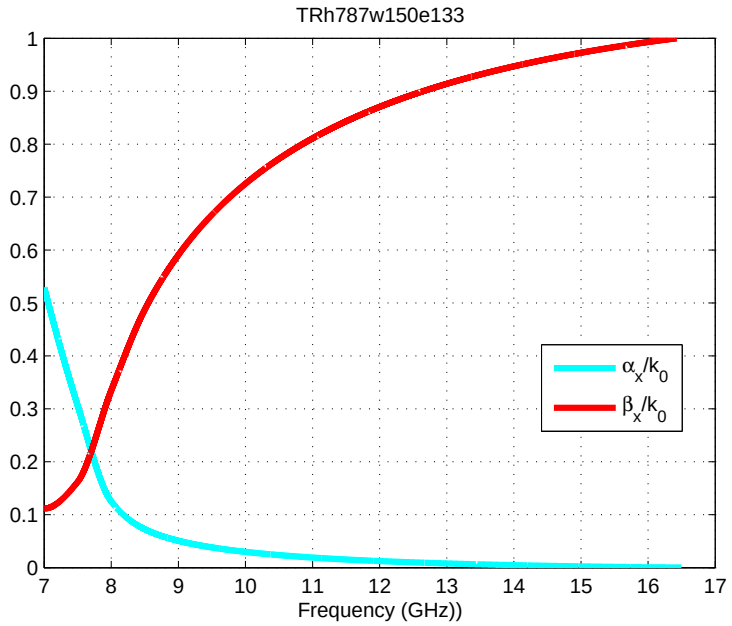

Figure 5.6: The normalized α_x and β_x curves in the leaky band for the THW antenna using substrate with ε_r=1.33 (h = 0.787 mm; w = 7.5 mm.)

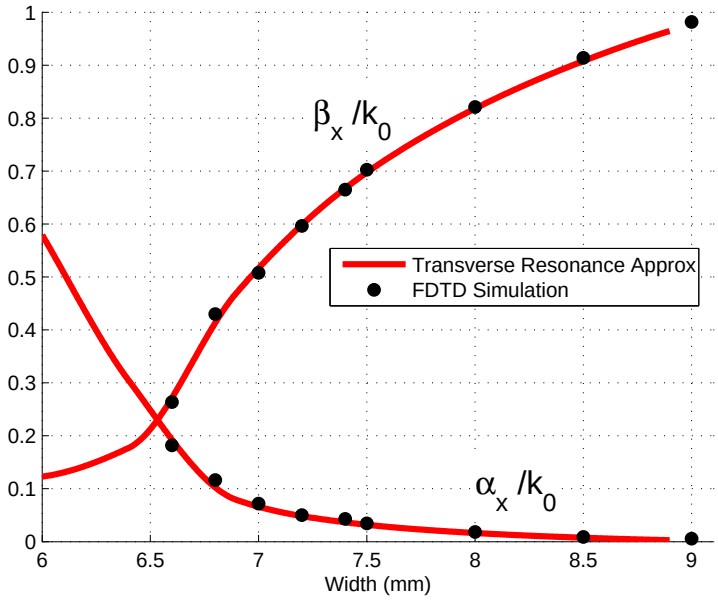

Figure 5.7: The effect of the width of the conductor on the propagation constant at 6.7 GHz for the THW antenna ($\varepsilon_r = 2.33$; h = 0.787 mm.)

5.4.2 Varying Height. Figure 4.18 illustrates the relationship between the height, or thickness, of the substrate and the propagation constant. Like permittivity, the height of the substrate is usually dictated by the material available. All antennas simulated and fabricated for this work used material that was 0.787 mm thick. As mentioned in the previous section, the transverse resonance solution includes an approximation that limits its applicability to thin substrates. The difference in β_x between FDTD and transverse resonance becomes noticeable for heights greater than approximately 1.1 mm.

5.4.3 Varying Width. Figure 5.7 shows that the propagation constant is very sensitive to the width of the conductor strip. As little as 0.1 mm difference in width will cause as much as 10% error in β_x. This sensitivity to width questions the ability to fabricate the wall with vias, since placement to even as little as 0.1 mm is difficult.

5.4.4 Frequency Scaling. The leaky frequency band can be scaled up or down by scaling the width and height inversely while using the same permittivity. For example, Table 5.2 shows the effect on frequency by halving the height and width. While the

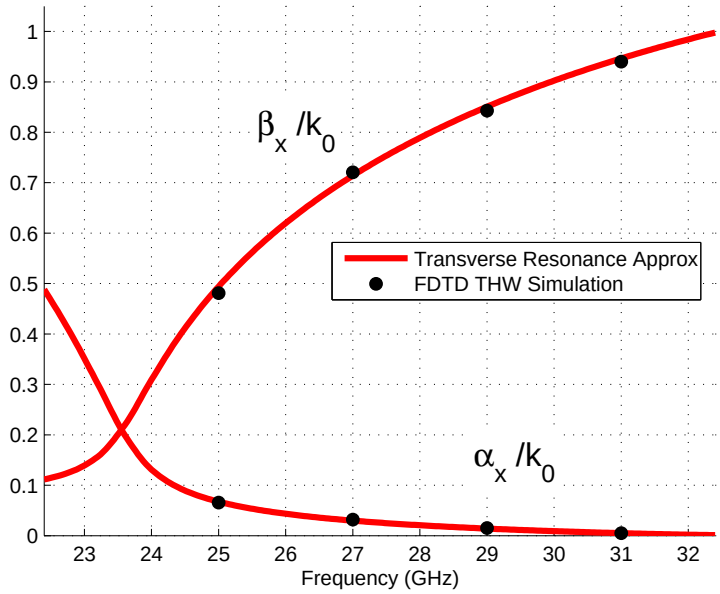

Figure 5.8: The center frequency has been scaled up by a factor of four by using a quarter of the height and a quarter of the width.

bandwidth appears to double, the effective bandwidth remains the same percentage of the center frequency, f_c.

Table 5.2: Scaling the frequency by a factor of two.

Bandwidth	2.4 GHz	4.8 GHz
f_c	7.08 GHz	14.16 GHz
w	15 mm	7.5 mm
h	787 μm	393.5 μm
ε_r	2.33	2.33

Figure 5.8 shows the effect of using one-fourth the width and one-fourth the height of the THW. The center frequency has quadrupled to 28.32 GHz. Frequency scaling does not prove useful for reduction of the FDTD simulation since cross section ratio of height to width is unchanged. However, this property could be useful to shrink the antenna to meet measurement facility size constraints. Conversely, fabrication may be made easier by increasing the size of the antenna.

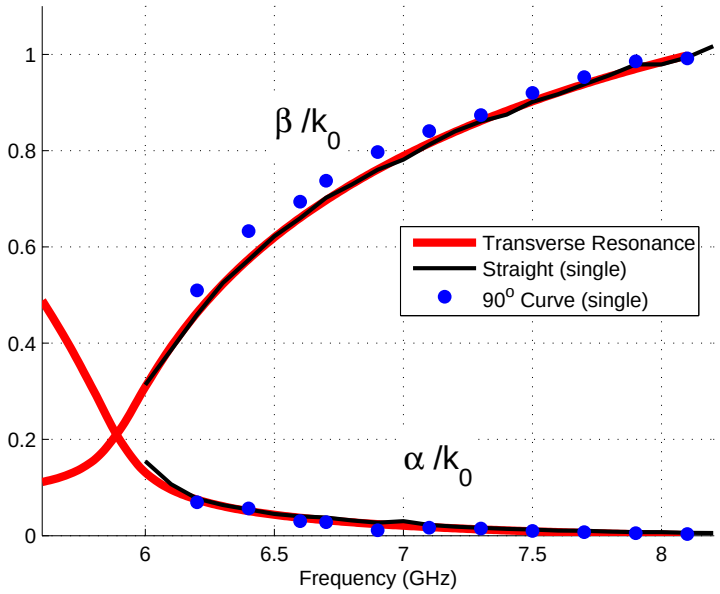

Figure 5.9: The THW antenna curved 90^o with a radius of approximately 93 mm.

5.5 Curvature

Constant curvature with the open end on the outward side was simulated at radii of 3.36, 4.23, 5.32, and 9.3 cm. Only 90^0 was possible to simulate for the largest radius, while 180^0 was used for all others. The size of the computational domain necessitated only single precision. Not enough information is available to extract k_x for frequencies whose λ_β is greater than twice the length of the arc. Figure 4.15 shows the relation between frequency and the wavelength of β_x. The curvature trials are summarized in Table 5.3. Figure 5.9 shows that curvature increases bandwidth by flattening β_x, predominantly for the lower frequencies, while keeping α_x relatively unaffected. Figures 5.10 through 5.12 indicate that as curvature decreases, the bandwidth decreases.

Table 5.3: Summary of curvature trials.

	180^0	180^0	180^0	90^0
Radius(cm)	3.36	4.23	5.32	9.3
Arc length (cm)	10.6	13.3	16.7	14.6
Largest λ_β possible (cm)	21.2	26.6	33.4	18.6
Lowest f possible	6.2 GHz	6.1 GHz	6.0 GHz	6.1 GHz
Approx Bandwidth	2.8 GHz	2.7 GHz	2.6 GHz	2.5 GHz

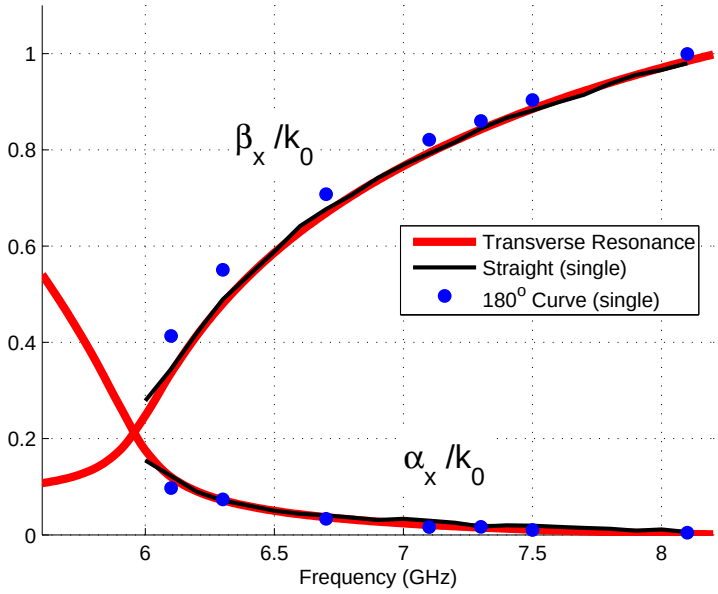

Figure 5.10: The THW antenna curved 180^o with a radius of approximately 53 mm.

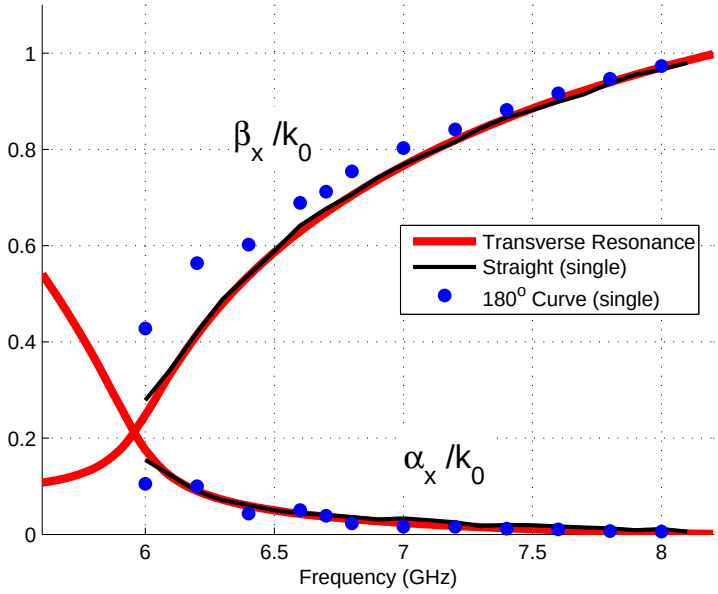

Figure 5.11: The THW antenna curved 180^o with a radius of approximately 42 mm.

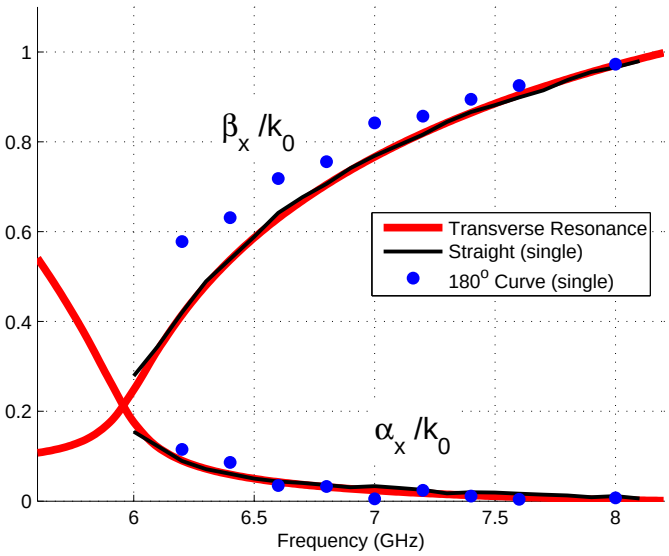

Figure 5.12: The THW antenna curved 180^o with a radius of approximately 34 mm.

Curvature with the wall on the outside appears to hamper the ability of the antenna to set-up the EH_1 mode. As seen in Figure 5.13, which is data from a 180^0 arc of radius 4.23 cm, destructive interference indicates the presence of the EH_0 mode.

5.6 Multiple Elements

From Equation (2.16) it is clear that the main beam is steerable in the longitudinal direction from near endfire to near broadside. A linear array of these elements should, therefore, be able to scan in two dimensions. A first step to developing such an array is to determine the required spacing between neighboring elements. Two elements were simulated next to each other at 7.2 GHz using double precision. The results were nearly identical regardless of whether the second element was excited or not. The effect on propagation constant by a neighboring element is shown in Figure 5.14. There appears to be little interaction between elements if they are separated by at least $0.25\lambda_s$ and virtually no interaction if the spacing is over $0.4\lambda_s$, where:

$$\lambda_s = \frac{\lambda_0}{\sqrt{\varepsilon_r}} \tag{5.1}$$

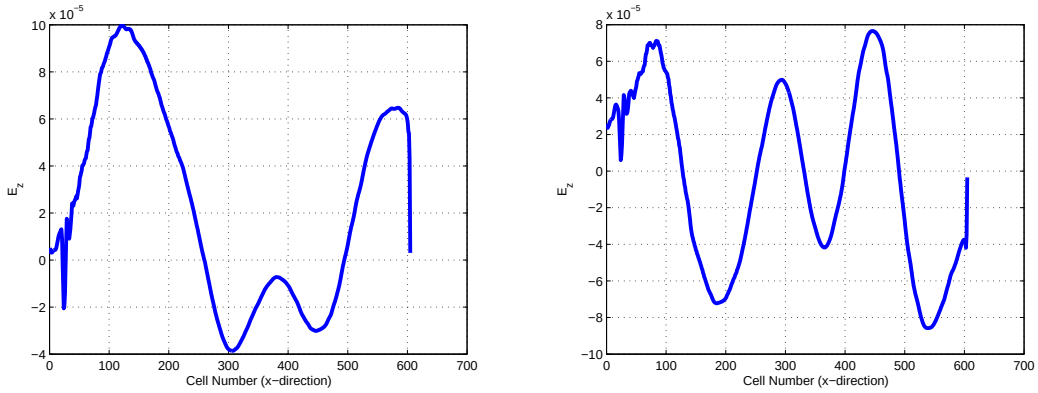

(a) (b)

Figure 5.13: Curvature with the wall on the outside produces field distributions, seen here at (a)6.4 GHz and (b) 7.4 GHz, that suggest the presence of multiple modes.

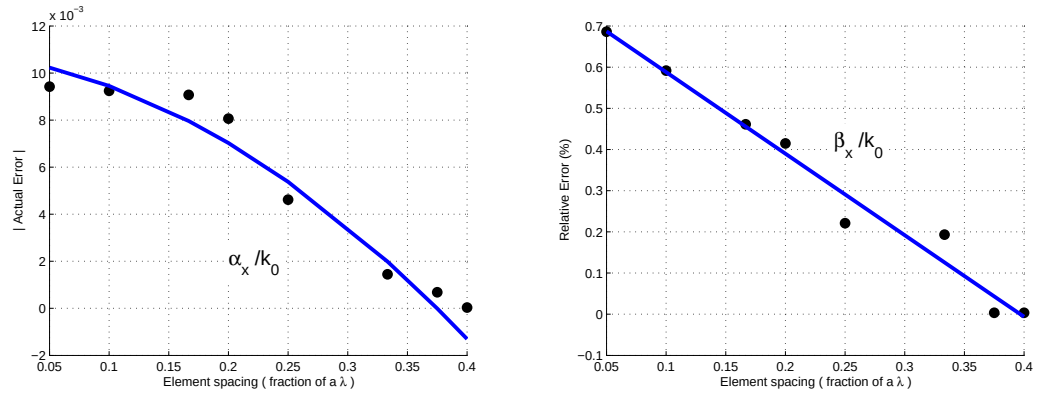

(a) (b)

Figure 5.14: (a) Actual error of $|\alpha_x|$ and (b) relative error of β_x from placing another element a fraction of a wavelength from the open end of the antenna. For both figures, the error is with respect to the propagation constant of a single element.

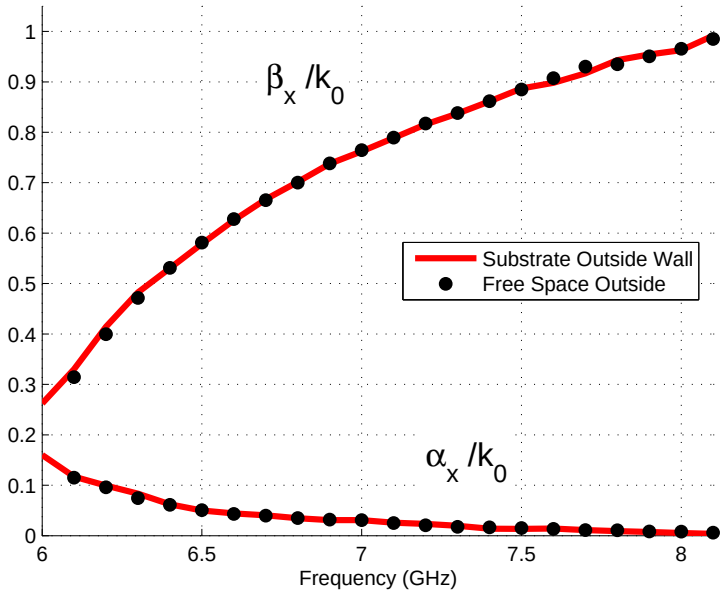

Figure 5.15: The propagation constant from FDTD simulations is unaffected by the removal of substrate outside of the wall.

5.7 Simplified Fabrication

Fabricating the THW antenna using vias soldered to the conducting strip and ground plate is time consuming and inaccurate. Precise placement of a 0.52 mm thick wire is quite difficult. As previously mentioned, Figure 5.7 shows that an error in width of as little as 0.1 mm can affect the propagation constant by as much as 10%. The spacing of the vias may also create a reactive component to the wall which could further alter the propagation constant. Replacing the vias with conductive copper tape was quick and simple. Figure 5.15 does not support the need for the substrate outside the wall, therefore, the wall could be created by cutting the substrate and ground plate away up to the location of the wall, applying copper tape to form the wall, and then soldering a replacement ground plate. The resulting antenna is pictured in Figure 5.16.

Figures 5.17 and 5.18 are comparisons of far-field patterns among the two THW antennas and the line source pattern from the FDTD-produced propagation constant. The magnitude of the backward lobes indicates that attenuation constant, α_x, of the THW antenna made with conductive tape more closely matches the FDTD data than does

Figure 5.16: THW antenna fabricated without vias.

the antenna utilizing vias. Position of the main lobe of each antenna indicates that β_x is nearly identical for each.

Table 5.4 summarizes the estimated error of the propagation constant of the THW antenna fabricated with conducting copper tape. Propagation constant was estimated with a line source pattern best fit match of the main and backward lobes. At 6.7 GHz, β_x has slightly more error than the antenna made with vias. Fabrication error making the width of the conducting strip slightly wider than designed is attributed. The width of the strip is more crucial and leads to more error for lower frequencies than higher frequencies.

Table 5.4: The THW antenna made with copper tape.

	6.7 GHz	7.2 GHz
Measured k_x/k_0	0.732 - j0.034	0.86 - j0.023
FDTD k_x/k_0	0.677 - j0.040	0.816 - j0.0252
β_x/k_0 Relative error	8.2 %	5.4 %

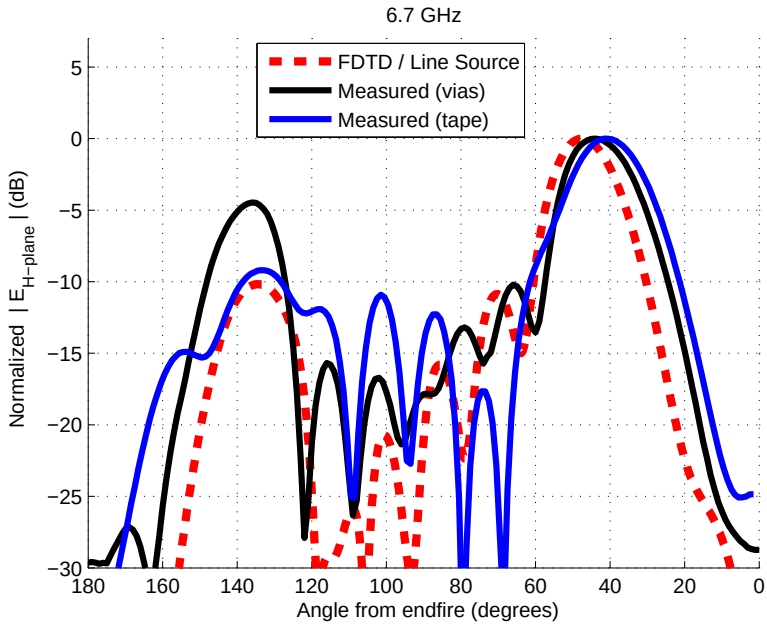

Figure 5.17: Comparison at 6.7 GHz of THW using vias, THW using conductive tape, and the line source - FDTD pattern estimate.

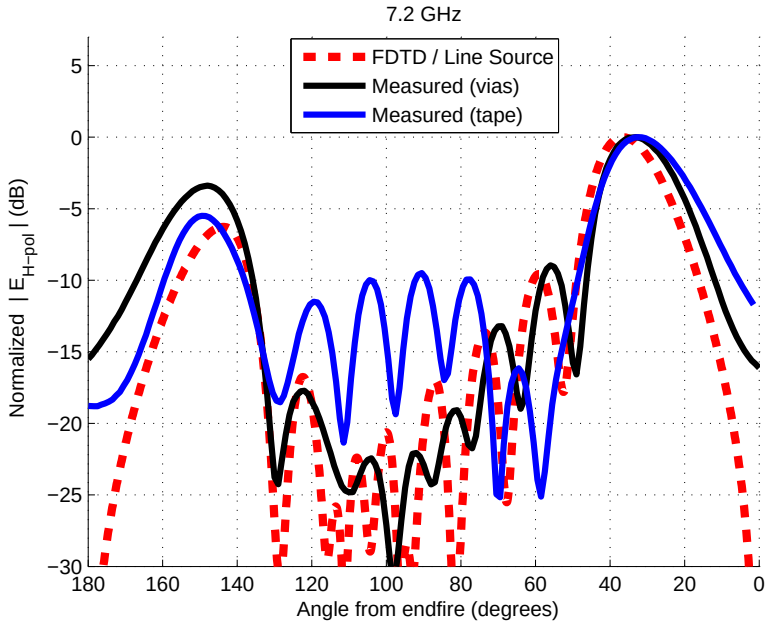

Figure 5.18: Comparison at 7.2 GHz of THW using vias, THW using conductive tape, and the line source - FDTD pattern estimate.

VI. Conclusions

This thesis provides the groundwork that will enable development of a lightweight, inexpensive, aerodynamic, and broadband antenna. Whether for radar or communication, an antenna with these properties would be a force multiplier for the smaller, limited payload air vehicles the United States Air Force will pursue in the coming years.

6.1 Summary of Results

A three dimensional Finite Difference Time Domain (FDTD) simulation was constructed to simulate various leaky wave microstrip antennas. FDTD was shown to be able to extract the propagation constant, which is useful in predicting antenna performance measures such as bandwidth and main bean direction. The antenna geometry was easily manipulated in FDTD to meet various testing requirements of different structures. Several means were found to decrease the number of cells required to accurately simulate the antennas allowing elaborate simulations with only a standard desktop PC with 1 GB of memory. The availability of high performance computing, which is typically required for such modelling, was shown to be not necessary for most geometries.

The FDTD simulation provided results within 1% of a transverse resonance approximation of the same structure. The transverse resonance model has been validated by other researchers with the Steepest Descent Contour [20, 30]. Measurements were also used for validation. A best fit line source far field pattern was matched to the measured pattern to estimate the propagation constant for comparison with the simulations. The ability to quantitively compare simulated antenna propagation constants with propagation constants of measured antennas was previously not available.

The Thiele Half Width (THW) antenna was shown to be an improvement over both the Thiele Full Width (TFW) antenna as well as the Menzel antenna. The propagation constant of the THW antenna behaved equivalently to the TFW antenna as anticipated by image theory. In addition, the non-excited side of the TFW antenna was shown to degrade the phase difference across the structure's width preventing effective radiation.

The vertical wall of the THW antenna was found to be more capable of blocking the fundamental mode than the antenna developed by Menzel [23].

Two THW antenna elements were excited in close proximity to test mutual interaction. No effect to the propagation constant of elements was observed if the spacing distance was greater than 0.4λ. This minimum spacing will allow multiple THW elements to adequately radiate as an array.

Bandwidth improvements were found to be inversely related to curvature of the THW antenna. Geometrical distortion may be a large source of error for the curved antennas simulated. Therefore, these findings need confirmation with measured or analytical results. The far-field line source pattern used is only valid for a straight antenna. A curved antenna can be fabricated and measured, however, the propagation constant cannot be estimated with the line source developed. A curved line source would be needed for comparison of the propagation constant with simulated data.

The bandwidth of the THW antenna can also be increased by using a lower permittivity dielectric constant; however, a commercially available substrate could not be found lower than 2.2. Lowering the dielectric constant has the drawback of a very low α_x across much of the leaky band, which hinders an effective radiator. Varying the width of the conducting strip or the height of the substrate were found to move the center frequency, but did not change the bandwidth as a percentage of center frequency. The width and height can be varied together to scale the center frequency. Frequency scaling can be used to decrease the length of the antenna to meet measurement facility size constraints or to increase the size of the antenna for ease of fabrication.

6.2 Follow-on Work

Knowledge gained from this thesis about the nature of the propagation constant as a function of curvature and element spacing is critical for future efforts to produce a spiral design. The Thiele antenna shows promise, but more work needs to be done before an effective, broadband, broad pattern antenna can be made. Further research of the THW would be aided by a faster simulation using more memory and a transformation of

the simulated fields to the far-field. Areas of analysis that could next be tackled include continuation of the curved geometry investigations and exploration of a full THW array. An important topic not addressed in this work is the feed.

6.2.1 FDTD Simulation. A larger simulation is advantageous for a host of reasons. Of course, more cells mean higher resolution and less geometrical distortion. A limitation of the FDTD method was that the propagation constant was not able to be determined when the length of the antenna was less than half of λ_β. Simulations were limited to 900,000 cells for double precision and 1,600,000 cells for single precision for 1 GB of computer memory. More memory would not prohibit extraction of the long λ_β propagation constants of low frequencies. Instead of terminating the structure into PML, a larger simulation would allow the antenna to instead be surrounded by free space, which would model the fields and currents of the actual antenna in addition to propagation constant extraction. The loss tangent of certain substrates may be large enough to require a lossy model, necessitating much more memory.

Computer memory is the factor limiting the simulation size. The solution is to create a parallel version of the code to allow several computers working the simulation simultaneously. The **E** field components of each cell are determined from that cell's previous time step as well as the directly adjacent **H** fields. The **H** field components update analogously. The **E** fields are not updated at the same time as the **H** fields, and vice versa. Therefore, breaking up the computational space allowing multiple processing of separate portions of the computational space simultaneously is possible. Many methods of parallelizing Matlab have been developed, including MatlabMPI, which is available in Wright-Patterson AFB's High Performance Computing facility.

The length of time needed to run the simulation was not a problem due to the large number of PC's that were available for this research. If time is an issue, as would likely be the case if the simulations were larger, Matlab should be abandoned for the field update loop of the current FDTD program. Fortran would provide a vast improvement in computational speed.

A curved line source approximation is needed to evaluate the curved simulation against a pattern measurement of a fabricated curved design. However, the line source approximation gives an indication of only the main lobes of the far-field pattern. Since the fields immediately above the simulated antenna are known, a near-field to far-field transformation would provide a more exact simulated pattern for comparison.

6.2.2 THW antenna. The best bandwidth improvements involve increasing α_x while not lowering β_x. This was shown to be the effect of curvature. Since the bandwidth of the THW antenna is increased by curvature, the natural next step is a spiral. Taper would likely further increase bandwidth and this could be investigated with the FDTD simulation. A substrate with a graded dielectric constant, although quite difficult to construct, could provide the benefits of increased bandwidth and a decreased backward lobe.

Since the main beam is frequency steerable, a linear array of THW antennas could allow a two dimensional scanning capability. Limited investigation shows that mutual coupling does not appear to be a factor in the leaky region if elements are separated by 0.4λ. Simulation of an array would require much more computation than even the curved trials. Parallel processing and a near-field to far-field transformation would enhance this investigation.

6.2.3 Feed. A proper impedance match with the source is vital to efficient power use by an antenna. Gain of the antenna would also be enhanced. The simulated fields inside the THW antenna should provide the information needed to characterize the impedance of the structure. An optimum feed could then be realized using the required matching stubs, although this match may only be effective for a narrow frequency band. Since the goal is a broadband antenna, a balun might be necessary to provide the desired insertion loss over the entire leaky band.

6.2.4 S-Parameter Measurements. Sheen developed an S-parameter extraction technique to de-embed alpha and beta from network analyzer measurements [37]. This method could be useful for geometries that are difficult to simulate. The drawback to this method is the high cost of building multiple designs.

TH.m

```
function TH(f,steps,sing)

%     3-D FDTD code with UPML absorbing boundary conditions
%     Date of this version:  21 Jan 2005
%*************************************************************************
%     PATTERNED AFTER CODE WRITTEN BY:
%                     Keely J. Willis, Ph.D. Student
%                     UW Computational Electromagnetics Laboratory
%                         Director: Prof. Susan C. Hagness
%*************************************************************************
%
%   INPUTS: 'f' IS THE EXCITATION FREQUENCY IN (Hz)
%           'steps' BEGINS TIME STEPPING IF '1', SKIPS TIME STEPPING TO ONLY DISPLAY
%               SIMULATION PARAMETERS IF '0'
%           'sing' SELECTS SINGLE PRECISION IF '1', DOUBLE PRECISION IF '0'
%
%*************************************************************************
%
%   SIMULATION 'name' of the form 'THexample67' where:
%
%           'TH' IS A THIELE HALF WIDTH (THW) ANTENNA
%               or 'TF' IS A THIELE FULL WIDTH (TFW) ANTENNA
%               or 'MENZEL' IS THE MENZEL ANTENNA
%               or 'THCURVEOUT' IS A CURVED THW WITH THE WALL OUTSIDE
%               or 'THCURVEIN' IS A CURVED THW WITH THE WALL INSIDE
%           'example' IS THE SPECIFIC CONFIGURATION, SUCH AS:
%               'loss' WHICH INCLUDES LOSS
%               'sing' WHICH IS SINGULAR PRECISION
%               'norm' WHICH IS LOSSLESS DOUBLE PRECISION 3:1:1
%               'smaller' WHICH IS A THINNER 'norm'
%               'exxx' WHICH IS 'norm' WITH ANOTHER DIELECTRIC
%               'hxxx' WHICH IS 'norm' WITH ANOTHER SUBSTRATE THICKNESS
%               'rxx' WHICH IS THE RADIUS OF CURVATURE (cm)
%           '67' IS THE EXCITATION FREQUENCY OF 6.7 GHz
```

```
%
%**********************************************************************
%
%   EXAMPLE OF THE SIMULATION MATLAB DISPLAY:
%           ---------------------------------*
%             THexample67 began at 13-Feb-2005 12:04:53.
%             Computational grid is 158790 cells.
%             Resolution is:  62.24  cells/wavelength.
%             Structure size: 66.9 X 7.50 X 0.787 (mm)
%             Cell size ratio: 2.99 : 1.00 : 1.00
%             Time steps:  13020 (dt= 0.3437 pS)
%
%           FDTD3D preprocessing took 1.55 seconds.
%
%           Period 1  of  30 took 9.14 minutes.
%                 (13-Jan-2005 12:14:07)
%                              "
%                              "
%            < DISPLAY FOR EACH PERIOD OF SOURCE >
%                              "
%                              "
%           Period 30  of  30 took 9.18 minutes.
%                 (13-Jan-2005 17:01:02)
%
%           End at 13-Feb-2005 17:01:35.
%**********************************************************************
%
%   OUTPUTS:
%       'THexample67.mat':  A FILE CONTAINING ALL OF THE SIMULATION DATA THAT WILL BE
%           USED TO EXTRACT THE PROPAGATION CONSTANT.
%
%       'THexample67QUART.mat':  A FILES SAVED AFTER A FOURTH OF THE SIMULATION IS
%           COMPLETE.  VERY USEFUL TO ESTIMATE THE REMAINING SIMULATION TIME.
%
%       'MTHexample67.mat':  AN OPTIONAL FILE CONTAINING FRAMES OF THE FIELDS.
%           (WARNING: THIS FILE CAN GET HUGE ~200 MB)
%
```

```
%       'THexample67.avi':  AN OPTIONAL FILE OF MOVIE IN COMPRESSED FORMAT
%
%************************************************************************
%************************************************************************


tic
Begin= datestr(now);        % STORE BEGINING TIME OF SIMULATION
fprintf('\n\n--------------------------------*');
name= [mfilename,'example',num2str(f/1e8)];
                            % CREATE A SIMULATION NAME
fprintf('\n%s began at %s.',name,Begin);
curve= 0;                   % '1' TO UPDATE PEC FOR CURVE
mov= 0;                     % '1' TO SAVE A MOVIE OF THE FIELDS
av= 0;                      % '1' TO SAVE .avi MOVIE (ONLY IF mov= '1')
if av                       % CREATE A .avi FILE TO BE WRITTEN TO
    aviobj = avifile([name,'.avi'],'fps',12,'quality',100);
end;

%************************************************************************
%       FREQUENCY
%************************************************************************
if sing c= single(299792458);   % speed of light (m/s)
else  c= 299792458;   end
omega= 2*pi*f;              % angular frequency (rad/s)
lambda= c/f;                % wavelength (m)
k= 2*pi/lambda;             % wavenumber (1/m)


%************************************************************************
%   MATERIAL PARAMETERS :  m=1: free space     m=2: Substrate
%************************************************************************
u0= pi*4e-7;                % permeability of free space (H/m)
e0= c^-2/u0;                % permittivity of free space (F/m)
lossTan= 0.00;              % lossless case
% lossTan= 0.0012;          % for RT/Duroid 5870
```

```
er=[1 2.33+j*lossTan*2.33]; % relative permitivity
e= e0*er;
sig= [zeros(1,length(er)) ];% electrical conductance
ur= [ones(1,length(er)) ];  % relative permeability
u= ur*u0;

for m= 1:length(er)         % CREATE COEFFICIENTS SPECIFYING MATERIAL FOR EACH CELL
    C.c1(m)= (2*e(m)-sig(m)*dt)/(2*e(m)+sig(m)*dt);
    C.c2(m)= 2*e(m)*dt/(2*e(m)+sig(m)*dt);
    C.c3(m)= C.c1(m);
    C.c4(m)= 1/(2*e(m).^2+e(m)*sig(m)*dt);
    C.c5(m)= (2*e(m)+sig(m)*dt);
    C.c6(m)= (2*e(m)-sig(m)*dt);

    D.d1(m)= 1;
    D.d2(m)= dt;
    D.d3(m)= 1;
    D.d4(m)= 1/(2*e(m)*u0);
    D.d5(m)= 2*e(m);
    D.d6(m)= 2*e(m);
end


%************************************************************************
%     GRID PARAMETERS
%************************************************************************
load Compare
pABx=round(pABx*100)/100;
B= pB(find(pABx==f/1e9));
L= c/B/f;                   % wavelength predicted by Transverse Resonance

X= 2*L;                     % length (m) (for approx 2 wavelengths)
Y= (7.42e-3);               % width of strip (m) GUESS: HALF CELL SHORTER
Zs= 787e-6;                 % thickness of substrate (m)
dz= Zs/5;                   % 5 cell thick substrate

if curve                    % 1.5:1.5:1 cell ratio
```

```
    dx= X/round(X/(1.5*dz));% size of <x> cell edge (m)
    dy= Y/round(Y/(1.5*dz));% size of <y> cell edge (m)

    r= 2/pi*X;              % RADIUS OF CURVATURE
    jstruct= round((r+Y-r/sqrt(2))/dy) +4;
    istruct= round(sqrt(2)*r/dx);
    if mod(istruct,2)
        istruct= round(sqrt(2)*r/dx)+1;
    end
    kstruct= Zs/dz;

else                        % 3:1:1 cell ratio
    istruct= round(X/3/dz); % size of structure (#cells) in <x>
    jstruct= round(Y/1/dz)+4;% size of structure (#cells) in <y>
    kstruct= Zs/dz;         % size of structure (#cells) in <z>
    dx= X/istruct;          % size of <x> cell edge (m)
    dy= .0075/(jstruct-3.5);% size of <y> cell edge (m)
                            % HALF-CELL CORRECTION MADE TO WIDTH OF CONDUCTING STRIP
end

if f/1e9 > 6.9      pml= 6; % thickness of PML region (# cells)
elseif f/1e9 > 6.6  pml= 8;
else                pml= 12;        end;
buffer= 2;                  % free space buffer above structure
pb= pml+buffer;

it= istruct+2*pml;          % size of total sim (#cells) in <x>
jt= jstruct+2*pml;          % size of total sim (#cells) in <x>
kt= kstruct+pb;             % size of total sim (#cells) in <x>
numcells= (it*jt*kt;        % TOTAL NUMBER OF CELLS
fprintf('\nComputational grid is %.0f cells.',numcells);


%**************************************************************************
%       CELL SIZE / TIME STEP
%**************************************************************************
DX= 1/dx; DY= 1/dy; DZ= 1/dz;% MULTIPLICATION IS SLIGHTLY FASTER THAN DIVISION
```

```
res= lambda/sqrt(2.33)/max([dx dy dz]);     % THE COARSEST RESOLUTION IN THE GRID
fprintf('\nResolution is:  %.2f  cells/wavelength.', res);
fprintf('\nStructure size: %.1f X %.2f X %.3f (mm)',...
    istruct*dx*1000, (jstruct-3.5)*dy*1000, kstruct*dz*1000);

cellx= dx/min([dx dy dz]);
celly= dy/min([dx dy dz]);
cellz= dz/min([dx dy dz]);
fprintf('\nCell size ratio: %.2f : %.2f : %.2f ', cellx, celly , cellz );

dt= .9/(c*sqrt(DX^2 + DY^2 + DZ^2));
                            % ENSURE dt IS LESS THAN COURANT CRITERIA
periods= 30;                % # periods of source (more for lower freqs)
TimeSteps= round(periods*round(1/(f*dt)));  % TOTAL NUMBER OF TIME STEPS
fprintf('\nTime steps:  %.0f (dt= %.4f pS)',TimeSteps,dt*1e12);


%**************************************************************************
%     SOURCE
%**************************************************************************
s0= 100;                    % SOURCE MAGNITUDE
n= 3;                       % number of periods of ramp
numramp= n*round(1/(f*dt));
ramp= ones(1,TimeSteps);
ramp(1:numramp)= ((1:numramp)/numramp).^3;  % CUBIC RAMP OVER FIRST THREE PERIODS
ramp= ramp(1:TimeSteps);
S0= s0*ramp;
source= S0.*sin(omega*((1:TimeSteps))*dt);  % CONSTANT FREQUENCY SOURCE
clear ramp s0 S0;


%**************************************************************************
%     INITIALIZE COMPUTATIONAL SPACE
%**************************************************************************
m=1;
if ~sing    field= InitializeFields(it,jt,kt);      % SET-UP A CHUNK OF MEMORY
else        field= InitializeFieldsSingle(it,jt,kt);    end
```

```
[C,D]= InitializeMainGrid(C,D,it,jt,kt,m);  % MAKE ALL CELLS FREE SPACE

Is= 1:it;
Js= 1:jt;
Ks= pb+1:kt;
m= 2;
[C,D]= GetMaterial(C,D,Is,Js,Ks,m);   % MAKE THE CELLS (Is,Js,Ks) SUBSTRATE

m= 1;
[C,D]= FillPML(C,D,dx,dy,dz,pml,pb,c,e,e0,u,dt,it,jt,kt,m);
                            % MAKE ALL OF THE PML MATCHED TO FREE SPACE
m= 2;
[C,D]= changePML(C,D,dx,dy,dz,pml,pb,c,e,e0,u,dt,it,jt,kt,m,Ks(1));
                            % MAKE Ks PML MATCHED TO SUBSTRATE

if curve                    % SPECIFY SOURCE POINT AND DISPLAY VECTOR
    ks= pb+round(kstruct/2);
    kd= ks;
    [field,is,js,id,jd,ANGLES]= InitializePEC(field,it,jt,kt,pb,pml,r,dx,dy,dz,Y,ks);
% [field,is,js,id,jd,ANGLES]= InitializePEC90(field,it,jt,kt,pb,pml,r,dx,dy,dz,Y,ks);

else
    % Location of current source
    is= pml+5;
    js= pml+5;
    ks= pb+3;

    % vector to display
    jd= js+1;
    kd= ks;
end

fprintf('\n\nFDTD3D preprocessing took %.2f seconds.\n',toc);

%       END OF PRE-PROCESSING--ONLY DO THE ABOVE ONCE
%**************************************************************************
```

```
if steps                    % BEGIN TIME STEPPING LOOP
    last= toc;
    flag= 1;
    for t=1:TimeSteps
        if flag
            if t > TimeSteps/4          % SEND A MESSAGE WHEN 1/4 DONE
                quartertime= toc-last;
                save([cd,'\Data\',name,'quart'], 'quartertime');
                flag= 0;
            end;
        end;
        if mod(t,round(1/(f*dt)))==0    % SAVE DATA ONCE A PERIOD
            fprintf('\nPeriod %.0f  of  %.0f took %.2f minutes. \n\t(%s)\n',...
                t/round(1/(f*dt)),periods,(toc-last)/60,datestr(now));
            last= toc;
            if curve
                for nn= 1:length(id)
                    EZDATA(nn)= field.Ez(id(nn),jd(nn),kd);
                end;
            else    EZDATA(t/round(1/(f*dt)),:)= field.Ez(:,jd,kd);    end;
        end

        field= UpdateE(field,C,D,it,jt,kt,DX,DY,DZ);    % UPDATE E FIELDS

        field.Ez(is,js,ks)=  source(t);                 %HARD SOURCE

        if curve            % ZERO THE E FIELDS THIS WAY TO REPRESENT PEC
            field.Ex= field.Ex .*field.pecEx;
            field.Ey= field.Ey .*field.pecEy;
            field.Ez= field.Ez .*field.pecEz;

        else                % ZERO THE E FIELDS THIS WAY
            field= addPECTH(field, it, jt, kt, pb, pml);
            %  field= addPECTF(field, it, jt, kt, pb, pml);
            %  field= addPECMENZ(field, it, jt, kt, pb, pml);
        end
```

```
    field= UpdateH(field,C,D,it,jt,kt,DX,DY,DZ);    % UPDATE H FIELDS

    if mov              % SAVE A FRAME OF FIELD DATA
        frame= 20;      % SAVE EVERY frameTH TIME STEP
        figure(2);
        if mod(t,frame)==0;
            timestep=int2str(t);

            tview=squeeze( field.Ez(:,:,kd) );
            subplot('position',[0.15 0.57 0.7 0.35])
            imagesc(tview');
            caxis([-0.1 0.1]);
            colorbar;
            axis image;
            title(['Ez:  View from above (+z); time step =',timestep]);
            xlabel('i coordinate');
            ylabel('j coordinate');

            sview=squeeze( field.Ez(:,jd,:) );
            subplot('position',[0.15 0.08 0.7 0.35])
            imagesc(sview');
            caxis([-0.1 0.1]);
            colorbar;
            axis image;
            title(['Ez: Cross-section (-y);  time step = ',timestep]);
            xlabel('i coordinate');
            ylabel('k coordinate');

            tt= t/frame;
            M(tt)= getframe(gcf);   % SAVE A FRAME FOR MOVIE
            if av                   % SAVE A FRAME FOR .avi MOVIE
                aviobj = addframe(aviobj,M(tt));
            end
        end;
    end;
end
```

```
    if mov
        movie(gcf,M,0,20);              % Matlab movie
        if av   aviobj = close(aviobj);  end % .avi MOVIE IS NOW IN CURRENT DIRECTORY
        save([cd,'\Data\M',name],'M');
        clear M;
    end

    clear field             % DON'T SAVE ALL OF THE FIELDS OR THE .mat FILE IS HUGE
    clear C D source;
    End= datestr(now);
    fprintf('\nEnd =  %s.\n\n',End);
    time= toc;
    save([cd,'\Data\',name]);
end
```

InitializeFields.m

```
function field= InitializeFields(it,jt,kt)
%   FUNCTION:
%      1. SET-UP MEMORY FOR NUMBER OF CELLS: (it,jt,kt) OF SIZE double
%      2. CREATE STRUCT 'field' THAT CONTAINS ALL OF THE FIELD COMPONENTS

field.Ex= zeros(it,jt+1,kt+1);
field.Ey= zeros(it+1,jt,kt+1);
field.Ez= zeros(it+1,jt+1,kt);

field.Dx = zeros(it,jt+1,kt+1);
field.Dy = zeros(it+1,jt,kt+1);
field.Dz = zeros(it+1,jt+1,kt);
field.Dxn= zeros(it,jt+1,kt+1);
field.Dyn= zeros(it+1,jt,kt+1);
field.Dzn= zeros(it+1,jt+1,kt);

field.Hx= zeros(it+1,jt,kt);
field.Hy= zeros(it,jt+1,kt);
field.Hz= zeros(it,jt,kt+1);

field.Bx = zeros(it+1,jt,kt);
field.By = zeros(it,jt+1,kt);
field.Bz = zeros(it,jt,kt+1);
field.Bxn= zeros(it+1,jt,kt);
field.Byn= zeros(it,jt+1,kt);
field.Bzn= zeros(it,jt,kt+1);
```

InitializeFieldsSingle.m

```
function field= InitializeFields(it,jt,kt)
%   FUNCTION:
%      1. SET-UP MEMORY FOR NUMBER OF CELLS: (it,jt,kt) OF SIZE single
%      2. CREATE STRUCT 'field' THAT CONTAINS ALL OF THE FIELD COMPONENTS

field.Ex= single(zeros(it,jt+1,kt+1));
field.Ey= single(zeros(it+1,jt,kt+1));
field.Ez= single(zeros(it+1,jt+1,kt));

field.Dx = single(zeros(it,jt+1,kt+1));
field.Dy = single(zeros(it+1,jt,kt+1));
field.Dz = single(zeros(it+1,jt+1,kt));
field.Dxn= single(zeros(it,jt+1,kt+1));
field.Dyn= single(zeros(it+1,jt,kt+1));
field.Dzn= single(zeros(it+1,jt+1,kt));

field.Hx= single(zeros(it+1,jt,kt));
field.Hy= single(zeros(it,jt+1,kt));
field.Hz= single(zeros(it,jt,kt+1));

field.Bx = single(zeros(it+1,jt,kt));
field.By = single(zeros(it,jt+1,kt));
field.Bz = single(zeros(it,jt,kt+1));
field.Bxn= single(zeros(it+1,jt,kt));
field.Byn= single(zeros(it,jt+1,kt));
field.Bzn= single(zeros(it,jt,kt+1));
```

InitializeMainGrid.m

```
function [C,D]= InitializeMainGrid(C,D,it,jt,kt,m)

%   FUNCTION:
%      1. SET-UP ALL CELLS TO CONTAIN MATERIAL 'm'

Ex= zeros(it,jt+1,kt+1);
Ey= zeros(it+1,jt,kt+1);
Ez= zeros(it+1,jt+1,kt);
Hx= zeros(it+1,jt,kt);
Hy= zeros(it,jt+1,kt);
Hz= zeros(it,jt,kt+1);

C.c1Ex= ones(size(Ex)).*C.c1(m);
C.c2Ex= ones(size(Ex)).*C.c2(m);
C.c3Ex= ones(size(Ex)).*C.c3(m);
C.c4Ex= ones(size(Ex)).*C.c4(m);
C.c5Ex= ones(size(Ex)).*C.c5(m);
C.c6Ex= ones(size(Ex)).*C.c6(m);

C.c1Ey= ones(size(Ey)).*C.c1(m);
C.c2Ey= ones(size(Ey)).*C.c2(m);
C.c3Ey= ones(size(Ey)).*C.c3(m);
C.c4Ey= ones(size(Ey)).*C.c4(m);
C.c5Ey= ones(size(Ey)).*C.c5(m);
C.c6Ey= ones(size(Ey)).*C.c6(m);

C.c1Ez= ones(size(Ez)).*C.c1(m);
C.c2Ez= ones(size(Ez)).*C.c2(m);
C.c3Ez= ones(size(Ez)).*C.c3(m);
C.c4Ez= ones(size(Ez)).*C.c4(m);
C.c5Ez= ones(size(Ez)).*C.c5(m);
C.c6Ez= ones(size(Ez)).*C.c6(m);

D.d1Hx= ones(size(Hx)).*D.d1(m);
D.d2Hx= ones(size(Hx)).*D.d2(m);
D.d3Hx= ones(size(Hx)).*D.d3(m);
```

```
D.d4Hx= ones(size(Hx)).*D.d4(m);
D.d5Hx= ones(size(Hx)).*D.d5(m);
D.d6Hx= ones(size(Hx)).*D.d6(m);

D.d1Hy= ones(size(Hy)).*D.d1(m);
D.d2Hy= ones(size(Hy)).*D.d2(m);
D.d3Hy= ones(size(Hy)).*D.d3(m);
D.d4Hy= ones(size(Hy)).*D.d4(m);
D.d5Hy= ones(size(Hy)).*D.d5(m);
D.d6Hy= ones(size(Hy)).*D.d6(m);

D.d1Hz= ones(size(Hz)).*D.d1(m);
D.d2Hz= ones(size(Hz)).*D.d2(m);
D.d3Hz= ones(size(Hz)).*D.d3(m);
D.d4Hz= ones(size(Hz)).*D.d4(m);
D.d5Hz= ones(size(Hz)).*D.d5(m);
D.d6Hz= ones(size(Hz)).*D.d6(m);
```

GetMaterial.m

```
function [C,D]= GetMaterial(C,D,I,J,K,mat)

%   FUNCTION:
%      1. UPDATE 'C' AND 'D' TO CHANGE THE MATERIAL IN CELLS (I,J,K) TO 'mat'

C.c1Ex(I,[J max(J)+1],[K max(K)+1])= C.c1(mat);
C.c2Ex(I,[J max(J)+1],[K max(K)+1])= C.c2(mat);
C.c3Ex(I,[J max(J)+1],[K max(K)+1])= C.c3(mat);
C.c4Ex(I,[J max(J)+1],[K max(K)+1])= C.c4(mat);
C.c5Ex(I,[J max(J)+1],[K max(K)+1])= C.c5(mat);
C.c6Ex(I,[J max(J)+1],[K max(K)+1])= C.c6(mat);

C.c1Ey([I max(I)+1],J,[K max(K)+1])= C.c1(mat);
C.c2Ey([I max(I)+1],J,[K max(K)+1])= C.c2(mat);
C.c3Ey([I max(I)+1],J,[K max(K)+1])= C.c3(mat);
C.c4Ey([I max(I)+1],J,[K max(K)+1])= C.c4(mat);
C.c5Ey([I max(I)+1],J,[K max(K)+1])= C.c5(mat);
C.c6Ey([I max(I)+1],J,[K max(K)+1])= C.c6(mat);

C.c1Ez([I max(I)+1],[J max(J)+1],K)= C.c1(mat);
C.c2Ez([I max(I)+1],[J max(J)+1],K)= C.c2(mat);
C.c3Ez([I max(I)+1],[J max(J)+1],K)= C.c3(mat);
C.c4Ez([I max(I)+1],[J max(J)+1],K)= C.c4(mat);
C.c5Ez([I max(I)+1],[J max(J)+1],K)= C.c5(mat);
C.c6Ez([I max(I)+1],[J max(J)+1],K)= C.c6(mat);

D.d1Hx([I max(I)+1],J,K)= D.d1(mat);
D.d2Hx([I max(I)+1],J,K)= D.d2(mat);
D.d3Hx([I max(I)+1],J,K)= D.d3(mat);
D.d4Hx([I max(I)+1],J,K)= D.d4(mat);
D.d5Hx([I max(I)+1],J,K)= D.d5(mat);
D.d6Hx([I max(I)+1],J,K)= D.d6(mat);

D.d1Hy(I,[J max(J)+1],K)= D.d1(mat);
D.d2Hy(I,[J max(J)+1],K)= D.d2(mat);
D.d3Hy(I,[J max(J)+1],K)= D.d3(mat);
```

```
D.d4Hy(I,[J max(J)+1],K)= D.d4(mat);
D.d5Hy(I,[J max(J)+1],K)= D.d5(mat);
D.d6Hy(I,[J max(J)+1],K)= D.d6(mat);

D.d1Hz(I,J,[K max(K)+1])= D.d1(mat);
D.d2Hz(I,J,[K max(K)+1])= D.d2(mat);
D.d3Hz(I,J,[K max(K)+1])= D.d3(mat);
D.d4Hz(I,J,[K max(K)+1])= D.d4(mat);
D.d5Hz(I,J,[K max(K)+1])= D.d5(mat);
D.d6Hz(I,J,[K max(K)+1])= D.d6(mat);
```

FillPML.m

```
function [C,D]= FillPML(C,D,dx,dy,dz,pml,pb,c,e,e0,u,dt,it,jt,kt,m)
%*************************************************************************
%     Program author: Keely J. Willis, Ph.D. Student
%                     UW Computational Electromagnetics Laboratory
%                         Director: Prof. Susan C. Hagness
%*************************************************************************
%   FUNCTION:
%      1. FILL THE OUTSIDE 'pml' NUMBER OF CELLS AS A POLYNOMIAL GRADED UNIAXIAL
%   PERFECTLY MATCHED LAYER (UPML) MATCHED TO FREE SPACE BY UPDATING 'C' AND 'D'
%
%*************************************************************************

rmax= exp(-16);             %   MAX DESIRED NORMAL REFLECTION
order= 4;                   %   ORDER OF GRADING

%   xxxxxxxxxxxxxxxxxxxxxxxxxxxxxx-varying material properties
d= pml*dx;                  % <x> THICKNESS OF PML (m)
sigmaMax= -(order+1)*log(rmax)*e0*c*.5/d;     % MAX <x> CONDUCTIVITY
sigfactor=sigmaMax/(dx*(d^order)*(order+1));

for i=1:pml
    x1=(pml-i+1)*dx;
    x2=(pml-i)*dx;
    sigma=sigfactor*(x1^(order+1)-x2^(order+1));
    facm=(2*e(m)-sigma*dt);
    facp=(2*e(m)+sigma*dt);

    % MATERIAL COEFFICIENTS FOR CELLS IN THE CENTER OF THE UPML
    C.c5Ex(i,:,:)=facp;
    C.c5Ex(it-i+1,:,:)=facp;
    C.c6Ex(i,:,:)=facm;
    C.c6Ex(it-i+1,:,:)=facm;
    D.d1Hz(i,:,:)=facm/facp;
    D.d1Hz(it-i+1,:,:)=facm/facp;
    D.d2Hz(i,:,:)=2*e(m)*dt/facp;
    D.d2Hz(it-i+1,:,:)=2*e(m)*dt/facp;
```

```
    D.d3Hy(i,:,:)=facm/facp;
    D.d3Hy(it-i+1,:,:)=facm/facp;
    D.d4Hy(i,:,:)=1/facp/u(m);
    D.d4Hy(it-i+1,:,:)=1/facp/u(m);

    x1=(pml-i+1.5)*dx;
    x2=(pml-i+0.5)*dx;
    sigma=sigfactor*(x1^(order+1)-x2^(order+1));
    facm=(2*e(m)-sigma*dt);
    facp=(2*e(m)+sigma*dt);

    % MATERIAL COEFFICIENTS FOR CELLS ON THE UPML BOUNDARY
    C.c1Ez(i,:,:)=facm/facp;
    C.c1Ez(it+1-i+1,:,:)=facm/facp;
    C.c2Ez(i,:,:)=2*e(m)*dt/facp;
    C.c2Ez(it+1-i+1,:,:)=2*e(m)*dt/facp;
    C.c3Ey(i,:,:)=facm/facp;
    C.c3Ey(it+1-i+1,:,:)=facm/facp;
    C.c4Ey(i,:,:)=1/facp/e(m);
    C.c4Ey(it+1-i+1,:,:)=1/facp/e(m);
    D.d5Hx(i,:,:)=facp;
    D.d5Hx(it+1-i+1,:,:)=facp;
    D.d6Hx(i,:,:)=facm;
    D.d6Hx(it+1-i+1,:,:)=facm;
end


%   yyyyyyyyyyyyyyyyyyyyyyyyyyyyy-varying material properties
d= pml*dy;                  % <y> THICKNESS OF PML (m)
sigmaMax= -(order+1)*log(rmax)*e0*c*.5/d;       % MAX <y> CONDUCTIVITY
sigfactor= sigmaMax/(dy*(d^order)*(order+1));

for j=1:pml
    y1= (pml-j+1)*dy;
    y2= (pml-j)*dy;
    sigma= sigfactor*(y1^(order+1)-y2^(order+1));
    facm= (2*e(m)-sigma*dt);
```

```
    facp= (2*e(m)+sigma*dt);

    % MATERIAL COEFFICIENTS FOR CELLS IN THE CENTER OF THE UPML
    C.c5Ey(:,j,:)=facp;
    C.c5Ey(:,jt-j+1,:)=facp;
    C.c6Ey(:,j,:)=facm;
    C.c6Ey(:,jt-j+1,:)=facm;
    D.d1Hx(:,j,:)=facm/facp;
    D.d1Hx(:,jt-j+1,:)=facm/facp;
    D.d2Hx(:,j,:)=2*e(m)*dt/facp;
    D.d2Hx(:,jt-j+1,:)=2*e(m)*dt/facp;
    D.d3Hz(:,j,:)=facm/facp;
    D.d3Hz(:,jt-j+1,:)=facm/facp;
    D.d4Hz(:,j,:)=1/facp/u(m);
    D.d4Hz(:,jt-j+1,:)=1/facp/u(m);

    y1= (pml-j+1.5)*dy;
    y2= (pml-j+0.5)*dy;
    sigma= sigfactor*(y1^(order+1)-y2^(order+1));
    facm= (2*e(m)-sigma*dt);
    facp= (2*e(m)+sigma*dt);

    % MATERIAL COEFFICIENTS FOR CELLS ON THE UPML BOUNDARY
    C.c1Ex(:,j,:)=facm/facp;
    C.c1Ex(:,jt+1-j+1,:)=facm/facp;
    C.c2Ex(:,j,:)=2*e(m)*dt/facp;
    C.c2Ex(:,jt+1-j+1,:)=2*e(m)*dt/facp;
    C.c3Ez(:,j,:)=facm/facp;
    C.c3Ez(:,jt+1-j+1,:)=facm/facp;
    C.c4Ez(:,j,:)=1/facp/e(m);
    C.c4Ez(:,jt+1-j+1,:)=1/facp/e(m);
    D.d5Hy(:,j,:)=facp;
    D.d5Hy(:,jt+1-j+1,:)=facp;
    D.d6Hy(:,j,:)=facm;
    D.d6Hy(:,jt+1-j+1,:)=facm;
end
```

```
%   zzzzzzzzzzzzzzzzzzzzz-varying material properties
d= pml*dz;                  % <z> THICKNESS OF PML (m)
sigmaMax= -(order+1)*log(rmax)*e0*c*.5/d;        % MAX <z> CONDUCTIVITY
sigfactor= sigmaMax/(dy*(d^order)*(order+1));

for k=1:pml
    z1=(pml-k+1)*dz;
    z2=(pml-k)*dz;
    sigma=sigfactor*(z1^(order+1)-z2^(order+1));
    facm=(2*e(m)-sigma*dt);
    facp=(2*e(m)+sigma*dt);

    % MATERIAL COEFFICIENTS FOR CELLS IN THE CENTER OF THE UPML
    C.c5Ez(:,:,k)=facp;
    C.c6Ez(:,:,k)=facm;
    D.d1Hy(:,:,k)=facm/facp;
    D.d2Hy(:,:,k)=2*e(m)*dt/facp;
    D.d3Hx(:,:,k)=facm/facp;
    D.d4Hx(:,:,k)=1/facp/u(m);

    z1=(pml-k+1.5)*dz;
    z2=(pml-k+0.5)*dz;
    sigma=sigfactor*(z1^(order+1)-z2^(order+1));
    facm=(2*e(m)-sigma*dt);
    facp=(2*e(m)+sigma*dt);

    % MATERIAL COEFFICIENTS FOR CELLS ON THE UPML BOUNDARY
    C.c1Ey(:,:,k)=facm/facp;
    C.c2Ey(:,:,k)=2*e(m)*dt/facp;
    C.c3Ex(:,:,k)=facm/facp;
    C.c4Ex(:,:,k)=1/facp/e(m);
    D.d5Hz(:,:,k)=facp;
    D.d6Hz(:,:,k)=facm;
end
```

```
%   <x> NORMAL PEC WALLS
C.c1Ez(1,:,:)=-1.0;
C.c1Ez(it+1,:,:)=-1.0;
C.c2Ez(1,:,:)=0.0;
C.c2Ez(it+1,:,:)=0.0;
C.c3Ey(1,:,:)=-1.0;
C.c3Ey(it+1,:,:)=-1.0;
C.c4Ey(1,:,:)=0.0;
C.c4Ey(it+1,:,:)=0.0;

%   <y> NORMAL PEC WALLS
C.c1Ex(:,1,:)=-1;
C.c1Ex(:,jt+1,:)=-1;
C.c2Ex(:,1,:)=0;
C.c2Ex(:,jt+1,:)=0;
C.c3Ez(:,1,:)=-1;
C.c3Ez(:,jt+1,:)=-1;
C.c4Ez(:,1,:)=0;
C.c4Ez(:,jt+1,:)=0;

%   <z> NORMAL PEC WALLS
C.c1Ey(:,:,1)=-1;
C.c2Ey(:,:,1)=0;
C.c3Ex(:,:,1)=-1;
C.c4Ex(:,:,1)=0;
```

ChangePML.m

```
function [C,D]= changePML(C,D,dx,dy,dz,pml,pb,c,e,e0,u,dt,it,jt,kt,m,K)
%************************************************************************
%     Program author: Keely J. Willis, Ph.D. Student
%                     UW Computational Electromagnetics Laboratory
%                         Director: Prof. Susan C. Hagness
%************************************************************************
%   FUNCTION:
%      1. CHANGE PML OF OUTSIDE CELLS OF LAYERS (K:kt) TO BE MATCHED TO MATERIAL
%           'm' BY UPDATING 'C' AND 'D'
%
%************************************************************************

rmax= exp(-16);             %   MAX DESIRED NORMAL REFLECTION
order= 4;                   %   ORDER OF GRADING

%   xxxxxxxxxxxxxxxxxxxxxxxxxxxxxx-varying material properties
d= pml*dx;                  % <x> THICKNESS OF PML (m)
sigmaMax= -(order+1)*log(rmax)*e0*c*.5/d;    % MAX <x> CONDUCTIVITY
sigfactor=sigmaMax/(dx*(d^order)*(order+1));

for i=1:pml
    x1= (pml-i+1)*dx;
    x2= (pml-i)*dx;
    sigma= sigfactor*(x1^(order+1)-x2^(order+1));
    facm= (2*e0-sigma*dt);
    facp= (2*e0+sigma*dt);

    % MATERIAL COEFFICIENTS FOR CELLS IN THE CENTER OF THE UPML
    C.c5Ex(i,:,K:end)=facp;
    C.c5Ex(it-i+1,:,K:end)=facp;
    C.c6Ex(i,:,K:end)=facm;
    C.c6Ex(it-i+1,:,K:end)=facm;
    D.d1Hz(i,:,K:end)=facm/facp;
    D.d1Hz(it-i+1,:,K:end)=facm/facp;
    D.d2Hz(i,:,K:end)=2*e(m)*dt/facp;
    D.d2Hz(it-i+1,:,K:end)=2*e(m)*dt/facp;
```

```
    D.d3Hy(i,:,K:end)=facm/facp;
    D.d3Hy(it-i+1,:,K:end)=facm/facp;
    D.d4Hy(i,:,K:end)=1/facp/u(m);
    D.d4Hy(it-i+1,:,K:end)=1/facp/u(m);

    x1= (pml-i+1.5)*dx;
    x2= (pml-i+0.5)*dx;
    sigma= sigfactor*(x1^(order+1)-x2^(order+1));
    facm= (2*e0-sigma*dt);
    facp= (2*e0+sigma*dt);

    % MATERIAL COEFFICIENTS FOR CELLS ON THE UPML BOUNDARY
    C.c1Ez(i,:,K:end)= facm/facp;
    C.c1Ez(it+1-i+1,:,K:end)= facm/facp;
    C.c2Ez(i,:,K:end)= 2*e(m)*dt/facp;
    C.c2Ez(it+1-i+1,:,K:end)= 2*e(m)*dt/facp;
    C.c3Ey(i,:,K:end)= facm/facp;
    C.c3Ey(it+1-i+1,:,K:end)= facm/facp;
    C.c4Ey(i,:,K:end)= 1/facp/e(m);
    C.c4Ey(it+1-i+1,:,K:end)= 1/facp/e(m);
    D.d5Hx(i,:,K:end)= facp;
    D.d5Hx(it+1-i+1,:,K:end)= facp;
    D.d6Hx(i,:,K:end)= facm;
    D.d6Hx(it+1-i+1,:,K:end)= facm;
end


%   yyyyyyyyyyyyyyyyyyyyyyyyyyyyy-varying material properties
d= pml*dy;                  % <y> THICKNESS OF PML (m)
sigmaMax= -(order+1)*log(rmax)*e0*c*.5/d;      % MAX <y> CONDUCTIVITY
sigfactor= sigmaMax/(dy*(d^order)*(order+1));

for j=1:pml
    y1= (pml-j+1)*dy;
    y2= (pml-j)*dy;
    sigma= sigfactor*(y1^(order+1)-y2^(order+1));
    facm= (2*e0-sigma*dt);
```

```
    facp= (2*e0+sigma*dt);

    % MATERIAL COEFFICIENTS FOR CELLS IN THE CENTER OF THE UPML
    C.c5Ey(:,j,K:end)= facp;
    C.c5Ey(:,jt-j+1,K:end)= facp;
    C.c6Ey(:,j,K:end)= facm;
    C.c6Ey(:,jt-j+1,K:end)= facm;
    D.d1Hx(:,j,K:end)= facm/facp;
    D.d1Hx(:,jt-j+1,K:end)= facm/facp;
    D.d2Hx(:,j,K:end)= 2*e(m)*dt/facp;
    D.d2Hx(:,jt-j+1,K:end)= 2*e(m)*dt/facp;
    D.d3Hz(:,j,K:end)= facm/facp;
    D.d3Hz(:,jt-j+1,K:end)= facm/facp;
    D.d4Hz(:,j,K:end)= 1/facp/u(m);
    D.d4Hz(:,jt-j+1,K:end)= 1/facp/u(m);

    y1= (pml-j+1.5)*dy;
    y2= (pml-j+0.5)*dy;
    sigma= sigfactor*(y1^(order+1)-y2^(order+1));
    facm= (2*e0-sigma*dt);
    facp= (2*e0+sigma*dt);

    % MATERIAL COEFFICIENTS FOR CELLS ON THE UPML BOUNDARY
    C.c1Ex(:,j,K:end)= facm/facp;
    C.c1Ex(:,jt+1-j+1,K:end)= facm/facp;
    C.c2Ex(:,j,K:end)= 2*e(m)*dt/facp;
    C.c2Ex(:,jt+1-j+1,K:end)= 2*e(m)*dt/facp;
    C.c3Ez(:,j,K:end)= facm/facp;
    C.c3Ez(:,jt+1-j+1,K:end)= facm/facp;
    C.c4Ez(:,j,K:end)= 1/facp/e(m);
    C.c4Ez(:,jt+1-j+1,K:end)= 1/facp/e(m);
    D.d5Hy(:,j,K:end)= facp;
    D.d5Hy(:,jt+1-j+1,K:end)= facp;
    D.d6Hy(:,j,K:end)= facm;
    D.d6Hy(:,jt+1-j+1,K:end)= facm;
end
```

InitializePEC.m

```
function [field,is,js,id,jd,ANGLES]=
                    InitializePEC(field,it,jt,kt,pb,pml,r,dx,dy,dz,Y,ks)

%**********************************************************************
%   FUNCTION:
%      1. ASSIGN LOCATION OF PEC FOR 180 DEGREE CURVE BY ZEROING TANGENTIAL E FIELDS
%      2. SPECIFY THE SOURCE CELL
%      3. SPECIFY CELLS TO BE RECORDED FOR PROPAGATION CONSTATNT EXTRACTION
%
%   OUTPUTS:
%       'field.pecEx','field.pecEy','field.pecEz':  SPECIFY CELLS OF E FIELDS TO BE
%           ZEROED TO MODEL PEC
%
%       'ANGLES':  A VECTOR OF ANGLES TO EACH (id,jd) CELL FROM CENTER OF CIRCLE
%
%       'id' AND 'jd':  SPECIFY THE FIELD DATA TO BE SAVED
%
%       'is' AND 'js':  SPECIFY THE SOURCE CELL(S)
%
%**********************************************************************

PEC= 0;

%   CREATE MEMORY LOCATIONS FOR PEC
field.pecEx= single(ones(it,jt+1,kt+1));
field.pecEy= single(ones(it+1,jt,kt+1));
field.pecEz= single(ones(it+1,jt+1,kt));

% Put ground plate on entire floor of computational space
Igx= 1:it;
Igy= 1:(it+1);
Jgx= 1:(jt+1);
Jgy= 1:jt;
Kg= (kt+1);
field.pecEx(Igx,Jgx,Kg)= PEC;
field.pecEy(Igy,Jgy,Kg)= PEC;
```

```
Kc= pb+1;                   % vertical location of strip
Kw= Kc:kt;                  % vertical location of wall
INSIDE= 1;                  % select inside or outside wall

% (dist0X,dist0Y) are the coordinates (m) of the center of the "circle"
dist0Y= r/sqrt(2) +jt*dy -dy*(2+pml);
dist0X= round(it/2)*dx;

id= 0;  jd= 0;   ANGLES= 0;
for x= 1:it
    for y= 1:jt
        % (distX,distY) are the coordinates (m) of the current cell at 'x' and 'y'
        distX= (x-1)*dx;
        distY= (y-1)*dy;

        % DIST is the distance from center of the "circle" to (distX,distY)
        DIST= sqrt((dist0X-distX)^2 +(dist0Y-distY)^2);

        if (DIST > r) & (DIST < (r+Y))
            field.pecEx(x,y,Kc)= PEC;               %Concucting strip
            field.pecEy(x,y,Kc)= PEC;               %Concucting strip
        end;

        if INSIDE           % PUT WALL ON INSIDE CURVE
            if abs(DIST-r) < (dy/2)
                field.pecEx(x,y,Kw)= PEC;
                field.pecEz(x,y,Kw)= PEC;
            end;
        else                % PUT WALL ON OUTSIDE CURVE
            if abs(r+Y-DIST) < (dy/2)
                field.pecEx(x,y,Kw)= PEC;
                field.pecEz(x,y,Kw)= PEC;
            end;
        end

        if INSIDE           % PUT SOURCE CELL AND DISPLAY VECTOR NEAR OUTSIDE EDGE
```

```
            is= pml+4;
            js= jt-pml-4;
            if abs(DIST-(r+Y-2*dy)) < (dy/2)
                ANGLES= [ANGLES atan2(dist0Y-distY,dist0X-distX)*180/pi];
                id= [id x];
                jd= [jd y];
            end;

        else                % PUT SOURCE CELL AND DISPLAY VECTOR NEAR INSIDE EDGE
            is= pml+Y-2;
            js= jt-pml-4;
            if abs(DIST-(r+2*dy)) < (dy/2)
                ANGLES= [ANGLES atan2(dist0Y-distY,dist0X-distX)*180/pi];
                id= [id x];
                jd= [jd y];
            end;
        end
    end;
end;
id(1)=[];  jd(1)=[];  ANGLES(1)=[];

if id==[] | jd==[]    error('YOU WON''T GET DATA, DUMMY');  end;
```

InitializePEC90.m

```
function [field,is,js,id,jd,ANGLES]= ...
                    InitializePEC90(field,it,jt,kt,pb,pml,r,dx,dy,dz,Y,ks)

%**********************************************************************
%   FUNCTION:
%      1. ASSIGN LOCATION OF PEC FOR 90 DEGREE CURVE BY ZEROING TANGENTIAL E FIELDS
%      2. SPECIFY THE SOURCE CELL
%      3. SPECIFY CELLS TO BE RECORDED FOR PROPAGATION CONSTATNT EXTRACTION
%
%   OUTPUTS:
%       'field.pecEx','field.pecEy','field.pecEz':  SPECIFY CELLS OF E FIELDS TO BE
%           ZEROED TO MODEL PEC
%
%       'ANGLES':  A VECTOR OF ANGLES TO EACH (id,jd) CELL FROM CENTER OF CIRCLE
%
%       'id' AND 'jd':  SPECIFY THE FIELD DATA TO BE SAVED
%
%       'is' AND 'js':  SPECIFY THE SOURCE CELL(S)
%
%**********************************************************************
PEC= 0;

%   CREATE MEMORY LOCATIONS FOR PEC
field.pecEx= ones(it,jt+1,kt+1);
field.pecEy= ones(it+1,jt,kt+1);
field.pecEz= ones(it+1,jt+1,kt);

% Put ground plate on entire floor of computational space
Igx= 1:it;
Igy= 1:(it+1);
Jgx= 1:(jt+1);
Jgy= 1:jt;
Kg= (kt+1);
field.pecEx(Igx,Jgx,Kg)= PEC;
field.pecEy(Igy,Jgy,Kg)= PEC;
```

```
Kc= pb+1;                   % vertical location of strip
Kw= Kc:kt;                  % vertical location of wall
INSIDE= 1;                  % select inside or outside wall

% (dist0X,dist0Y) are the coordinates (m) of the center of the "circle"
dist0Y= r/sqrt(2) +jt*dy -dy*(2+pml);
dist0X= round(it/2)*dx;

id= 0;  jd= 0;   ANGLES= 0;
for x= 1:it
    for y= 1:jt+1
        % (distX,distY) are the coordinates (m) of the current cell at 'x' and 'y'
        distX= (x-1)*dx;
        distY= (y-1)*dy;

        % DIST is the distance from center of the "circle" to (distX,distY)
        DIST= sqrt((dist0X-distX)^2 +(dist0Y-distY)^2);

        if (DIST > r) & (DIST < (r+Y))
            field.pecEx(x,y,Kc)= PEC;               %Concucting strip
            field.pecEy(x,y,Kc)= PEC;               %Concucting strip
        end;

        if INSIDE           % PUT WALL ON INSIDE CURVE
            if abs(DIST-r) < (dy/2)
                field.pecEx(x,y,Kw)= PEC;
                field.pecEz(x,y,Kw)= PEC;
            end;
        else                % PUT WALL ON OUTSIDE CURVE
            if abs(r+Y-DIST) < (dy/2)
                field.pecEx(x,y,Kw)= PEC;
                field.pecEz(x,y,Kw)= PEC;
            end;
        end

        if INSIDE           % PUT SOURCE CELL AND DISPLAY VECTOR NEAR OUTSIDE EDGE
             if x==(pml+5)
```

```
                if abs(DIST-(r+Y-2*dy)) < (dy/2)
                    is= x;
                    js= y;
                end;
            end;
            if abs(DIST-(r+Y-2*dy)) < (dy/2)
                ANGLES= [ANGLES atan2(dist0Y-distY,dist0X-distX)*180/pi];
                id= [id x];
                jd= [jd y];
            end;
        else                % PUT SOURCE CELL AND DISPLAY VECTOR NEAR INSIDE EDGE
            if x==(pml+5)
                if abs(DIST-(r+Y-2*dy)) < (dy/2)
                    is= x;
                    js= y;
                end;
            end;
            if abs(DIST-(r+2*dy)) < (dy/2)
                ANGLES= [ANGLES atan2(dist0Y-distY,dist0X-distX)*180/pi];
                id= [id x];
                jd= [jd y];
            end;
        end
    end;
end;
id(1)=[];  jd(1)=[];  ANGLES(1)=[];

if id==[] | jd==[]    error('YOU WON''T GET DATA, DUMMY');  end;
```

UpdateE.m

```
function field= UpdateE(field,C,D,it,jt,kt,DX,DY,DZ)
%
%   FUNCTION:
%      1. UPDATE E FIELD COMPONENT OF ALL CELLS FOR ONE TIME STEP BASED ON EXAMPLE OF
%       EQ. 7.74 OF COMPUTAIONAL ELECTRODYNAMICS BY TAFLOVE/HAGNESS 2ND ED.
%

field.Dxn(:,2:jt,2:kt)= C.c1Ex(:,2:jt,2:kt).*field.Dx(:,2:jt,2:kt)...
    +C.c2Ex(:,2:jt,2:kt).*( (field.Hz(:,2:jt,2:kt)-field.Hz(:,1:jt-1,2:kt))*DY ...
                           -(field.Hy(:,2:jt,2:kt)-field.Hy(:,2:jt,1:kt-1))*DZ );

field.Dyn(2:it,:,2:kt)= C.c1Ey(2:it,:,2:kt).*field.Dy(2:it,:,2:kt)...
    + C.c2Ey(2:it,:,2:kt).*( (field.Hx(2:it,:,2:kt)-field.Hx(2:it,:,1:kt-1))*DZ ...
                            -(field.Hz(2:it,:,2:kt)-field.Hz(1:it-1,:,2:kt))*DX );

field.Dzn(2:it,2:jt,:)= C.c1Ez(2:it,2:jt,:).*field.Dz(2:it,2:jt,:)...
    + C.c2Ez(2:it,2:jt,:).*( (field.Hy(2:it,2:jt,:)-field.Hy(1:it-1,2:jt,:))*DX ...
                            -(field.Hx(2:it,2:jt,:)-field.Hx(2:it,1:jt-1,:))*DY );

field.Ex(:,2:jt,2:kt)=  C.c3Ex(:,2:jt,2:kt).*field.Ex(:,2:jt,2:kt)...
    + C.c4Ex(:,2:jt,2:kt).*( C.c5Ex(:,2:jt,2:kt).*field.Dxn(:,2:jt,2:kt)...
                            -C.c6Ex(:,2:jt,2:kt).*field.Dx(:,2:jt,2:kt) );

field.Ey(2:it,:,2:kt)=  C.c3Ey(2:it,:,2:kt).*field.Ey(2:it,:,2:kt)...
    + C.c4Ey(2:it,:,2:kt).*( C.c5Ey(2:it,:,2:kt).*field.Dyn(2:it,:,2:kt)...
                            -C.c6Ey(2:it,:,2:kt).*field.Dy(2:it,:,2:kt) );

field.Ez(2:it,2:jt,:)=  C.c3Ez(2:it,2:jt,:).*field.Ez(2:it,2:jt,:)...
    + C.c4Ez(2:it,2:jt,:).*( C.c5Ez(2:it,2:jt,:).*field.Dzn(2:it,2:jt,:)...
                            -C.c6Ez(2:it,2:jt,:).*field.Dz(2:it,2:jt,:) );

field.Dx=field.Dxn;
field.Dy=field.Dyn;
field.Dz=field.Dzn;
```

UpdateH.m

```
function field= UpdateH(field,C,D,it,jt,kt,DX,DY,DZ)
%
%   FUNCTION:
%      1. UPDATE H FIELD COMPONENT OF ALL CELLS FOR ONE TIME STEP BASED ON EXAMPLE OF
%       EQ. 7.74 OF COMPUTAIONAL ELECTRODYNAMICS BY TAFLOVE/HAGNESS 2ND ED.
%

field.Bxn(2:it,:,:)= D.d1Hx(2:it,:,:).*field.Bx(2:it,:,:)...
    - D.d2Hx(2:it,:,:).*( (field.Ez(2:it,2:jt+1,:)-field.Ez(2:it,1:jt,:))*DY ...
                         -(field.Ey(2:it,:,2:kt+1)-field.Ey(2:it,:,1:kt))*DZ );

field.Byn(:,2:jt,:)= D.d1Hy(:,2:jt,:).* field.By(:,2:jt,:)...
    - D.d2Hy(:,2:jt,:).*( (field.Ex(:,2:jt,2:kt+1)-field.Ex(:,2:jt,1:kt))*DZ ...
                         -(field.Ez(2:it+1,2:jt,:)-field.Ez(1:it,2:jt,:))*DX );

field.Bzn(:,:,2:kt)= D.d1Hz(:,:,2:kt).* field.Bz(:,:,2:kt)...
    - D.d2Hz(:,:,2:kt).*( (field.Ey(2:it+1,:,2:kt)-field.Ey(1:it,:,2:kt))*DX ...
                         -(field.Ex(:,2:jt+1,2:kt)-field.Ex(:,1:jt,2:kt))*DY );

field.Hx(2:it,:,:)= D.d3Hx(2:it,:,:).*field.Hx(2:it,:,:)+ D.d4Hx(2:it,:,:)...
    .*(D.d5Hx(2:it,:,:).*field.Bxn(2:it,:,:) - D.d6Hx(2:it,:,:).*field.Bx(2:it,:,:));

field.Hy(:,2:jt,:)= D.d3Hy(:,2:jt,:).*field.Hy(:,2:jt,:)+ D.d4Hy(:,2:jt,:)...
    .*(D.d5Hy(:,2:jt,:).*field.Byn(:,2:jt,:) - D.d6Hy(:,2:jt,:).*field.By(:,2:jt,:));

field.Hz(:,:,2:kt)= D.d3Hz(:,:,2:kt).*field.Hz(:,:,2:kt)+ D.d4Hz(:,:,2:kt)...
    .*(D.d5Hz(:,:,2:kt).*field.Bzn(:,:,2:kt) - D.d6Hz(:,:,2:kt).*field.Bz(:,:,2:kt));

field.Bx=field.Bxn;
field.By=field.Byn;
field.Bz=field.Bzn;
```

AddPECTH.m

```
function field= addPECTH(field, it, jt, kt, pb, pml)
%
%   FUNCTION:
%      1. ASSIGN ZERO THICKNESS PEC FOR A THW ANTENNA TO BY ZEROING
%       TANGENTIAL E FIELDS CORRESPONDING TO CONDUCTOR LOCATIONS
%

Icx= 1:it;
Icy= 1:(it+1);
Jcx= pml+3:(jt+1)-pml-2;
Jcy= pml+3:jt-pml-2;
Kc= pb+1;
field.Ex(Icx,Jcx,Kc)= 0;     %Concucting strip
field.Ey(Icy,Jcy,Kc)= 0;     %Concucting strip


Igx= 1:it;
Igy= 1:(it+1);
Jgx= 1:(jt+1);
Jgy= 1:jt;
Kg= (kt+1);
field.Ex(Igx,Jgx,Kg)= 0;     %Ground Plate
field.Ey(Igy,Jgy,Kg)= 0;     %Ground Plate


% wall is no longer on the pml
Iwx= 1:it;
Iwz= 1:(it+1);
Jw= (jt+1)-pml-2;
Kwx= pb+1:(kt+1);
Kwz= pb+1:kt;
field.Ex(Iwx,Jw,Kwx)= 0;     %Concucting wall
field.Ez(Iwz,Jw,Kwz)= 0;     %Concucting wall
```

AddPECTF.m

```
function field= addPECTF(field, it, jt, kt, pb, pml)
%
%   FUNCTION:
%      1. ASSIGN ZERO THICKNESS PEC FOR A TFW ANTENNA TO BY ZEROING
%       TANGENTIAL E FIELDS CORRESPONDING TO CONDUCTOR LOCATIONS
%

Icx= 1:it;
Icy= 1:(it+1);
Jcx= pml+3:(jt+1)-pml-2;
Jcy= pml+3:jt-pml-2;
Kc= pb+1;
field.Ex(Icx,Jcx,Kc)= 0;    %Concucting strip
field.Ey(Icy,Jcy,Kc)= 0;    %Concucting strip


Igx= 1:it;
Igy= 1:(it+1);
Jgx= 1:(jt+1);
Jgy= 1:jt;
Kg= (kt+1);
field.Ex(Igx,Jgx,Kg)= 0;    %Ground Plate
field.Ey(Igy,Jgy,Kg)= 0;    %Ground Plate


Iwx= 1:it;
Iwz= 1:(it+1);
Jw= round(jt/2)+1;
Kwx= pb+1:(kt+1);
Kwz= pb+1:kt;
field.Ex(Iwx,Jw,Kwx)= 0;    %Concucting wall
field.Ez(Iwz,Jw,Kwz)= 0;    %Concucting wall
```

AddPECMENZ.m

```
function field= addPECMENZ(field, it, jt, kt, pb, pml, dx)
%
%   FUNCTION:
%      1. ASSIGN ZERO THICKNESS PEC FOR A MENZEL ANTENNA TO BY ZEROING
%       TANGENTIAL E FIELDS CORRESPONDING TO CONDUCTOR LOCATIONS
%

width= jt-2*pml-4;          % WIDTH OF STRUCTURE (CELLS)
sloty= round(width/4);      % PEC ON BOTH <y> SIDES OF EACH SLOT
slotx= round(sloty/2);      % PEC BETWEEN SLOTS IN <x>
pecx= round(slotx/1);       % SLOT <x>

Icx= 1:it;
Icy= 1:(it+1);
Jcx= pml+3:pml+3+sloty;
Jcy= pml+3:pml+2+sloty;
Kc= pb+1;
field.Ex(Icx,Jcx,Kc)= 0;
field.Ey(Icy,Jcy,Kc)= 0;    %Top long

Icx= 1:it;
Icy= 1:(it+1);
Jcx= (jt+1)-pml-2-sloty:(jt+1)-pml-2;
Jcy= jt-pml-1-sloty:jt-pml-2;
field.Ex(Icx,Jcx,Kc)= 0
field.Ey(Icy,Jcy,Kc)= 0;    %Bottom long

Icx= 1:pml+2*pecx;
Icy= 1:pml+2*pecx+1;
Jcx= pml+3+sloty+1:(jt+1)-pml-sloty-3;
Jcy= pml+2+sloty+1:jt-pml-sloty-2;
field.Ex(Icx,Jcx,Kc)= 0;
field.Ey(Icy,Jcy,Kc)= 0;    %First

Icx= pml+slotx+2*pecx+1:pml+slotx+3*pecx;
Icy= pml+slotx+2*pecx+1:pml+slotx+3*pecx+1;
```

```
field.Ex(Icx,Jcx,Kc)= 0;
field.Ey(Icy,Jcy,Kc)= 0;    %Second

for n= 1:5
Icx= Icx+slotx+pecx;
Icy= Icy+slotx+pecx;
field.Ex(Icx,Jcx,Kc)= 0;
field.Ey(Icy,Jcy,Kc)= 0;    %Third - Seventh
end;

Icx= Icx(1)+slotx+pecx:it;
Icy= Icy(1)+slotx+pecx:it+1;
field.Ex(Icx,Jcx,Kc)= 0;
field.Ey(Icy,Jcy,Kc)= 0;    %Eighth

Igx= 1:it;
Igy= 1:(it+1);
Jgx= 1:(jt+1);
Jgy= 1:jt;
Kg= (kt+1);
field.Ex(Igx,Jgx,Kg)= 0;    %Ground Plate
field.Ey(Igy,Jgy,Kg)= 0;    %Ground Plate
```

ViewData.m

```
% function [A,B]= ViewData(view)
%
%   FUNCTION:
%      1. READ DATA FROM THW, TFW, OR MENZEL SIMULATION
%      2. PROCESS DATA
%      3. COMPUTE \alpha AND \beta
%      4. PLOT \alpha AND \beta
%      5. SAVE \alpha AND \beta TO EXCEL SPREADSHEET
%
clear all
close all
clc

% ALLOW USER TO CHOOSE TRIAL TO EVALUATE
[view, pathname]= uigetfile;
load([pathname,view]);

% DISPALY THE RAW DATA
for n= 1:floor(periods)
    figure
    EZ= EZDATA(n,:);
    plot(1:length(EZ),EZ,'linewidth',2)
    ylabel(' E_z ');
    xlabel(' Cell Number (x-direction) ');
    title([' Period #:  ',num2str(n)]);
    grid on
end

% Ez:  GET ABOUT TWO GOOD WAVES.  IT MAY NOT BE POSSIBLE TO GET TWO WAVELENGTHS.
% ADJUST 'start' AND 'stop' TO GET AS MUCH DATA AS POSSIBLE.  AT LEAST A HALF
% WAVELENGTH IS REQUIRED TO CONTINUE.
if f/1e9 < 6.1    start= is+40;
elseif f/1e9 < 7.1    start= is+10;
else start= is+3; end;

if f/1e9 < 6.3    stop= 500;
```

```
elseif f/1e9 < 6.6    stop= 300;
elseif f/1e9 < 7.0    stop= 150;
else stop= 100; end;

% NORMALIZE
Max= find(abs(Ez(start:start+stop))==max(abs(Ez(start:start+stop))));
Ez= Ez((start+Max):stop+start+Max)/Ez((start+Max));

% Es:  INTERPOLATE MORE POINTS IF NECCESSARY
points= 1;
x= (1:length(Ez))+start+Max-1;
xs= (1:(1/points):length(Ez))+start+Max-1;
Es = spline(x,Ez,xs);
dxs= dx/points;

% USE LOG(Es) TO DETERMINE 'A' AND 'B'
logEs= real(log(Es));
figure
plot(xs*dxs,logEs,'b','linewidth',3);
grid on
xlabel('Distnace from source (m)');
ylabel('ln { E_z }  (dB) ');

% FIND NULL LOCATIONS: 'nullEz', PEAK LOCATIONS: 'slopeX', AND PEAK VALUES: 'slopeY'
slopeX= 1;  slopeY= 0;  nullEs= 0;  down= 1;
for nn= 4:length(logEs)
    if down & logEs(nn)>logEs(nn-1) & logEs(nn-1)>logEs(nn-2)
        down= 0;
        nullEs= [nullEs (nn-2)*dxs];
    elseif ~down & logEs(nn)<logEs(nn-1) & logEs(nn-1)<logEs(nn-2)
        down= 1;
        slopeX= [slopeX (nn-2)];
        slopeY= [slopeY logEs(nn-2)];
    end;
end
Lbeta= nullEs(4)-nullEs(2);
B= 2*pi/Lbeta;
```

```
peak1= 1;
peak2= 3;
A= ( slopeY(peak1)-slopeY(peak2) )/( (slopeX(peak2)-slopeX(peak1))*dxs );

% NORMALIZED EXPONENTIAL CURVE FITTING 'A' AND 'B'
EsMatch= exp(-A*xs*dxs-j*B*xs*dxs)/max(exp(-A*xs*dxs-j*B*xs*dxs));

% COMPARE DATA TO MATCHED CURVE
figure
hold on
plot(x,log(Es),'r','linewidth',4);
plot(x,log(EsMatch),'k','linewidth',2);
hold off
ylabel('Ez');
xlabel('X-direction cell number');
title(view);
legend('FDTD',['\alpha/k_0= ',num2str(round(A/k*100)/100),'\beta/k_0= ',num2str(B/k)])
grid on

% COMPARE LOG DATA TO LOG MATCHED CURVE
figure
hold on
plot(x,(Es),'r','linewidth',4);
plot(x,(EsMatch),'k','linewidth',2);
hold off
ylabel('Ez');
xlabel('X-direction cell number');
title(view);
legend('FDTD',['\alpha/k_0= ',num2str(round(A/k*100)/100),'\beta/k_0= ',num2str(B/k)])
grid on

% SAVE DATA TO EXCEL SPREADSHEET TO BE RECORDED
format long
data= [ f/1e9   A/k    B/k ];
N = xlsread('C:\Documents and Settings\Ashley\Desktop\NewSimData',name);
N= [N; data];
xlswrite('C:\Documents and Settings\Ashley\Desktop\NewSimData',N,name,'A2');
```

ViewDataCurve.m

```
% function [A,B]= ViewDataCurve(view)
%
%   FUNCTION:
%      1. READ DATA FROM CURVE SIMULATION
%      2. PROCESS DATA
%      3. COMPUTE \alpha AND \beta
%      4. PLOT \alpha AND \beta
%      5. SAVE \alpha AND \beta TO EXCEL SPREADSHEET
%

clear all
close all
clc

% ALLOW USER TO CHOOSE TRIAL TO EVALUATE
[view, pathname]= uigetfile;
load([pathname,view]);

% DISPALY THE RAW DATA
for n= 1:floor(periods)
    figure
    EZ= EZDATA(n,:);
    plot(1:length(EZ),EZ,'linewidth',2)
    ylabel(' E_z ');
    xlabel(' Cell Number (x-direction) ');
    title([' Period #:  ',num2str(n)]);
    grid on
end
% figure
% plot(1:length(angles),angles,'b','linewidth',2)
% title('raw angles')
% grid on
% xlabel('cell number');
% ylabel('Angle (degrees) ');

% UNWRAP THE ANGLE
```

```
R= r+Y-2*dy;        % radius of "circle"
P= 2*pi*R;          % perimeter of "circle"
E= Ez(floor(periods),:);
clear Ez
angles= unwrap(angles);
% figure
% plot(1:length(angles),angles,'b','linewidth',2)
% title('unwrapped angles')
% grid on
% xlabel('cell number');
% ylabel('Angle (degrees) ');

% ORDER THE ANGLES
A=0;  Ez=0;
for aa= 1:length(angles)
    for a= 1:length(A)
        if angles(aa)< A(a)
            A= [A(1:(a-1)) angles(aa) A(a:end)];
            Ez= [Ez(1:(a-1)) E(aa) Ez(a:end)];
            break;
        elseif a==length(A)
            A= [A angles(aa)];
            Ez= [Ez E(aa)];
        end
    end
end
A(1)=[];  Ez(1)=[];
% figure
% plot(1:length(A),A,'b','linewidth',2)
% title('ordered angles')
% grid on
% xlabel('cell number');
% ylabel('Angle (degrees) ');

% CHANGE ANGLE TO POSITION
dist= (A)/360*P;  % vector of positions of each point along antenna "arc"
% figure
```

```
% plot(1:length(dist),dist,'b','linewidth',2)
% title('angles turned to distances')
% grid on
% xlabel('cell number');
% ylabel('Arc distance to source (m) ');

% RAW LOG DATA TO BE ANALYZED
figure
plot(dist,log(Ez),'b','linewidth',2)
title('raw')
grid on
xlabel('cell number');
ylabel('| E_z | ');

% FIND SOURCE
is= find(log(Ez)==max(log(Ez)));

% Ez:  GET ABOUT TWO GOOD WAVES.  IT MAY NOT BE POSSIBLE TO
% GET TWO WAVELENGTHS.  ADJUST 'start' AND 'stop' TO GET AS MUCH DATA AS
% POSSIBLE.  AT LEAST A HALF WAVELENGTH IS REQUIRED TO CONTINUE.
if f/1e9 < 6.1    start= is+50;
elseif f/1e9 < 7.1    start= is+50;
else start= is+30; end;

if f/1e9 < 6.3    stop= 300;
elseif f/1e9 < 6.6    stop= 300;
elseif f/1e9 < 7.0    stop= 150;
else stop= 200; end;

% NORMALIZE
Max= find(abs(Ez(start:start+stop))==max(abs(Ez(start:start+stop))));
Ez= Ez((start+Max):stop+start+Max)/Ez((start+Max));
dist= dist(start+Max:stop+start+Max);
% figure
% plot(1:length(Ez),Ez,'b','linewidth',2)
% title('short and normal')
% grid on
```

```
% xlabel('cell number');
% ylabel('| E_z | ');


% USE LOG(Es) TO DETERMINE 'A' AND 'B'
logEz= real(log(Ez));
figure
plot(dist,logEz,'b','linewidth',2)
title('log')
grid on
xlabel('cell number');
ylabel('ln | E_z |  (dB) ');

% FIND NULL LOCATIONS 'nullEz', PEAK LOCATIONS 'slopeX', AND, PEAK VALUES
% 'slopeY'
slopeX= dist(1);  slopeY= 0;  nullEz= dist(1);  down= 1;
for nn= 4:length(logEz)
    if down & logEz(nn)>logEz(nn-1) & logEz(nn-1)>logEz(nn-2)
        down= 0;
        nullEz= [nullEz dist(nn-2)];
    elseif ~down & logEz(nn)<logEz(nn-1) & logEz(nn-1)<logEz(nn-2)
        down= 1;
        slopeX= [slopeX dist(nn-2)];
        slopeY= [slopeY logEz(nn-2)];
    end;
end
Lbeta= (nullEz(4)-nullEz(2));
B= 2*pi/Lbeta;
A= ( slopeY(1)-slopeY(3) )/( (slopeX(3)-slopeX(1)) );

% NORMALIZED EXPONENTIAL CURVE FITTING 'A' AND 'B'
EzMatch= exp(-A*dist-j*B*dist)/max(exp(-A*dist-j*B*dist));

% COMPARE DATA TO MATCHED CURVE
figure
hold on
plot(dist,Ez,'r','linewidth',4);
```

```
plot(dist,real(EzMatch),'k','linewidth',2);
hold off
ylim([-1 1.5]);
ylabel('Ez');
xlabel('X-direction cell number');
title(view);
legend('FDTD',['\alpha/k_0= ',num2str(round(A/k*100)/100),'\beta/k_0= ',num2str(B/k)])
grid on

% COMPARE LOG DATA TO LOG MATCHED CURVE
figure
hold on
plot(dist,log(Ez),'r','linewidth',4);
plot(dist,log(real(EzMatch)),'k','linewidth',2);
hold off
ylabel('Ez');
xlabel('X-direction cell number');
title(view);
legend('FDTD',['\alpha/k_0= ',num2str(round(A/k*100)/100),'\beta/k_0= ',num2str(B/k)])
grid on

% SAVE DATA TO EXCEL SPREADSHEET TO BE RECORDED
data= [ f/1e9   A/k    B/k time];
N = xlsread('C:\Documents and Settings\Ashley\Desktop\NewSimData',name);
N= [N; data];
xlswrite('C:\Documents and Settings\Ashley\Desktop\NewSimData',N,name,'A2');
```

LineSource.m

```
function LineSource(th1,th2,f)
%
%   OUTPUT:  PLOTS SHOWING LINE SOURCE APPROXIMATION OF THE FAR-FIELD
%       PATTERN OF THIELE HALF WIDTH ANTENNA GENERATED FROM ALPHA AND BETA
%
%   INPUTS:
%           \alpha AND \beta FROM MEASUREMENTS, SIMULATION, AND/OR TRANS RES APPROX
%           'th1' IS THE REFLECTION ANGLE FROM THE FAR END
%           'th2' IS THE REFLECTION ANGLE FROMTHE NEAR (SOURCE) END
%           'f' IS THE EXCITATION FREQUENCY
%
%


c= 299792458;               % speed of light (m/s)
omega= 2*pi*f;              % angular frequency (rad/s)
lambda= c/f;                % wavelength (m)
k0= 2*pi/lambda;            % wavenumber (1/m)
u0= pi*4e-7;                % permeability of free space (H/m)
e0= c^-2/u0;                % permittivity of free space (F/m)

load TRh787w15e233          % GET TRANSVERSE RESONANCE DATA FOR 'f'
alphaT= round(AA(find(round(freqs*100)/100==f/1e9))*1000)/1000;
betaT= round(BB(find(round(freqs*100)/100==f/1e9))*100)/100;

if f== 6.7e9
    load F67                        % MEASURED DATA
    az= F67(:,1)-90;
    mag= fliplr(F67(:,2)')';
    ph= F67(:,3);
    alphaF= 0.0404245257377625;     %PUT FDTD DATA HERE
    betaF= 0.676644325256347;       %PUT FDTD DATA HERE

    load gmz67                      % MEASURED DATA
    GMZaz= gmz67(:,1)-90;
    GMZmag= (gmz67(:,2)')';
    GMZph= gmz67(:,3);
```

```
elseif f== 7.2e9
    load F72                        % MEASURED DATA
    az= F72(:,1)-90;
    mag= fliplr(F72(:,2)')';
    ph= F72(:,3);
    alphaF= 0.0251624081283808;     %PUT FDTD DATA HERE
    betaF= 0.816086113452911;       %PUT FDTD DATA HERE

    load gmz72                      % MEASURED DATA
    GMZaz= gmz72(:,1)-90;
    GMZmag= (gmz72(:,2)')';
    GMZph= gmz72(:,3);

else
    error('NO DATA FOR THAT FREQUENY');
end;

phi= (0:.1:180)*pi/180;
percent= 4/100; % ADD 4% TO gamma TO ACCOUNT FOR "LINE SOURCE/ANTENNA LENGTH ISSUE"
r= 100;                     % distance to far field -- 2.0 (m) is adequate)
L= .19;                     % length of antenna (m)


% TRANSVERSE RESONANCE FORWARD WAVE
gammaT= (betaT*(1+percent))*k0-j*(alphaT*(1+percent))*k0;
OmT= L/2*(k0*cos(phi)-gammaT);
ET= (sin(phi).*sin(OmT)./OmT);                      % NORMALIZED
maxEtr= phi(find(abs(ET)==max(abs(ET))));           % LOCATION OF MAIN BEAM
ErT= exp(-alphaT*k0*L)*abs(ET)*exp(-j*th1);         %   RETURN WAVE
Er2T= exp(-alphaT*k0*L)*ErT*exp(-j*th2);            %   RETURN-RETURN WAVE
Er3T= exp(-alphaT*k0*L)*Er2T*exp(-j*th1);           %   RETURN-RETURN-RETURN WAVE
EtotalT= abs(ET) +fliplr(ErT) +Er2T +fliplr(Er3T);  % ALL TRANSVERSE RESONANCE WAVES

% FDTD FORWARD WAVE
gammaF= (betaF*(1+percent))*k0-j*(alphaF*(1+percent))*k0;
OmF= L/2*(k0*cos(phi)-gammaF);
```

```
EF= (sin(phi).*sin(OmF)./OmF);                      % NORMALIZED
maxEfdtd= phi(find(abs(EF)==max(abs(EF))));         % LOCATION OF MAIN BEAM
ErF= exp(-alphaF*k0*L)*abs(EF)*exp(-j*th1);         %  RETURN WAVE
Er2F= exp(-alphaF*k0*L)*ErF*exp(-j*th2);            %  RETURN-RETURN WAVE
Er3F= exp(-alphaF*k0*L)*Er2F*exp(-j*th1);           %  RETURN-RETURN-RETURN WAVE
EtotalF= abs(EF) +fliplr(ErF) +Er2F +fliplr(Er3F);  % ALL FDTD WAVES


% DISPLAY MEASURED DATA AND FDTD/TR LINE SOURCE APPROXIMATIONS
figure
hold on;
plot((phi*180/pi)+.5, 20*log10(EtotalF/max(EtotalF)), 'r--','linewidth', 4);
plot(az,mag-max(mag),'k','linewidth',3);
plot(GMZaz+2.5,GMZmag-max(GMZmag),'b','linewidth',3);
hold off;
grid on;
set(gcf,'Color',[1;1;1]);
set(gca,'XDir','reverse')
axis([0 180 -30 7]);
title([num2str(f/1e9),' GHz']);
legend('FDTD / Line Source','Measured (vias)','Measured (tape)');
% legend('Line Source','Measured (tape)');
xlabel([' Angle from endfire (degrees)']);
ylabel(' Normalized  | E_{H-pol} | (dB)');

% DISPLAY BOTH POLAR AND RECTANGULAR
figure
subplot(2,1,1)
hold on;
plot((phi*180/pi), 20*log10(EtotalF/max(EtotalF)), 'b','linewidth', 3);
plot(maxEfdtd*ones(20,1),linspace(-30,0,20),'r','linewidth', 3);
hold off;
grid on;
set(gcf,'Color',[1;1;1]);
set(gca,'XDir','reverse')
axis([0 180 -30 10]);
title([num2str(f/1e9),' GHz','  \alpha /k_0= ',num2str(alphaF),...
```

```
    ' \beta /k_0= ',num2str(betaF)]);
% legend('FDTD / Line Source','Measured');
xlabel([' Angle from endfire (degrees)']);
ylabel(' Normalized  | E_{\theta} | (dB)');
text(130,5,[' Main Beam: ',num2str(maxEfdtd),'^o '],'FontSize',14,...
                            'BackgroundColor','w','EdgeColor','r','Linewidth',3);

subplot(2,1,2)
p= find(abs(real(20*log10(Etotalf)+30)) <.05);
polar(phi(p(1):p(2)), 20*log10(EtotalF(p(1):p(2))/max(EtotalF))+30);
ylim([0 45])
ylabel('Normalized | E_\theta | (dB)');

% APPROX MAIN BEAM
MAINtr= acos(betaT)*180/pi
MAINfdtd= acos(betaF)*180/pi

% MAIN BEAM DATA
maxEtr=maxEtr*180/pi
maxEfdtd=maxEfdtd*180/pi
```

TransRes.m

```
function [A,B]=TransRes(f,h,w,er)

% WRITTEN BY:   Dr. Gary Thiele
% MODIFIED BY:   Greg Zelinski
% LAST MODIFIED:  21NOV2004
%
% INPUT:    'f' is frequency (Hz)
%           'h' is the substrate height (m)
%           'w' is the conductor width (m)
%           'er' is the relative permittivity of the substrate
%
% OUTPUTS:  'A' is the attenuation constant normalized with free space wavenumber
%           'B' is the phase constant normalized with free space wavenumber
%
% SOURCE:  K. S. Lee, ''Microstrip Line Leaky Antenna'', Ph.D. diss.,
%           Polytechnic Institute 1986

c= 299792458;               % speed of light
u0= pi*4e-7;                % free space permeability
e0= c^-2/u0;                % free space permittivity
k0= 2*pi*f/c;               % free space wavenumber
k= k0*sqrt(er);             % wavenumber in medium

m= 1:50;                    % summation truncation
delta= (er-1)/(er+1);
Q= sum( (-delta).^m.*log(m) );

syms kxe                    % symbolic variable
kz= sqrt(k^2 - kxe^2);
alpha = kz/k0;
kx= sqrt(1-alpha^2)*k0;
gamma = 0.5772-1;

fe = -2*kxe*h/pi*( ( log(j*kx*h) +gamma )/er  +2*Q  -log(2*pi) );

del = kz*h/pi*( (1-er)/er*( log(j*kx*h) +gamma ) + 2*Q  );
```

```
chi = 2*atan( kz/kxe*tanh(del) ) - fe;

trans= chi -kxe*w +pi;      % TRANSVERSE RESONANCE EQUATION FOR EH_1
solkxe= solve(trans);       % solution of symbolic variable kxe
prop= sqrt(k^2 - solkxe^2);
B = real(prop/k0);
A = abs(imag(prop/k0));
```

MakeTransResFile.m

```
%   MakeTransResFile.m
%
%   OUTPUT:
%           1. SAVES .mat FILE TO THE CURRECT DIRECTORY.
%                   'freqs' IS A VECTOR OF THE FREQUENCIES (Hz)
%                   'AA' IS A VECTOR OF \alpha/k0
%                   'BB' IS A VECTOR OF \beta/k0
%           2. PLOT OF DATA
%
%   NAMING CONVENTION:
%           'TRh787w150e233.mat' IS FOR AN ANTENNA OF
%           HEIGHT 787e-6 (m); HALF WIDTH 7.5 (mm); AND DIELECTRIC CONSTANT 2.33
%
%**************************************************************************
clear all
close all
clc
format compact
tic
getData = 0;                % use "1" to get data or "0" to just plot

if getData
    range= (6:.1:8.2)*1e9;  % FREQUENCIES

    %for MENZEL'S antenna:
    h= .787*1e-3;
    w= 15e-3;
    er = 2.33;

    for r= 1:length(range)
        last= toc;
        [A(r),B(r)]=TransRes(range(r),h,w,er);
        fprintf('\nFrequency %.0f of %.0f took %.1f s.',r,length(range),toc-last);
    end

    % interpolate Transverse Resonance data to 1 MHz increments
```

```
    freqs= range(1):1e6:range(end);
    AA = pchip(range,A,freqs);       % pchip or spline
    BB = pchip(range,B,freqs);

    file= ['TRh',num2str(round(w*1e6)),'w',num2str(round(w*1e4)),...
                                                    'e',num2str(round(er*100))];
    save(file);

else
    file= 'TRh787w150e233';
    load(file);
end

figure
plot(freqs,AA,'c',freqs,BB,'r','linewidth',3);
xlabel ('Frequency (GHz))')
legend('\alpha/k_0 ','\beta/k_0 ')
title ([file,''])
grid on
set(gcf,'Color',[1;1;1]);

time= toc/60;
fprintf('\n\n\tTransRes took %.2f minutes.\n\n', time);
```

DataReader.m

```
%   DataReader.m
%
%   PLOTS A COMPARISON BETWEEN TRANSVERSE RESONANCE AND ONE OR MORE DATA  SETS
%
clear all
close all
clc
load Compare;               % GET TRANSVERSE RESONANCE DATA

name= '180curveS';          % ENTER A DATA SET TO DISPLAY
N = xlsread('C:\Documents and Settings\Ashley\Desktop\NewSimData',name);
f= N(:,1);      a= N(:,3);      b= N(:,6);

name2= 'Single';            % ENTER ANOTHER DATA SET TO DISPLAY
N2 = xlsread('C:\Documents and Settings\Ashley\Desktop\NewSimData',name);
f2= N2(:,1);    a2= N2(:,2);    b2= N2(:,6);

figure
hold on
plot(freqs,AA,'r','linewidth',4);
plot(f2,a2,'k','linewidth',2);
plot(f,a,'b.','MarkerSize',20);
plot(freqs,BB,'r','linewidth',4);
plot(f2,b2,'k','linewidth',2);
plot(f,b,'b.','MarkerSize',20);
hold off
axis([5.6 8.2 0 1.1]);
set(gcf,'Color',[1;1;1]);
xlabel('Frequency (GHz)');
text(6.7,.85,'\beta /k_0','BackgroundColor','w','FontSize',16);
text(7,.15,'\alpha /k_0','BackgroundColor','w','FontSize',16);
legend('Transverse Resonance','Straight (single)',...
                                        '180^o Curve (single)','Location','East');
grid on
```

1. Andrew, William V., Constantine A. Balanis, and Panayiotis A. Tirkas. "A Comparison of the Berenger Perfectly Matched Layer and the Lindman Higher Order ABC's for the FDTD Method". *IEEE Microwave and Guided Wave Letters*, Vol. 5, No. 6:192–194, June 1995.

2. Bagby, Jonathan S., Dennis P. Nyquist, Ching-Her Lee, and Yi Yuan. "Identification of Propagation Regimes on Integrated Microstrip Transmission Lines". *IEEE Transactions on Microwave Theory and Techniques*, Vol. 41, No. 11:1887–1894, November 1993.

3. Balanis, Constantine. *Advanced Engineering Electromagnetics*. John Wiley & Sons, Inc., New York, NY, 1989.

4. Balanis, Constantine. *Antenna Theory: Analysis and Design*. John Wiley & Sons, Inc., New York, NY, second edition, 1997.

5. Berenger, Jean-Pierre. "A Perfectly Matched Layer for the Absorption of Electromagnetic Waves". *Journal of Computational Physics*, Vol. 114:185–200, October 1994.

6. Boukamp, Joachim and Rolf H. Jansen. "Spectral Domain Investigation of Surface Wave Excitation and Radiation by Microstrip Lines and Microstrip Disk Resonators". *Proceedings of the 1983 European Microwave Conference*, September 5-8, 1983.

7. Chang, David C. and Edward F. Kuester. "Total and Partial Reflection from the End of a Parallel-Plate Waveguide with an Extended Dielectric Slab". *Radio Science*, Vol. 16, No. 1:1–13, January-February 1981.

8. Chew, Weng Cho and Nicholas V. Shuley. "A 3-D Perfectly Matched Medium from Modified Maxwells Equations with Stretched Coordinates". *Microwave Optical Technology Letters*, Vol 7:599–604, September 1994.

9. Ermert, Helmut. "Guided Modes and Radiation Characteristics of Covered Microstrip Lines". *Archiv fur Elektronik und Ubertragungstechnik (AEU)*, Band 30, Heft 2:65–70, April 1976.

10. Ermert, Helmut. "Guiding and Radiation Characteristics of Planar Waveguides". *Microwaves, Optics, and Acoustics*, Vol. 3, No. 2:59–62, March 1979.

11. Goldstone, L. O. and Arthur A. Oliner. "Leaky Wave Antennas I: Rectangular Waveguides". *IRE Transactions on Antennas and Propagation*, Vol. 7, Issue 4:307–319.

12. Grimm, Jerry Michael and Dennis P. Nyquist. "Spectral Analysis Considerations Relevant to Radiation and Leaky Modes of Open-Boundary Microstrip Transmission Line". *IEEE Transactions on Microwave Theory and Techniques*, Vol. 41, No. 1:150–153, January 1993.

13. IEEE. "IEEE Standard 145-1983: Standard Definitions of Terms for Antennas". June 1983.

14. Kantartzis, Nikolaos V. and Theodoros Tsiboukis. "A Comparative Study of the Perfectly Matched Layer, the Superabsorption Technique, and Several Higher-Order ABC's for the FDTD Algorithm in Two and Three Dimensional Problems". *IEEE Transactions on Magnetics*, Vol. 33, No. 2:1460–1463, March 1997.

15. Kashiwa, T., T. Onishi, and I. Fukai. "Analysis of Microstrip Antennas on a Curved Surface Using the Conformal Grids FD-TD Method". *IEEE Transactions on Antennas and Propagation*, Vol. 42:423–427, March 1994.

16. Katz, Daniel S., Eric T. Thiele, and Allen Taflove. "Validation and Extension to Three Dimensions of the Berenger PML Absorbing Boundary Condition for FD-TD Meshes". *Microwave and Guided Wave Letters*, Vol. 4, No. 8:268–270, August 1994.

17. Kuester, Edward F., Robert T. Johnk, and David C. Chang. "The Thin-Substrate Approximation for Reflection from the End of a Slab-loaded Parallel-Plate Waveguide with Applications to Microstrip Patch Antennas". *IEEE Transactions on Antennas and Propagation*, Vol. AP-30, No. 5:910–917, September 1982.

18. Kumar, Girish and K. P. Ray. *Broadband Microstrip Antennas*. Artech House, Boston, MA, 2003.

19. Kunz, Karl S. and Ray J. Luebbers. *The Finite Difference Time Domain Method for Electromagnetics*. CRC Press, Ann Arbor, MI, 1993.

20. Lee, Kun Sam. *Microstrip Line Leaky Wave Antennas*. Ph.D. thesis, Polytechnic Institute of New York, 1986.

21. Lin, Yu-De and Jyh-Wen Sheen. "Mode Distinction and Radiation Efficiency Analysis of Planar Leaky-Wave Line Source". *IEEE Transactions on Microwave Theory and Techniques*, Vol. 45, No. 10:1540–1543, October 1997.

22. Marcuvitz, Nathan. "On Field Representations in Terms of Leaky Modes and Eigenmodes". *IRE Electromagnetic Wave Theory Symposium*, Vol. 4, Issue 3:192–194, July 1956.

23. Menzel, Wolfgang. "A New Travelling-Wave Antenna in Microstrip". *Archiv fur Elektronik und Ubertragungstechnik (AEU)*, Band 33, Heft 4:137–140, April 1979.

24. Mesa, Francisco and David R. Jackson. "Investigation of Integration Paths in the Spectral Domain Analysis of Leaky Modes on Printed Circuit Lines". *IEEE Transactions on Microwave Theory and Techniques*, Vol. 50, No. 10:2267–2275, October 2002.

25. Mesa, Francisco, David R. Jackson, and Manuel J. Freire. "Evolution of Leaky Modes on Printed-Circuit Lines". *IEEE Transactions on Microwave Theory and Techniques*, Vol. 50, No. 1:94–104, January 2002.

26. Michalski, Krzysztof A. and Dalian Zheng. "Rigorous Analysis of Open Microstrip Lines of Arbitrary Cross Section in Bound and Leaky Regimes". *IEEE Transactions on Microwave Theory and Techniques*, Vol. 37, No. 12:2005–2010, December 1989.

27. Mur, G. "Absorbing Boundary Conditions for the Finite Difference Approximation of the Time-Domain Electromagnetic Field Equations". *IEEE Transactions on Electromagnetic Compatibility*, Vol. EMC-23:377–382, November 1981.

28. Noujeim, Karam M. "Wave propagation Characteristics of a Reactively Loaded Microstrip". *IEEE Microwave Theory and Techniques Digest*, 821–824, 2003.

29. Oliner, Arthur A. "Leakage from Higher Modes on Microstrip Line with Applications to Antennas". *Radio Science*, Vol. 22, No. 6:907–912, November 1987.

30. Oliner, Arthur A. and K. S. Lee. "The Nature of the Leakage From Higher Modes on Microstrip Line". *IEEE MTT-S International Microwave Symposium Digest*, 57–60, 1986.

31. Pozar, David M. *Microwave Engineering*. John Wiley, New York, NY, second edition, 1998.

32. Pozar, David M. and David H. Schaubert. *Microstrip Antennas: The Analysis and Design of Microstrip Antennas and Arrays*. John Wiley, New York, NY, 1995.

33. Prescott, Deane T. and Nicholas V. Shuley. "Reflection Analysis of the FDTD Boundary condition – Part II: Berenger's PML Absorbing Layers". *IEEE Transactions on Microwave Theory and Techniques*, Vol. 45, No. 8:1171–1178, August 1997.

34. Qian, Y., B. C. C. Chang, T. Itoh, K. C. Chen, and C. K. C. Tzuang. "High Efficiency and Broadband Excitation of Leaky Mode in Microstrip Antennas". *IEEE Microwave Theory and Techniques Digest*, 1419–1422, 1999.

35. Sheen, David M., Sami M. Ali, Mohamed D. Abouzahra, and Jin Au Kong. "Application of the Three Dimensional Finite Difference Time-Domain Method to the Analysis of Planar Microstrip Circuits". *IEEE Transactions on Microwave Theory and Techniques*, Vol. 38, No. 7:849–857, July 1990.

36. Sheen, David Mark. *Numerical Modeling of Microstrip Circuits and Antennas*. Ph.D. thesis, Massachusetts Institute of Technology, 1991.

37. Sheen, Jyh-Wen, Yu-De Lin, and Tai-Lee Chen. "A Leaky-Mode S-Parameter Extraction Technique for Efficient Design of the Microstrip Line Leaky-Wave Antenna". *IEEE Microwave Theory and Techniques Digest*, 175–178, 1999.

38. Taflove, Allen. *Advances in Computational Electrodynamics: The Finite Difference Time-Domain Method*. Artech House, Boston, MA, second edition, 1998.

39. Taflove, Allen and Susan Hagness. *Computational Electrodynamics: The Finite Difference Time-Domain Method*. Artech House, Boston, MA, second edition, 2000.

40. Tzuang, Ching-Kuang C. "Leaky-Mode Perspective on Printed Antenna". *Proceedings of the National Science Council, Republic of China*, Vol. 23, No. 4:544–548, May 1999.

41. Walter, Carlton H. *Traveling Wave Antennas*. McGraw-Hill, New York, NY, 1965.

42. Yau, D., N. V. Shuley, and L. O. McMillan. "Characteristics of Microstrip Leaky-Wave Antenna Using the Method of Moments". *IEE Proc. Microwave Antennas and Propag*, Vol. 146, No. 5:324–328, October 1999.

43. Yee, Kane S. "Numerical Solution of Initial Boundary Value Problems Involving Maxwell's Equations in isotropic Media". *IEEE Transactions on Antennas and Propagation*, Vol. AP-14, No. 3:302–307, May 1966.

REPORT DOCUMENTATION PAGE

Form Approved
OMB No. 0704-0188

1. REPORT DATE *(DD-MM-YYYY)*	2. REPORT TYPE	3. DATES COVERED *(From - To)*
21-03-2005	Master's Thesis	Dec 2003 - Mar 2005

4. TITLE AND SUBTITLE
Finite Difference Time Domain (FDTD) Analysis of a Leaky Traveling Wave Microstrip Antenna

5a. CONTRACT NUMBER

5b. GRANT NUMBER

5c. PROGRAM ELEMENT NUMBER

6. AUTHOR(S)
Zelinski, Gregory M., First Lieutenant, USAF

5d. PROJECT NUMBER

5e. TASK NUMBER

5f. WORK UNIT NUMBER

7. PERFORMING ORGANIZATION NAME(S) AND ADDRESS(ES)
Air Force Institute of Technology
Graduate School of Engineering and Management (AFIT/EN)
2950 Hobson Way
WPAFB OH 45433-7765

8. PERFORMING ORGANIZATION REPORT NUMBER
AFIT/GE/ENG/05-24

9. SPONSORING/MONITORING AGENCY NAME(S) AND ADDRESS(ES)
Air Force Research Laboratories (AFRL/SNRR), (AFMC)
Attn: Dan Janning
2241 Avionics Circle
WPAFB OH 45433-7765
DSN 785-4120 x3544 Email: Dan.Janning@wpafb.af.mil

10. SPONSOR/MONITOR'S ACRONYM(S)

11. SPONSOR/MONITOR'S REPORT NUMBER(S)

12. DISTRIBUTION/AVAILABILITY STATEMENT
APPROVED FOR PUBLIC RELEASE; DISTRIBUTION UNLIMITED

13. SUPPLEMENTARY NOTES

14. ABSTRACT

This thesis provides the groundwork that will enable development of a lightweight, inexpensive, aerodynamic, and broadband antenna. Whether for radar or communication, an antenna with these properties would be a force multiplier for the smaller, limited payload air vehicles the United States Air Force will pursue in the coming years.

Several microstrip antennas using the first higher order mode were simulated with the Finite Difference Time Domain (FDTD) method. The propagation constant of each antenna was extracted from the resulting field distribution for comparison with a transverse resonance approximation, measured far-field patterns, and other simulated antennas. Variations of the geometry were explored to investigate field propagation, improve the far-field pattern, and improve bandwidth. A simplified fabrication method was demonstrated that shorten production time and improved the far-field pattern.

15. SUBJECT TERMS
Antennas, traveling waves, propagation, microwave frequency, finite difference theory, difference equations, numerical analysis, time domain, fabrication, antenna radiation patterns, bandwidth.

16. SECURITY CLASSIFICATION OF:			17. LIMITATION OF ABSTRACT	18. NUMBER OF PAGES	19a. NAME OF RESPONSIBLE PERSON
a. REPORT	b. ABSTRACT	c. THIS PAGE			Michael L. Hastriter, Maj, USAF
U	U	U	U	158	19b. TELEPHONE NUMBER *(Include area code)* 937-255-3636 x4652